POLITECNICO DI MILANO
DEPARTMENT OF CIVIL AND ENVIRONMENTAL ENGINEERING
DOCTORAL PROGRAMME IN ENVIRONMENTAL AND INFRASTRUCTURE ENGINEERING

POROUS SURFACES FOR PERMEABLE PAVEMENT: CLOGGING AND FILTRATION MECHANISMS

Doctoral Dissertation of:
Mariana Marchioni

Supervisor:
Prof. Gianfranco Becciu

Co-Supervisor:
Prof. John Sansalone

Tutor:
Prof. Gianfranco Becciu

The Chair of the Doctoral Program:
Prof. Alberto Guadagnini

29th Cycle – 2013/2018

"I maintain that the only purpose of science is to ease the hardship of human existence. If scientists, intimidated by self-seeking people in power, are content to amass knowledge for the sake of knowledge, then science can become crippled, and your new machines will represent nothing but new means of oppression."

Bertolt Brecht, The life of Galileo.

Contents

List of figures

List of tables

Abstract[1]

Urbanization growth ultimately affects the hydrological cycle reducing infiltration and evapotranspiration, directing most of the stormwater to the sewer system and so increasing flood risk ((ISTAT), [4]). This situation is intensified by the "heat islands" effect where the higher temperatures in densely populated areas ultimately enhance precipitation (Alves Filho and Ribeiro, [5]). When washing off impermeable surfaces, runoff transports particulate matter (PM) loads and PM-bound chemicals generated by anthropogenic, biogenic activities and infrastructure. Diffuse non-source discharge from rainfall-runoff processes is currently the major source of receiving water impairment (Sansalone, Hird, [6]).

The traditional urban drainage management has become impractical in current urbanization scenarios, pushing towards comprehensive measures that promote infiltration on its source (Becciu, Ghia, [7]) (Lamera, Becciu, [8]). These measures are commonly known as SuDs (sustainable urban drainage systems) and propose different solutions to achieve a long term and sustainable urban drainage management, acting both on runoff volume and pollutants load (Marchioni and Becciu, [9]).

One way to reduce runoff volume is through the reduction of impervious areas. This can be achieved by reducing the development area, promoting infiltration or disconnecting the impermeable areas from the municipal drainage system (Field and Tafuri, [10]). There are many practices on this approach, such as permeable pavements, infiltration trenches, green roofs, detention reservoirs.

Permeable pavement act on both runoff water volume and pollutants load. It can be described as an infiltration system on which runoff infiltrates through a permeable layer or other stabilized permeable surface (Field and Tafuri, [10]). Permeable pavement operates on runoff volume through retention and infiltration. Runoff pollutant load can be reduced by mechanisms of sedimentation, filtration, adsorption, biodegradation and volatilization and water quality can be enhanced by nutrient, sludge, metals and hydrocarbons removal (Woods-Ballard, Kellagher, [11]).

Besides stormwater control, other aspects can be incorporated into SuDS strategies based on permeable paving, such as water reuse (Pratt, [12]) (Imran, Akib, [13]), energy saving (Sañudo-Fontaneda, Castro-Fresno, [14]) , temperature decreasing (Asaeda and Ca, [15]), (Smith, [16]), (Sarat and Eusuf, [17]). Using photocatalytic cement incorporated on the pavement it can also act on air pollution (de Melo, Trichês, [18]).

[1] Parts of this research were published on the following:
[1] Andrés-Valeri, V.C., et al., *Laboratory assessment of the infiltration capacity reduction in clogged porous mixture surfaces.* Sustainability, 2016. **8**(8): p. 751.
[2] Brugin, M., et al., *Clogging potential evaluation of porous mixture surfaces used in permeable pavement systems.* European Journal of Environmental and Civil Engineering, 2017: p. 1-11.
[3] Marchioni, M. and G. Becciu, *Experimental Results On Permeable Pavements In Urban Areas: A Synthetic Review.* International Journal of Sustainable Development and Planning, 2015. **10**(6): p. 806-817.

Those results can be increased when permeable pavements and vegetation are jointly considered (Scholz and Uzomah, [19]).

Dry deposition PM deposited on the surface of permeable pavements decrease water infiltration until unsatisfactory performance. Clogging is influence by the surface pore structure and the PM granulometric indices, blocking the connected porosity (Kia, Wong, [20]). Pollutants loads partition on PM fractions allowing physical separation through filtration mechanisms (Sansalone and Cristina, [21]).

The line of implementation of new technologies often begins with academic research on laboratory level, then prototypes and full-scale tests leading to market availability. At this point become necessary to develop guidelines, standards and regulations. Permeable pavements have already reached this line and related technologies are fully market available and research is focused on optimization. The most considered research issues are improving surface materials and studying the clogging phenomena. Research activities can be addressed to observe, monitor and predict clogging through modelling, laboratory and field experiments. It’s also necessary to have a trustworthy evaluation test methods and to set efficient maintenance procedures.

This research investigates aspects of runoff volume and pollutant load on porous asphalt[2] (PA) and pervious concrete[2] (PC) that are commonly used as surface on permeable pavement through an experimental plan. A rainfall simulator was developed to measure on laboratory runoff volume and hydraulic conductivity on initial conditions and under the effect of sediments load. Part of the porous asphalt specimens were analyzed with x-ray micro-CT tomography (XRT) to obtain pore structure parameters. Dry deposition (PM) was sampled on four different locations in Milan (Italy) and was obtained the accumulation rate and granulometric indices. The laboratory and field results were used to model permeability and filtration mechanism.

The results showed the efficiency of both type of tested materials (PC and PA) for runoff volume reduction and pollutants load removal under the tested conditions. The permeability model showed that the falling head permeameter does not yield a darcyan hydraulic conductivity. The filtration mechanism model showed good accordance between measured and modeled results.

[2] This type of material is refer on literature as porous, pervious or permeable. In this text is adopted the term porous asphalt as seen on the European Committee for Standardization (CEN) and pervious asphalt as on ASTM international. Is important to notice that a material can be “porous” but not present a permeability consistent with a permeable pavement use.

1. Introduction

1.1. Scenario

Urbanization can be understood on two aspects, demographically, i.e. the population residing on the defined urban areas and on the means of proportion urban, i.e. the territorially aspect based on land use, diffusion and concentrations indicators. There is not actually a directly correlation between these two aspects and especially on the European context it's possible to observed urban area growth with a stable or decrease on resident population. Urban growth is correlated positively with economic growth ((ISTAT), [4]).

On the demographically point of view, more than half of the world's population (54%) currently lives in urban areas and this number is project to reach 66% in 2050. In Italy today 69 per cent of the population resides on urban area and is estimated to reach 78 per cent in 2050 (United Nations, [22]), (Figure 1).

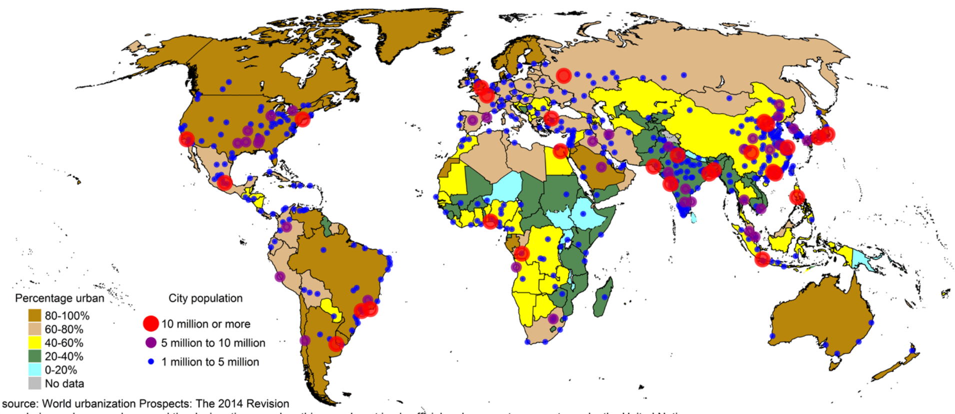

Data source: World urbanization Prospects: The 2014 Revision
The boundaries and names shown and the designations used on this map do not imply official endorsement or acceptance by the United Nations.
Dotted line represents approximately the Line of Control in Jammu and Kashmir agreed upon by India and Pakistan.
The final status of Jammu and Kashmir has not yet been agreed upon by the parties.
Final boundary between the Republic of Sudan and the Republic of South Sudan has not yet been determined.

Figure 1 – Percentage of urban population (United Nations, [22]).

Urban area however does not have a defined confine on the city limits and expands uncontrolled and disordered towards the peripheral zone on the phenomena known as city sprawling, causing an increase in land take and soil sealing (Gibelli and Salzano, [23, (FAO-UN), [24]). Land take is the conversion of agricultural, natural or semi-natural land cover to a anthropogenic area. A part of this area will result on soil sealing, i.e. the permanent covering of an area of land and its soil with impermeable artificial materials such as asphalt or concrete, for example through buildings and roads. The ratio between the sealed area and the total area can be named soil sealing index and range from 0,95 for dense residential areas to 0,1 for park and villas. ((FAO-UN), [24]). The main impacts of soil sealing are on soil biodiversity, carbon storage, the microclimate due the lack of evapotranspiration and vegetation reduction and the alteration of the hydrological cycle. To minimize these effects urban planners and managers should minimize the conversion of green areas, support re-use already build-up areas and infrastructures that allow infiltration and minimize soil sealing ((FAO-UN), [24]).

The city of Milan (Italy) registered an important urban area growth after the Second World War (Figure 2) (Becciu, Ghia, [7]).

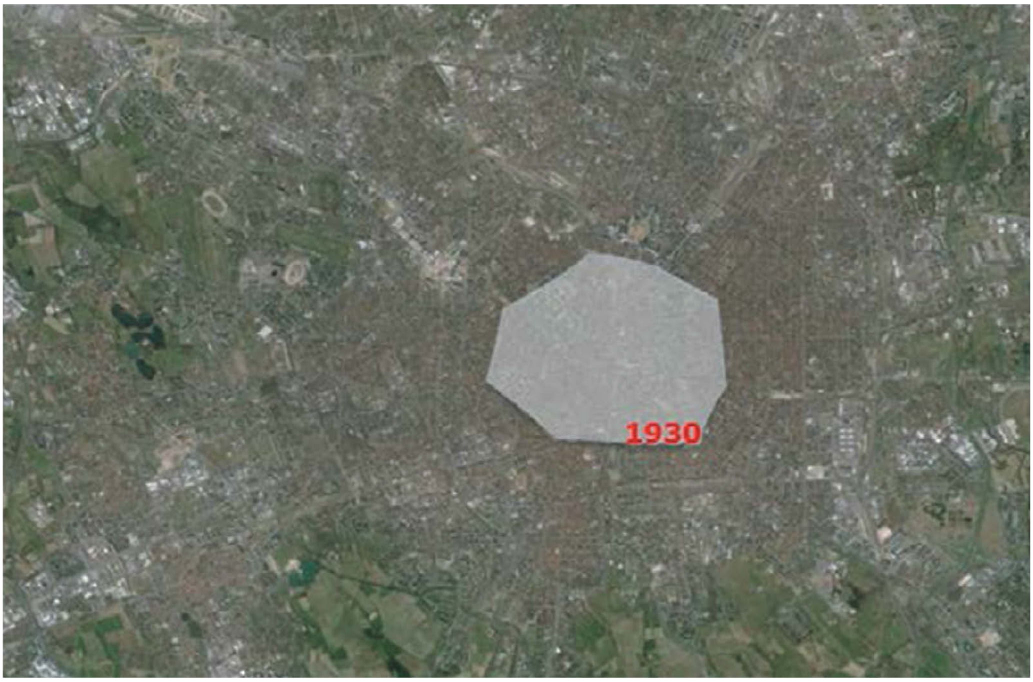

Figure 2 - Comparison of Milan (Italy) urban area on 1930 and now.

1.2. Urbanization impacts on the hydrological cycle

The hydrological cycle includes many processes occurring continuously with no beginning and end, when water evaporates from oceans and land surface to the atmosphere, water vapor is transported and lifted to the atmosphere until it condenses and precipitates on the land or the oceans. Precipitated water may be intercepted by vegetation, became overland flow over the ground surface, infiltrate into the ground, flow through the soil as subsurface flow and discharge into streams as surface runoff. Much of the intercepted water and surface runoff returns to the atmosphere through evaporation. The infiltrated water may percolate deeper to recharge groundwater, later emerging in springs or seeping into streams to form surface runoff and finally flowing out to the sea or evaporating into the atmosphere in the continuous hydrological cycle (Chow, Maidment, [25])

This cycle is modified due to urbanization resulting on reduction on soil infiltration, groundwater recharge and evapotranspiration with the most part of the water volume being direct to the sewer system increasing flooding risk. Figure 3 illustrates the hydraulic alterations on the annual water balance comparing a pre and post-development scenario on a real case. The evapotranspiration reduces from 40 per cent of the total precipitation to 25 per cent and the groundwater recharge from 50 per cent to 30 per cent with most of the water on the post-development (45 per cent) being directed for the sewer system (Becciu and Paoletti, [26]).

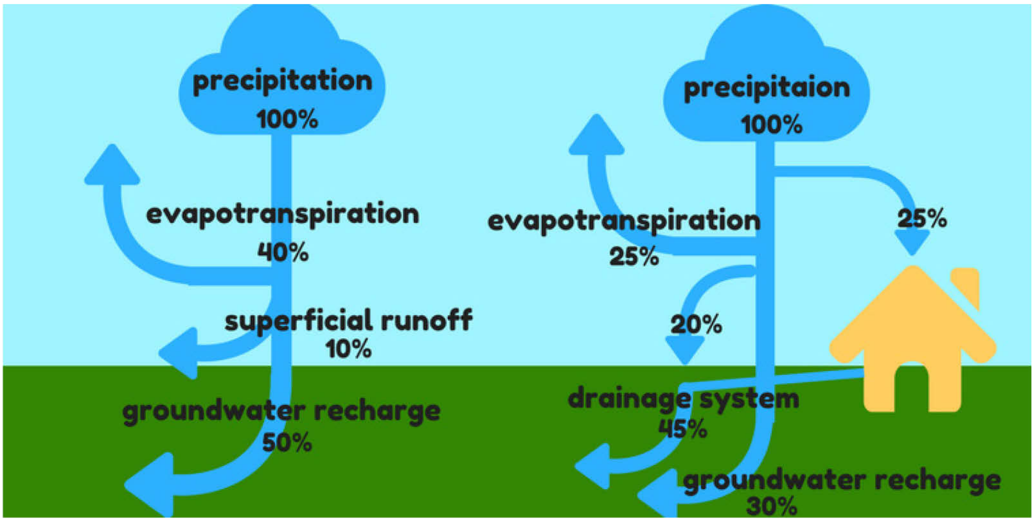

Figure 3 - Water balance example comparing a pre-development (left) with a post-development scenario (right). Adapted from (Becciu and Paoletti, [26]).

During an extreme rainfall event, i.e. events that produce relevant runoff, the evapotranspiration normally substrates 10% of the total volume of precipitation leaving 90% available for infiltration and superficial runoff. On a pre-development situation is typically observed a 25% superficial runoff and 65% infiltration for highly permeable natural catchments on low return period events (2-5 years), reaching 60% - 30% partition runoff/infiltration for low permeability and higher return periods events (50-100 years). Migrating towards to the post-development scenario there is an important reduction on soil infiltration due to impermeabilization and increasing on runoff volume, having a 50%-45% runoff/infiltration for low return period events and 85%-10% for high return periods (Becciu and Paoletti, [26]).

There is also increasing of flow velocity on street and sewer channels that result on increasing the peak flow during a rainfall event and a lower concentration time on the subcatchment. Therefore, soil sealing has a double impact increasing both runoff water volume and peak. On Figure 4 is possible to observe the increase on peak flow and runoff volume on the post-development situation on the generic example of a runoff hydrograph comparing the pre and post-development scenario (Woods Ballard, Wilson, [27]).

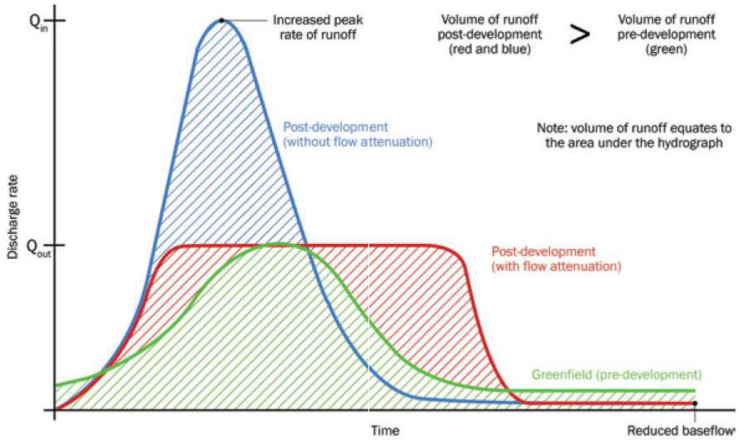

Figure 4 - Example of runoff hydrograph (Woods Ballard, Wilson, [27]).

Table 1 summons up the resulting impacts from imperviousness surfaces, for example the increased volume of runoff and peak flow that causes flooding that eventually leads to habitat loss, erosion, channel widening and streambed alteration on streams (Water, [28, (USEPA), [29]).

Table 1 – Impacts from increases on imperviousness surfaces. Adapted from ((USEPA), [29]).

	Resulting impacts				
Increased imperviousness leads to:	**Flooding**	**Habitat loss (e.g., inadequate substrate, loss of riparian areas, etc.)**	**Erosion**	**Channel widening**	**Streambed alteration**
Increased volume	●	●	●	●	●
Increased peak flow	●	●	●	●	●
Increased peak flow duration	●	●	●	●	●
Increased stream temperature	●(1)	●			
Decreased base flow		●			
Changes in sediment loadings	●	●	●	●	●

(1) Update impact according results found on (Kertesz and Sansalone, [30])

In the city of Milan the Seveso river registered 342 floods (i.e. 2,4 per year) from 1878 to 2018, but from 1976 the frequency registered was 2,6 per year with a total of 108 floods events. This can be a consequence of the urban area growth (Figure 2) (Becciu, Ghia, [7]).

1.3. Urbanization impacts on water chemistry

The term “urban diffuse pollution”, also known as non-point pollution, indicates a collective of pollutants that doesn’t originate from a single source but are products of land use and human activity in the urban area (Woods-Ballard, Kellagher, [11]). PM plays the role of a vector for the transport of these pollutants, such as heavy metals, organics and nutrients, and they end up being washed out by stormwater eventually reaching streams (Sansalone, Kuang, [31]); (McDowell-Boyer, Hunt, [32]) (Marchioni and Becciu, [9])). The chemical analysis of stormwater in comparison with wastewater showed a higher presence of heavy metals and comparable or higher values for BOD and COD (Table 2 and Table 3).

Table 2 – Annual constituent loadings (ton_m) in rainfall-runoff and wastewater from selected sites (National Water Quality Inventory: 1996 Report to United States Congress)

	Urban stormwater(1)	**Combined sewer system(2)**	**Industrial discharges(3)**
Zinc (Zn)	217,7	32,14	59,9
Lead (Pb)	59,9	2,5	14,2
Copper (Cu)	51,3	9,5	57,6
Nitrogen	13.607,0	5443,3	Not avaiable
Phosphorous	544,3	51,3	Not avaiable
BOD(4)	4309,0	635,0	Not avaiable

(1) Metropolitan Washington DC. Drainage area: 455 km2 (Anacostia watershed, Washington D.C.); annual precipitation = 980,4 mm/y; population within drainage area = 823.000 (current as of 1990); % impervious area = 22,5%.
(2) Blue Pains, Washington D.C.; waste stream includes combined sewer system and domestic sewer system; service population of 2,0 million (current as of 1990).
(3) Maryland e Virgina 1987 toxic release inventory.

A study held on Hamilton County (Ohio, United States) compared the stormwater runoff with wastewater flow considering an urban area of 5200 hectares (52 km^2) of roadways and a population of approximately 800.000 people generating domestic wastewater flows, finding an approximately equivalent annual load of total suspended solids (TSS) and chemical oxygen demand (COD) (Table 3, (Sansalone, Koran, [33])

Table 3 - Comparison of urban highway stormwater versus untreated municipal wastewater from Cincinnati, Ohio, on an annual basis (Sansalone, Hird, [6])

	Urban Stormwater Runoff (1)	Untreated Municipal Wastewater (2)
Flow	4,5 x 10^{10} L	7,72 x 10^{10} L
COD (mg/L)	350	500
TSS (mg/L)	200	220
Zn_T (µg/L)	4500	75
Pb_T (µg/L)	150	35
Cd_T (µg/L)	12	1

(1) Stormwater generated from 40 km2 interstate and arterial road pavement.
(2) Wastewater flowrates from service population of 800.000.

Anthropogenic activities, especially vehicular traffic, produce pollutants load that will accumulate on impervious surfaces (Table 4 and Table 5).

Table 4 - Sources of pollution from impermeable surfaces (Woods Ballard, Wilson, [27]).

Source	Typical pollutants
Atmospheric deposition	Phosphorous, nitrogen, sulphur, heavy metals(1), hydrocarbons, particulate matter
Traffic – exhausts	Hydrocarbons, MTBE (methyl tert-butlyl elther), cadmium, platinum, palladium, rhodium
Traffic – wear and corrosion	Particulate matter, heavy metals(1)
Leaks and spillages (eg from road vehicules)	Hydrocarbons, phosphates, heavy metals(1), glycols, alcohols
Litter/ animal faeces	Bacteria, viruses, phosphorous, nitrogen
Vegetation/ landscape maintenance	Phosphorous, nitrogen, herbicides, insecticides and fungicides
Soil erosion	Sediment, phosphorous, nitrogen, herbicides, insecticides and fungicides
De-icing activities	Grit, choride, sulphate, heavy metals(1), glycol, cyanide, phosphate
Cleaning activities	Sediment, phosphorous, nitrogen, detergents, hydrocarbons
Sewer misconnections	Bacteria, detergents, organic matter and textiles
Illegal disposal of chemicals and oil	Hydrocarbons, various chemicals

(1) Heavy metals include: lead, cadmium, copper, chromium nickel, zinc, mercury. Not all heavy metals are present in all cases.

On Table 5 is shown the pollutants loads resulting especifically from vehicular traffic found on highways. Sources like exhaust, automobile parts wear, lubricating, infrastructure parts will contribute with heavy metals and other pollutants.

Table 5 - Primary source of urban and highway stormwater pollutants **((USEPA), [34])**.

Constituent	Primary sources
Lead (Pb)	Leaded fuels (auto exhaust), tire wear, lubricating oil and grease, bearing wear, anti-caking agent used in deicing salt.
Zinc (Zn)	Vulcanized-rubber-tire wear (zinc-oxide filler material), galvanized steel, infrastructure, motor oil (stabilizing additive), grease.
Iron (Fe)	Auto-body rust, steel highway structures, moving engine parts.
Copper (Cu)	Metal plating, bearing and bushing wear, moving engine parts, brake-lining wear, fungicides and insecticides.
Cadmium (Cd)	Tire wear (filler material), insecticides, zinc-galvanized surfaces.
Chromium (Cr)	Metal plating, moving engine parts, brake-lining wear.
Nickel (Ni)	Diesel-fuel gasoline (exhaust) and lubricating oil, metal plating, bushing wear, brake-lining wear, asphalt paving.
Manganese (Mn)	Moving engine parts.
Bromide (Br^-)	Auto exhaust.
Cyanide (Cn^-)	Anti-cake compound (ferric, ferro-cyanide, etc.) used to keep deicing salt granular.
Chloride (Cl^-)	Deicing salts.
Sulphates ($SO4^-$)	Roadway beds, fuel, deicing salts.
Petroleum	Spills, leaks, or blow-by of motor lubricants, antifreeze and hydraulic fluids, asphalt surface leachate.
PCBs	Spraying of highway-o-ways, background atmospheric deposition, PCB catalyst in tires.
Rubber	Tire wear.
VSS	Tire wear, asphalt abrasion.
Asbestos	Clutch and brake lining wear.

1.4. Sustainable urban drainage systems

Runoff will occur regardless the existence of a suitable urban drainage system, therefore depending on the system's quality there will be benefits or harm for the population. The urban drainage system comprises two main subsystems, the initial drainage system, or micro drainage, and macro drainage systems, that are responsible for directing and controlling the stormwater runoff and modify the natural system for runoff retaining and containment. They aim is to dispel the runoff from its generation, just transferring the runoff from one point to another downstream basin ((BR), [35, (BR), [36]). Until the seventies the hygienist philosophy was adopted on urban water management where the water was considered a health hazard and should be promptly conveyed away from its source. After the seventies it was already observed the need to change approach and to manage water floods as also the necessity to promote water treatment working mainly on the impacts already established (Table 6).

Table 6 - Urban water management development stages (Tucci, [37]).

Period	Philosophy	Description
Until 1970	Hygienist	Water supply without water treatment, stormwater direct downstream through channels
1970 – 1990	Corrective	Water treatment, flood management through runoff quantity & quality control acting mostly on the impacts
After 1990	Sustainable	Land use management respecting hydraulic invariance concept, SuDS promoting especially infiltration and diffuse pollution control

The conventional approach, however, became impractical on the growing urbanization scenario and a sustainable point of view started to be prefer. The term sustainable can be defined as something causing little or no damage to the environment and therefore able to continue for a long time. In urban drainage management that can be achieved when stormwater is infiltrated or at least temporary retained on its source to avoid drainage system saturation and consequently floods. In the city of Milan, to solve the Seveso river floods would be necessary to build at least five storage tanks with an estimated costs of 130 million Euros punctuating the necessity to change approach (Becciu, Ghia, [7]). The philosophy behind these new measures is to maintain the condition of drainage after developing the closest possible to the natural pre-development introducing the hydraulic invariance concept. They are commonly referred as SuDS (Sustainable Drainage Systems) (Woods Ballard, Wilson, [27]), Stormwater BMPs (Best Management Practices) (Field and Tafuri, [10]) ((USEPA), [29])or LID (Low-Impact Development stormwater drainage systems) (Elliott and Trowsdale, [38]). The aim of these measures is to minimize the impacts of urbanization acting in quantity and quality of runoff and promote opportunities on amenities and biodiversity (Woods Ballard, Wilson, [27]).

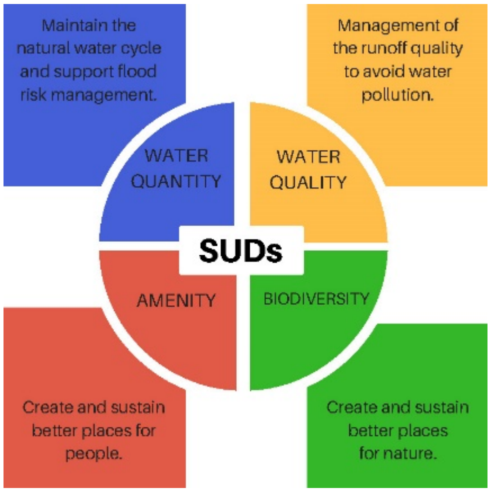

Figure 5 - Pillars of SuDS (Woods-Ballard, Kellagher, [11]).

SuDs will have six main functions: rainwater harvesting, pervious surfacing, infiltration, conveyance, storage and treatment (Woods Ballard, Wilson, [27]) (Table 7).

Table 7 - Functions of SuDS components (Woods Ballard, Wilson, [27]).

SuDS components	Description
Rainwater harvesting system	Components that capture rainwater and facilitate its use within the building environment.
Pervious surfacing systems	Structural surfaces that allow water to infiltrate reducing runoff such as permeable pavement and green roofs. May include subsurface storage.
Infiltration systems	Components that facilitate the infiltration of water on the ground, often include temporary storage zones to accommodate runoff volumes before slow release to the soil.
Conveyance systems	Components that convey flows to downstream storage systems, can also provide flow and volume control and treatment, e.g. swales.
Storage systems	Components that control the flows and, when possible, volumes of discharge released. May also provide further runoff treatment, e.g. ponds, wetlands and detention basin.
Treatment systems	Components that remove or facilitate the degradation of contaminants present in the runoff.

There are many types of SuDs available, such as permeable pavements, infiltration trenches, roofs reservoirs, detention reservoirs. They can be designed to attend one or more design criteria acting on runoff quantity (volume and peak flow), water quality, amenities and biodiversity (Table 8).

Table 8 - SuDS types and design criteria (Woods Ballard, Wilson, [27]).

SuDS type	Description	Design criteria						
			Water quantity					
				Runoff volume				
		Collection Mechanism	Peak flow	Small events	Large events	Water quality	Amenity	Biodiversity
Rainwater harvesting systems	Systems that collect runoff from roofs or paved surfaces	P		●	●	●		
Green roofs	Planted soil layers on the roof buildings	S	○	●		●	●	●
Infiltration systems	Systems that collect and store runoff allowing to infiltrate into the soil	P	●	●	●	●	●	●
Proprietary treatment systems	Subsurface structures design to provide runoff water treatment	P				●		
Filter strips	Grass strips that promote runoff water sedimentation and filtration	L		●		●	○	○
Filter drains	Shallow stone-filled trenches that provide attenuation, conveyance and treatment runoff	L	●	○		●	○	○
Swales	Vegetable channels used to convey and treat runoff	L	●	●	●	●	●	●
Bioretention systems	Shallow landscaped depressions that allow runoff to pond temporarily on the surface before filtering through vegetation and underlying soils	P	●	●	●	●	●	●
Trees	Trees within soil-filled tree pits, tree planters or structural soils used to collect, store and treat runoff	P	●	●		●	●	●
Permeable pavement	Structural paving through which runoff can soak and subsequently be stored in the subbase beneath and/or allowed to infiltrate into the ground below	S	●	●	●	●	○	○

SuDS type	Description	Design criteria						
			Water quantity					
				Runoff volume				
		Collection Mechanism	Peak flow	Small events	Large events	Water quality	Amenity	Biodiversity
Attenuation storage tanks	Large, below ground voided spaces to temporarily store runoff before infiltration, controlled release or use	P	●					
Detention basin	Vegetation depressions that store and treat runoff	P	●	●		●	●	●
Ponds and wetlands	Permanent pools of water used to facilitate runoff treatment where runoff can also be store in attenuation zone above the pool	P	●			●	●	●

Note: P – point, L – lateral, S – Surface, ● – likely valuable contribution to delivery of design criteria, ○ – some potential contribution to delivery of design criteria if specifically included on the design.

The ideal is combine different practices to be able to manage and treat runoff the most efficient way (Woods Ballard, Wilson, [27]). To select a particular practice it is necessary to considered urban factors, social, economic and environmental issues, including the drainage area, the infiltration capacity of the soil, groundwater level, land slope, area availability, presence sediments, among others ((BR), [35]). The West Great Western Park in Oxfordshire, United Kingdom is an example of project where different types and components where used in combination to reach design criteria and attend local regulations (Figure 6 and Figure 7) (Pyke, [39]). Permeable pavement was used on the local traffic roads with water outflow on conveyance ditches placed around the pavement. Runoff from the collector road goes to swales while rainfall collect on roofs goes to the detention pond.

Figure 6 – Combination of SuDS at the Great Western Park in Oxfordshire, United Kingdom designed by Allen Pyke Associates (Pyke, [39]).

Figure 7 - Great Western Park in Oxfordshire, United Kingdom showing different SuDS types (from left to right: permeable pavement, detention basin, swale).

On (Ahiablame, Engel, [40]) a model was used to predict the impact on runoff volume and quality by applying a sustainable drainage approach on a watershed level in two cities in Indiana (United States) and it was found that the implementation of a mix of rain barrels/cisterns and permeable pavement could lead to a 2-12% runoff reduction on watershed level. Although the results might appear small the authors point out that it cannot be considered irrelevant, especially considering the gain on water quality. (Gnecco and Palla, [41]) model the impact of using green roofs and permeable pavements to reduce impervious areas on a subcatchment on Genoa (Italy) achieving resilience by both peak and volume runoff in a 36% conversion scenario. On (Sansalone, Raje, [42]) it was model for a parking lot the response pre and post-development and after retrofitting using a linear infiltration reactor achieving a scenario similar with the pre-development (Figure 8). The surface runoff of 1,37 m pre-development increased for 6,39 m post-development but after the implementation of SuDs return to a similar surface runoff of initial conditions (1,36 m).

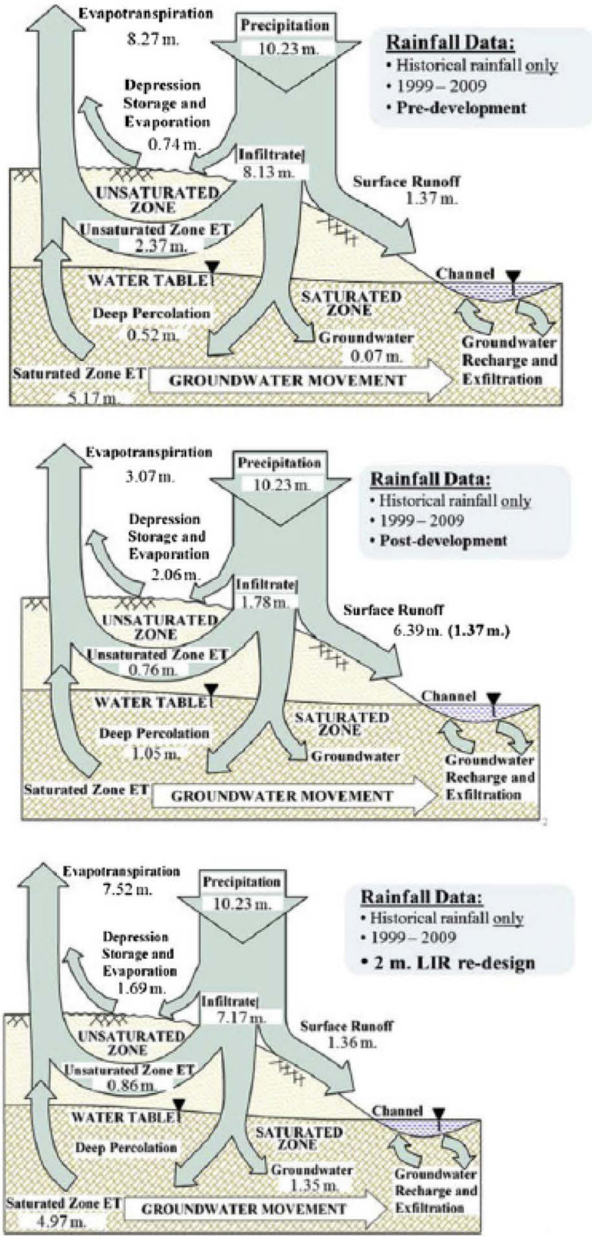

Figure 8 - Long-term hydrologic cycle components for pre, post-development and for retrofitting with SuDS (Sansalone, Raje, [42]).

1.5. Integrate water management regulations

The stormwater management guideline is an important tool for municipalities provide efficient water management. This guideline is support by the land use, environmental and water resources regulations and interfaces with urban planning, transportation, sanitation and solid waste guidelines. The management referred to general and local program management and the agencies involved (Figure 9).

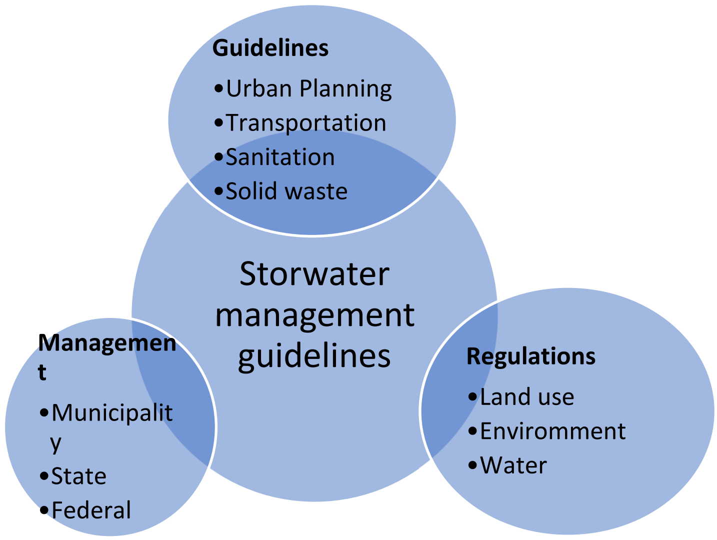

Figure 9 - Stormwater management guideline interfaces (Tucci, [37]).

Several water regulations mentioned the concept of hydraulic invariance. In Europe the European Union Water Framework Directive ((EU), [43]) encourages a holistic approach on water management and establishes water quality objectives and classification for surface water. In the United Kindgom this directive was transposed as legislation in 2003 (Kingdom, [44]). In United States the EPA Clean Water Act mention carrying grants and technical assistance to incentive the adoption of stormwater BMPs (Act, [45]). In Washington D.C., for example, there is a stormwater fee based on impervious area with a discount for whoever decide to adopt SuDs, referred there as green infrastructure ((US), [46, (US), [47, (US), [48]) ((US), [49]).

In Italy the hydraulic invariance concept is mentioned on a recent regulation from the Lombardia region demanding a maximum discharge on the sewer system of 10 l/s ha or 20 l/s.ha depending of the land use.

Stormwater municipality guidelines also referred to the hydraulic invariance concept and incentive the adoption on SuDS, some examples are the cities of Vancouver, Canada, North Carolina, United States, Sao Paulo and Porto Alegre, Brazil.

2. Permeable pavement

2.1. Definition and main aspects

Permeable pavements are defined as those having open spaces (joints or pores) in its structure where water and air can pass through and can be used for roads, parking lots, courtyards, among others. The surface receives directly traffic load and must also allow water to infiltrate promptly. There are various surfaces available, such as: precast concrete blocks, in placed porous concrete, porous asphalt, concrete grids, porous aggregates, grass, plastic grids, granular materials and loose decks (Ferguson, [50]). The ones that provide vehicular support are the concrete blocks, used on permeable interlocking concrete pavement, pervious concrete and porous asphalt. A more recent definition describes permeable pavement as having a surface with porous asphalt, pervious concrete or permeable interlocking concrete pavement and multiple permeable layers to store storm water until it infiltrates on subgrade soil or is collected by an underdrain (Weiss, Kayhanian, [51]). By allowing water infiltration permeable pavement ultimately result on reduction of surface water runoff volume while the porous structure function as a filter retaining part of the sediments and reducing the pollutants load.

On Figure 10 there is an example of a supermarket parking lot with permeable interlocking concrete pavement permeable pavement. More examples of permeable pavements are gathered on Appendix 1.

Figure 10 – Supermarket parking lot. Vipiteno (Italy).

Early studies on permeable pavements date from the seventies and were mostly conducted on laboratory, normally using simulation rainfall (Pratt, [52]). The first full-scale tests were held on the eighties such as (Smith, [16]) in the United States, using concrete grid pavements, (Hogland, Niemczynowicz, [53]) in Sweden with porous asphalt, (Fujita, [54]), (Suda, Yamanaka, [55]) in Japan, using pervious concrete blocks and on (Pratt, [56]) (United Kingdom) using concrete blocks with voids. Some of those parking lots continued to be monitored throughout the nineties (Pratt, [12, Pratt, Mantle, [57]) while similar researches were conducted in another locations, as shown on Table 9. Those studies mostly evaluated the efficiency of pavements on reducing runoff volume and pollutant removal testifying its effectiveness as SUDs.

Table 9 – Full scale tests using permeable pavement (adapted from (Marchioni and Becciu, [3]).

Country	City	Reference	Installed	Surface	Runoff		Others
					Volume	Pollutants load	
United States	Dayton	(Smith, [9])	1981	Grid	●		Temperature
Sweden	Lund	(Hogland, Niemczynowicz, [10])	-	PA	●	●	Clogging
United Kingdom	Nottingham	(Pratt, [11]) (Pratt, Mantle, [12]) (Pratt, [13])	1986	PICP	●	●	-
France	Rezè	(Legret, Colandini, [14]) (Legret and Colandini, [15])	1991(1)	PA		●	-
France	Nantes	(Pagotto, Legret, [16])	-	PA	●	●	-
Japan	Kuki	(Asaeda and Ca, [17])	-	PICP			Temperature
Germany	Stadtlohn Stukenbrock	(Dierkes, Kuhlmann, [18])	1987(1) 1996	PICP	● ●	●	Clogging
United States	Cincinnati	(Teng and Sansalone, [58]) (Sansalone and Teng, [59])	1996	PC	●	●	PER (partial exfiltration reactor)
Canada	Ontario	(Gerritts and James, [19])	-	PICP	●	●	-
United Kingdom	Edinburgh	(Schlüter and Jefferies, [20])	2000(1)	PICP	●	-	Modelling outflow
United Kingdom	New Castle	(Knapton, Cook, [21])	1999	PICP			Mechanical properties
United States	Renton	(Brattebo and Booth, [22])	1996		●	●	-
United States	Various	(Bean, Hunt, [23])	-	Grid, PICP, Grid, PICP	●	●	-
Brazil	Porto Alegre	(Acioli, [24]), (Jabur, [25]) (Pellizzari, [26])	2004	Grid	●		-
United States	Various	(Dreelin, Fowler, [27])	2006	Grid	●	●	-
Belgian	Various	(Beeldens and Herrier, [28])	2003	Grid, PICP	●		-
Canada	Calgary	(Van Duin, Brown, [29])	2005	PICP	●		Clogging
United Kingdom	NewCastle	(Knapton and McBride, [30])	2009	PICP			Mechanical properties
United States	North Carolina	(Collins, Hunt, [31])	1999	Grid, PICP, PA	●	●	-
Brazil	São Paulo	(Virgiliis, [32]), (Pinto, [33])	2008	PICP, PA	●		-
United States	New Jersey	(Borst, [34]) (Brown and Borst, [60])	2009	PICP, PA, PC	●	●	Temperature
New Zeland	Christchurch	(Morgenroth, Buchan, [35])	2007	PC			Soil contamination
United Kingdon	Central Scotland	(Newman, Aitken, [36])	2008	Macro-pervious system		●	-
Italy	Puglia	(Ranieri, Colonna, [61])	2010(1)	PA	●		Hydraulic conductivity measurements

Country	City	Reference	Installed	Surface	Runoff		Others
					Volume	Pollutants load	
Spain	Valencia	(Casal-Campos, Jefferies, [62]) (Perales-Momparler, Jefferies, [63])	2012	PC	●		
Spain	Santander	(Castro-Fresno, Andrés-Valeri, [64, Sañudo-Fontaneda, Andrés-Valeri, [65, Gomez-Ullate, Novo, [66]), (Sañudo-Fontaneda, Andres-Valeri, [67])	2006	PC, PA	●	●	Clogging
Italy	Calabria	(Brunetti, Šimůnek, [68, Carbone, Brunetti, [69])	2014	PICP	●		Hydrological modelling

(1) estimated year
Note: PICP: permeable interlocking concrete pavement, PA: porous asphalt, PC: pervious concrete

The practical information for permeable pavement, such as cross section, materials, design, is normally find on product association guidelines like INTERPAVE ((INTERPAVE), [70]), ICPI (Interlocking Concrete Pavement Institute) (Smith, [71]) ASSOBETON (Pilotti and Tomirotti, [72])for interlocking concrete pavement , NCMA (National Ready-Mix Concrete Association) (TENNIS et al, 2004) for porous concrete and NAPA (National Asphalt Pavement Association) (Hansen, [73]) for porous asphalt.

2.1.1.Effect on runoff quantity

The primary role of a permeable pavement is reduce runoff volume and promote hydrograph attenuation, and this feature was considered on the majority of initial researches. (Smith, [16]) monitored a parking lot with concrete grip pavers fill with grass that drained into a storm outlet recording the runoff for 11 storm events. Those events were compared to a simulated runoff from a similar impervious area. The grid lot coefficient of runoff ranged from 0.00 (zero) to 0.35 while the impervious lot was 1.00 for all events demonstrating the runoff reduction expected. The temperature was also monitored finding lower air temperature on the concrete grid pavement.

After the full scale tests held with porous asphalt by (Hogland, Niemczynowicz, [53]), due to observed difficulties on cleaning, (Pratt, [56]) tested concrete blocks for permeable interlocking concrete pavement on a full scale test held in Nottingham. The units had holes with 25 mm diameter filled with 5-10 mm gravel, the same used as bedding layer. The open graded base was constructed with four different stones (gravel, blast furnace slag, granite, limestone) and was separated of the bedding layer by a geotextile to prevent material loss. The site was undersealed by a plastic membrane to collect the pavement outflow. The period of discharge is delayed by many hours after the rainfall, while on an impermeable pavement usually by them all the runoff is discharged attesting hydrograph attenuation. In one event, after the rainfall, 42% (9mm) of a 21.6 rainfall was discharged on the permeable pavement. After a 30 days period it was observed a range of 55% to 75% runoff for the different bases. The same full scale test was addressed on (Pratt, Mantle, [57]) and shown a runoff average for 37% on gravel, 34% on blast furnace slag, 47% on granite and 45% on limestone, considering 62 rainfall events.

(Suda, Yamanaka, [55]) tested permeable interlocking concrete pavement with pervious concrete blocks. After testing various mix designs it was manufactured an experimental batch and the blocks were tested using rainfall simulation, finding out that on a 50 mm/h intensity rainfall the water infiltrated without runoff for the first 30 minutes. On a field test the water infiltration was visually confirmed although it was observed a reduction on permeability due to clogging after 6 months of use.

The type of surface can affect the pavement performance, for example (Acioli 2005) monitored for a year a parking lot in Porto Alegre, Brazil, finding out 5% of runoff on porous asphalt and 2,3% on concrete grids fill with grass.

On (Pagotto, Legret, [74]) a porous asphalt pavement was observed for a year them compared to a conventional asphalt pavement previous installed on the same site. In this case the porous asphalt was installed over an impervious surface, therefore could not be considered a fully permeable pavement. Comparing the results, the flow volume was actually higher on the porous asphalt, with 7825 m^3/ha versus 5840 m^3/ha on the conventional asphalt, and although the measurements were made on a one year gap it is possible to infer that the permeable base is essential to guarantee the reduction of runoff volume. On the other side, the response time mean, i.e., elapse time between the rain and the beginning of the flow, was higher on the porous asphalt (2:30 versus 1:15 on conventional asphalt) meaning that the system function on hydrograph attenuation. Besides the infiltration purposes, porous asphalt is often used for avoiding aquaplaning and water splashing, reducing the risk of accidents and also reducing noise.

Still regarding the base, (Acioli, [75]) noticed that during the entire monitoring time the storage capacity of the base reservoir never exceed 25%, meaning that the design method oversized the base thickness, which would be uneconomical. Also on (Pinto, [76]), that monitored a permeable pavement designed and constructed by (Virgiliis, [77]) in São Paulo, Brazil, the full capacity of the base reservoir wasn't reached, reassuring the importance of an accurate design method. The author enumerates the required information for designing a permeable pavement: existence of contribution area, precipitation data considering time of concentration and return period, base and surface material characteristics regarding porosity and permeability, subgrade slope and if the pavement promotes full, partial or no infiltration on the subgrade. None of the design methods analyzed on (Pinto, [76]) referred to all features. Also, (Pinto, [76]) highlights that problems during construction could have create early clogging, also stressing the importance to comprise construction good practices.

Besides the importance of the surface material and base material, the subgrade soil can also influence on the pavement's performance.,. In order to attested the feasibility also on clay soils, (Dreelin, Fowler, [78]) monitored for a year a pavement installed over this type of soil and it generated 93% less runoff than a reference conventional pavement. Also, in cases of low permeability subgrade the permeable pavement can include a drainage tube to outlet the water excess. (Bean, Hunt, [79]) registered lower infiltration rate on permeable pavements over clay soils when compared with sandy soils, likely due to surface clogging due to the presence of fine particles on the site.

The full scale tests above were built mostly for research, while (Beeldens and Herrier, [80]) monitored the runoff performance on existing pavements using a double ring infiltrometer. The approximately 50 sites up to 10 years of life use with permeable interlocking concrete pavement were located in Belgian and shown acceptable overall performance on surface infiltration and storage capability, highlighting the importance of the base thickness and the subgrade soil infiltration rate. That study can attests the feasibility of the systems on real case scenarios.

The full scale and fields tests provide reliability on the systems and a natural second step was to develop models on the system behavior providing tools for developers. Using the Erwin 3.0 rainfall-runoff model with adaptations ((USEPA), [81, Schlüter and Jefferies, [82]) modelled the outflow volume on an existing permeable pavement on Edinburgh (Scotland) achieving acceptable agreement for both peak flow and volume. On a review on models for sustainable drainage systems (Elliott and Trowsdale, [38]) found out 40 models and analyzed 10 that were available and with sufficient information. None of the models analyzed feature the full scope of the system and usually addressed planning preliminary design information. Therefore, although it is already available a range of models it still lacks on a broader tool that could easily help from planning to application of sustainable urban drainage systems. (Brunetti, Šimůnek, [68]) obtained satisfactory accuracy using a mechanistic model, HYDRUS-1D, to describe the hydraulic behavior of permeable pavement installed at the University of Calabria.

The United States Environmental Protection Agency's Storm Water Management Model (SWMM) can be used with this purpose of simulated the hydraulic response behavior in long-term applications for permeable pavements. Using this model (Qin, Li, [83]) investigate the impact of SUDs on a China development and (Sansalone, Raje, [42]) on a Florida development attesting the effectiveness of applying permeable pavement.

2.1.2.Effects on runoff pollutants load

Pollutants load removal is another important feature on permeable pavement. (Pratt, [56]) analyzed the short and long term variations in pollutants discharges, using four different stones as base to produce a range of quality discharges, i.e. pH and alkalinity could be reduced by using blast furnace slag, while reduction of hardness and lead discharge could be achieved by using limestone. However, in long term, the stone variations were small, meaning limited chemical degradation. Analyzing suspended solid variations, (Pratt, [56]) measured a range from near 0 (zero) to 50 mg/l while on an impermeable pavement it can fluctuated from 30 mg/l to 300 mg/l, with peaks of 1000 mg/l, hence the permeable pavement not only shown reduced concentration of suspended solids but also greater stability. On the same study the four type bases were subjected to a 10 years rainfall laboratory simulation and it was analyzed fine sediments, organic material and lead accumulation through the layers of the pavement. With small variations the larger part of the output sediments were trapped above the geotextile, on the gravel layer.

The pollutants removal was also addressed in a full-scale test held on Rezé, France by (Legret, Colandini, [84]) using a porous asphalt surface, porous bitumen stabilized base, crushed stones sub-base and a geotextile above the subgrade. After analyzing about 30 rainfall events and comparing with a nearby impermeable pavement, the permeable pavement showed a decrease about 64% for suspended solids and 79% on lead. After 4 years, the structure of the pavement was analyzed revealing that the micropollutants tend to accumulate on the pervious asphalt and the geotextile level, not being observed contamination on the soil. The same test was held on (Legret and Colandini, [85]) observing also a reduction on the following pollution contaminants – suspended solids, Pb, Cu, Cd and Zn – on the permeable pavement discharge. Samples extracted from the pavement structure and soil bellow shown that metal pollutants are mainly retained on the porous asphalt and the soil doesn’t present contamination after the 8 years that the permeable pavement was operational.

It has been then discussed the role of the geotextile on the pollutant removal on (Kirkpatrick, Campbell, [86]) where was achieved 93,1% removal of hydrocarbons without the use of geotextile. In fact, on (Dierkes, Kuhlmann, [87]) the tests conducted with porous concrete interlocking pavement found out that most of the heavy metals were trapped on the upper layer of the porous concrete blocks, conclusion find also on (Mullaney, Rikalainen, [88]) where up to 60% of the metals on a equivalent of 20 years of sediments where also trapped on the upper layers, with or without geotextile.

Instead of analyzing the water outflow, (Morgenroth, Buchan, [89]) tested the soil bellow 25 sites being no pavement, conventional pavement and permeable pavement and discovered alterations on soil physical and chemical characterizes that could impact vegetation. According to (Morgenroth, Buchan, [89]) permeable pavement can alter soil pH which affects soil solubility, reducing concentrations of Al, Fe and Mg while increasing Na concentration. The effect will depend upon the soil initial conditions.

Although the studies already mentioned focus on more traditional stormwater pollutants, the effect of microorganism must also be taken in account. For instance, fecal pollution can cause health risks by affecting water sources and economical loss by beaches closures (McCarthy, Hathaway, [90]). On (Tota-Maharaj and Scholz, [91]) the use of interlocking permeable pavement combined with titanium dioxide on laboratory experiment was able to completely remove from runoff Escherichia coli, total coliforms and faecal Streptococci through the photocatalytic reaction.

As from runoff volume, models were created to simulated the pollutants removal on SUDs. (Imteaz, Ahsan, [92]) analyzed the accuracy of the Model of Urban Stormwater Improvement Conceptualization (MUSIC) by comparing with field measurements. The work comprises bioretention systems, grass swale and permeable pavement. For both studied cases on permeable pavement the model overestimates the flow removal and consequently the pollutants removal, that in this case suspended solids, Total Phosphorus and Total Nitrogenous. Therefore, the author suggests that the model still needs adjustments and for better accuracy a physically based deterministic model should be developed. Also, the already mentioned EPA SWMM can be also used to model runoff quality (Kipkie, [93]), (Sansalone, Raje, [42]) (Qin, Li, [83]).

2.2. Cross section

The permeable pavement structure is composed by surface/wearing course, base, subbase, subgrade and, when necessary, drainage pipes for overflow (Ferguson, [50]) (Figure 11). The surface should allow water infiltration and resist traffic. The pavement base/subbase is similar to a conventional one, the main difference being the aggregates porosity, which must be such that allows the base to function as a reservoir (Smith, [94]). The high porosity results on less strength, for that reason permeable pavements are normally applied on areas with low volume traffic and with limited heavy vehicle loading (Hein, Swan, [95]).

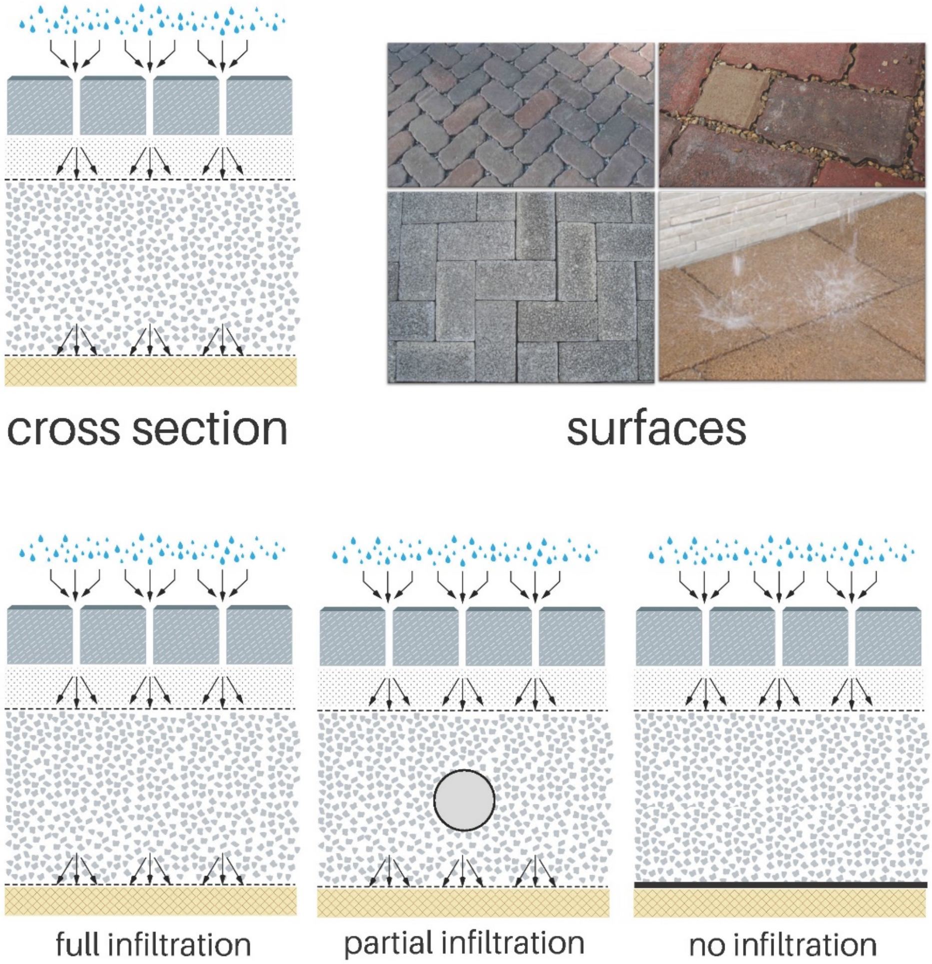

Figure 11 - Cross section, types of surface and infiltration types.

Permeable pavement goes against one of the main premises of paving by allowing water infiltration and retention. In a conventional paving project, the main purpose on drainage is to prevent the structure to become saturated or exposed to high levels of moisture for long periods of time; thereby it is essential to promptly remove all water that falls over the surface of the pavement (Suzuki, Azevedo, [96]). To avoid that water remains on the base enough time to cause pavement damage permeable pavement can present three infiltration profiles: full, partial or no infiltration. When the soil has enough permeability (10^{-6} to 10^{-3} m/s), i.e. sandy, gravel soils, it's possible to allow full stormwater infiltration on the subgrade. When the permeability is lower it's necessary to complement the system with and underdrain and in the cases with low hydraulic conductivity (10^{-10} to 10^{-8}), expansible soils, risk of contamination or high water table it's recommend to impermeabilized the subgrade and directed all stormwater with drainage tubes. The (Table 10) (BSI, [97]) gives an indication to choose type of infiltration profile.

Table 10 – Guidance on selection of infiltration profiles (BSI, [97]).

		Total infiltration	Partial infiltration	No infiltration
Permeability of subgrade defined by coefficient of permeability, K (m/s)	10^{-6} to 10^{-3}	●	●	●
	10^{-8} to 10^{-6}	x	●	●
	10^{-10} to 10^{-8}	x	x	●
Highest recorded water table within 1.000 mm of formation level		x	x	●
Pollutants present in subgrade		x	x	●

The recommended surfaces are pre-cast concrete blocks for interlocking concrete pavement, in placed pervious concrete and porous asphalt. Interlocking concrete pavement consists in solid units of concrete laid side by side to bear traffic loads (Ferguson, [50]). They can allow water to infiltrate through enlarges joints, open voids or, in case of pervious concrete, through it pores. The units are installed on a bedding layer of coarse aggregate, and, depending on the paving type, coarse joint material.

Pervious concrete consists of a highly permeable structure that allows water to infiltrate and evaporate going opposite of conventional concrete, where the air voids must be minimized (Sansalone, Kuang, [98]). That structure is achieved by removing the fine material of the mix design and using single sized aggregates. Numerous researches have been conducted on pervious concrete for features and test methods ((Batezini and JT, [99]),(Neithalath, Weiss, [100]), (Ranieri, Colonna, [61])), mix design methods (Zheng, Chen, [101]) and to improve properties ((Bonicelli, Crispino, [102, Bonicelli, Giustozzi, [103]) (Chen, Wang, [104]). Porous concrete, by nature, has lower mechanical strength than conventional concrete and therefore is important to find the right balance between voids and resistance to achieved good performance. Another feature that should be taken in account is raveling and clogging. Likewise, porous concrete, porous asphalt consists in one single size, no fines, aggregates that provide a high void structure that allows water to infiltrate. Polymer additives may be used to improved characteristics and allow use on heavier traffic (Knappenberger, Jayakaran, [105]).

A geotextile membrane can be used bellow the base to protect the soil and improve sediments retention.

2.3. Mechanical behavior

Independently of the surface, the structural and hydraulic behavior is highly dependent of the permeable base aspects. On (Pratt, [56]) and (Dierkes, Kuhlmann, [87]) it was evaluated various materials and porosities for permeable bases. (Knapton and McBride, [106]) conducted a full scale test on Newcastle using a device named Newcastle University Load Facility (NUROLF) that consisted on a truck powered by a 60 HP electric motor that simulated various combinations of speed, acceleration and braking with a maximum axle load of 14 t. This device was used on a permeable interlocking concrete pavement with an open graded base and it was concluded that the pavement would perform properly regarding to channeling when axle loads would not exceed 6000 kg. Surpassing that value would result on deformation, and would be necessary to use some stabilization to the open graded based. This work gave base to the design method on (BSI, [97]). On (Legret, Colandini, [84]) and (Knapton and McBride, [106]) it was also considered an open base stabilized with bitumen to improve structural performance.

Later studies have also evaluate the performance under heavy traffic (Knapton and McBride, [106]) (Jones, [107]). (Knapton and McBride, [106]) conducted full scale trials on permeable interlocking concrete pavement and four base sections being coarse graded aggregate, coarse graded aggregate stabilized with cement, dense bitumen Macadam and coarse graded aggregate reinforced with geogrid. The area was saturated with water to present the worst case scenario and them was trafficked by an eight wheel rigid truck loaded beyond its normal capacity. After 6000 cumulative standard axles the rut depths was 37 mm,10 mm, 6 mm and 32 mm for Tests 1 to 4, respectively. Considering 20 years of design life, the corresponding rut depths would be 30 mm, 7 mm, 5 mm and 27 mm for Tests 1 to 4 for respectively. Being 40 mm rut the failure criterion for flexible pavement with Load Category 3 accordingly the UK Classification, all pavements are considered suitable for Load Category 3 and Tests 2 and 3 are also suitable for Load Category 4.

On laboratory level (Jones, [107]) used a ME (Mechanical-Empirical) approach to develop permeable pavement designs also considering heavy traffic. The method consists basically on first characterize the materials on laboratory, use computer models to evaluate pavement performance, submit the best designs to empirical validation and calibration of failure mechanisms and performance through accelerated pavement testing and field test sections. The author obtained several preliminary design tables for both porous concrete and porous asphalt considering not only the mechanical properties but also the hydraulic properties.

2.4. Design

When designing the pavement is necessary to have two distinct approaches: mechanical design and hydrological design. Hydrological takes account of the infiltrate water volume and its outflow, while the mechanical consider the traffic loads and subgrade support taking account of the structural resistance of the pavement. The design will establish a structure thickness that attend both criteria.

The design process starts by defining site constraints, such as but not limit to: potential infiltration for contamination, presence of aquifer, distance of the water table; permitted water discharge from site, permitted runoff discharge from site, infiltration close to buildings and then is chosen the infiltration profile (Table 10).

The mechanical design starts by determine the structural support from the subgrade using the CBR (California bearing ratio) and the loading depending of the traffic, then the thickness of the surface layer, that will depend of the chosen type (PICP, PC, PA) and the total structure thickness using a conventional pavement design. There is not a design procedure adopted for all surfaces types, for porous asphalt NAPA recommend the use of the design method proposed by The American Association of State Highway and Transportation Officials (AASHTO) ((AASHTO), [108]) (Hansen, [109]), however (Hein, Swan, [95]) proposes an adaption for porous asphalt to account the lower resistance due to the higher porosity. On permeable concrete interlocking concrete pavement (Smith, [71]) proposes a method considering the permeable base.

On the hydraulic design the surface should allow high infiltration and then the design defines the base and subbase thickness to storage water considering the porosity. Common methods for storage volumes may be used, for example the curve number and the rational method (Weiss, Kayhanian, [51]). ICPI proposes a method considering the limit of storage time to avoid pavement damage (Smith, [71]).

(Beeldens and Herrier, [80]) suggests cross sections designs for different traffic ad soil conditions.

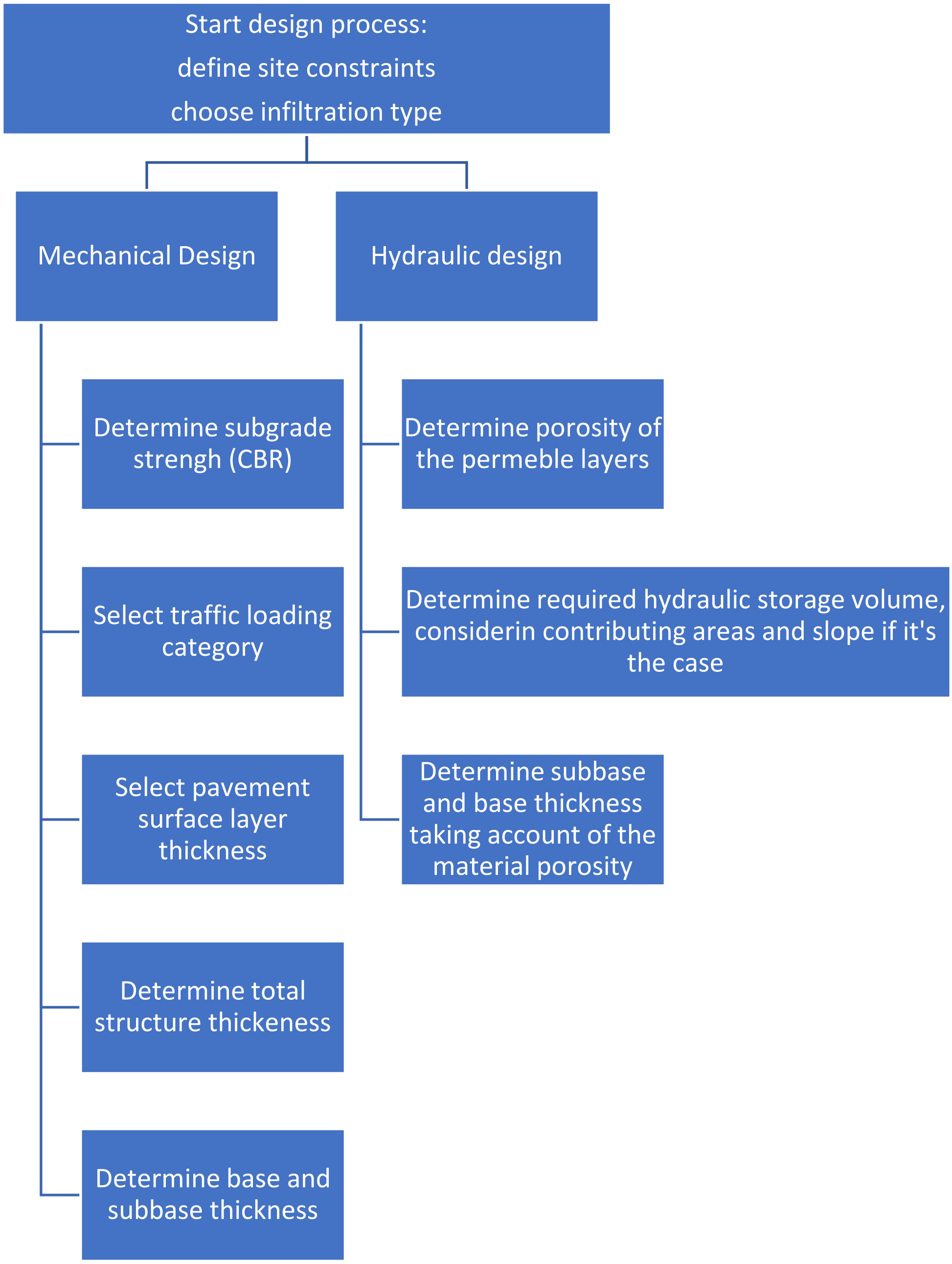

Figure 12 - Pervious pavement design flow (adapted from (Woods Ballard, Wilson, [27])).

2.5. Service life and maintenance

A traditional pavement normally has a design life from 10-20 years that will depend of the load, normally vehicular traffic. On permeable pavement there is the important effect of clogging caused by sediments deposited on the pavement (Brugin, Marchioni, [2]). After testing a number of pavements using a infiltrometer, (Borgwardt, [110]) concluded that after 20 years a permeable pavement could lost 80% of its initial infiltration rate. Considering that clogging would certainly happen it is importance to study the possibility of a simple and effectively maintenance. Performance evaluation methods and prediction modelling are necessary to program a maintenance routine. Truck sweeping, vacuuming and air jet are the most common maintenance methods. The frequency can vary to at least once a year or more, even 3 or 4 times a year depending on the pavement surroundings (Kia, Wong, [20]). This aspect of permeable pavement is further discussed on Item 3.3.

On Figure 13 there is an example of permeable interlocking concrete pavement permeable pavement completely clogged. There were reports that it was used a non-conformity material on the joints that blocked the water infiltration.

Figure 13 - Clogged permeable interlocking concrete pavement permeable pavement. Ibirapuera Park, São Paulo (Brazil).

2.6. Evaluation

Many of the studies mentioned conducted evaluation test methods, but for practical matters it becomes essential to have both an accurate and simple method to evaluate the permeable pavement performance especially regarding municipality acceptance. It’s possible to evaluate the infiltration through the infiltration rate, which indicates the rate that water infiltrates into the soil (de Sousa Pinto, [111]). Common in soil classification, a soil that shows an infiltration rate above 4.10 cm/s is considered having good permeability (ABNT, [112, Terzaghi, Peck, [113]). A permeable pavement, thus, should present a similar range in order to behave as a permeable soil (Marchioni and Silva, [114]). In Germany it is required that permeable pavements present an infiltration coefficient above 2.7 x10-5 m / s (Dierkes, Kuhlmann, [87]). However is important to notice that the infiltration coefficient is highly dependent of the test method, an aspect that is going to be further discussed (Ranieri, Colonna, [61]).

In soils, that rate can be directly determined by in place tests or using a constant head permeameter, and also via indirect means, as a variable head permeameter or by size distribution analyze (Terzaghi, Peck, [113]). (Bean, Hunt, [79]) adjusted a soil test method for permeable pavements and based on this study it was drafted the ASTM C1701 (ASTM, [115]). This method has been reviewed by (Smith, Earley, [116]) and (Li, Kayhanian, [117]), whom also analyzed the National Center for Asphalt Technology (NCAT) test method, similar with the ((CEN), [118]). They both attested the effectiveness of the ASTM C 1701 (ASTM 2009) (ASTM, [115]). The test method was successfully applied on field tests by (Borst, [119]) (Marchioni and Silva, [114]) (Jabur, [120]) (Sañudo-Fontaneda, Andres-Valeri, [67]) confirming its simple operation and accurate results. There is also available a similar test specifically for permeable interlocking concrete pavement ASTM C1781 / C1781M – 15.

Figure 14 - ASTM C 1781 test procedure (ABCP collection).

The CEN EN 12697-19 ((CEN), [121]) and CEN EN 12697-40 ((CEN), [118]) both mention permeability for bituminous porous mixtures, whereas the first propones a laboratory test using a constant head permeameter and the second an in situ test using a falling head permeameter. (Gibelli and Salzano, [23, Ranieri, Colonna, [61]) examined the EN BS EN 12697-40 ((CEN), [118]) and a number of tests.

For samples with high permeability is more accurate to use a constant head permeameter, however for simplification and especially on field tests the falling head permeameter is used more often. Comparing results with different permeameters it was noticed that the hydraulic conductivity obtained with constant head and falling head permeameter yield different results (Ranieri, Colonna, [61]).

Italian manufactures often refer to soil standards to measure permeability on permeable pavement on the lack of a specific standard.

2.7. Standards

Standards may address general aspects, product specifications and test methods, evaluation and design. In the European Committee for Standardization (CEN) there aren't specific standards for permeable pavement. In the British Standard Institution (BSI) however is available the "BS 7533-13:2009. Pavements constructed with clay, natural stone or concrete pavers. Guide for the design of permeable pavements constructed with concrete paving blocks and flags, natural stone slabs and setts and clay pavers" which was used as reference for the development of the ABNT (*Associacao Brasileira de Normas Técnicas*) NBR 16416. Besides the mechanical and hydraulic design criteria, the standard gives requirements for all pavement layers considering only the permeable interlocking concrete pavements.

The ASTM International (ASTM) has test method standards for pervious concrete and a test method for infiltration rate for pervious concrete and permeable concrete interlocking pavement. The European Committee for Standardization (CEN) and UNI (*Ente Italiano di Normazione*) have standards on porous asphalt specifications and test methods including infiltration (Table 11).

Table 11 - Standards mentioning permeable pavement.

Committee	Number	Description
CEN / UNI	EN 13108-7:2006	Bituminous mixtures - Material specifications - Part 7: Porous Asphalt
CEN / UNI	EN 12697-19:2012	Bituminous mixtures - Test methods for hot mix asphalt - Part 19: Permeability of specimen
CEN / UNI	EN 12697-40:2012	Bituminous mixtures - Test methods for hot mix asphalt - Part 40: In situ drainability
ASTM	C1688/C1688M-14a	Standard Test Method for Density and Void Content of Freshly Mixed Pervious Concrete
ASTM	C1754/C1754M-12	Standard Test Method for Density and Void Content of Hardened Pervious Concrete
ASTM	C1747/C1747M-13	Standard Test Method for Determining Potential Resistance to Degradation of Pervious Concrete by Impact and Abrasion
ASTM	C1701/C1701M-09	Standard Test Method for Infiltration Rate of In Place Pervious Concrete

ASTM	C1781 / C1781M - 15	Standard Test Method for Surface Infiltration Rate of Permeable Unit Pavement Systems
BSI	BS 7533-13:2009	Pavements constructed with clay, natural stone or concrete pavers. Guide for the design of permeable pavements constructed with concrete paving blocks and flags, natural stone slabs and setts and clay pavers
ABNT	NBR 16416	*Pavimentos permeáveis de concreto: requisitos e procedimentos*
NC	NLT-327 00	*Permeabilidad in sítu de pavimentos drenantes con el permeámetro LCS*

3. Runoff quantity

The runoff generates on a rainfall-runoff event depend of losses due to abstractions. The ultimately goal of permeable pavement is to reduce runoff acting mostly with infiltration and depression storage. In the case of porous surfaces, the pore structure will affect permeability and capability to infiltrate runoff. The pore structure also affects the pavement behavior on its service life due to clogging.

3.1. Rainfall-runoff transformation

Runoff is the flow of water on the surface of the earth and has its origin on precipitation. Flood runoff is a result from short-duration highly intensity rainfall, long-duration low-intensity rainfall. (Maidment, [122]). Only a part of the precipitation convert into superficial runoff because of the hydrological losses due to abstractions such as evapotranspiration, vegetable interception, depression storage and infiltration, where the last two are more quantitative relevant (Becciu and Paoletti, [26]). Abstractions are normally taken account by the means of runoff coefficient, being the ratio of the peak rate of direct runoff to the average intensity of the storm (Chow, Maidment, [25]). The runoff coefficient varies from 0.13-0.35 for lawns to 0.70-0.95 on downtown area (Maidment, [122]). This parameter is used on the rational method to calculated the peak flow and is difficult to estimated, being normally obtained through tables with suggested values (Maidment, [122]). The runoff coefficient gives only an indication because in reality the loss is not uniform during an event.

Permeable pavements are designed to reduce superficial runoff by acting on infiltration and depression storage. Laboratory and full scale tests had measured runoff coefficient with values as 0 – 0,45 considering various types of permeable pavement surfaces and period of observation (de Araújo, Tucci, [123]). A 10 years simulation using SWMM comparing a conventional pavement scenario and a permeable pavement could reduce runoff from 6,39 m to 1,36 m, regaining a runoff comparable with the pre-development scenario (Sansalone, Raje, [42]), (Figure 8).

Infiltration is the process of water penetrating from the ground surface into de soil. In the soil case the infiltration rate is influenced by soil surface conditions and its vegetative cover and the soil properties such as porosity and hydraulic conductivity and the current moisture content (Chow, Maidment, [25]). On permeable pavement the water infiltrates on the pavement surface, in the case of this research though the porous of pervious concrete or porous asphalt.

3.2. Flow through porous media

A porous material can be defined as a bound solid containing holes or voids, connected or non-connected dispersed within in a random or regular manner. A fluid can only flow through interconnected pores, named effective pore space, while all the total pores is named total pore space (Collins 1976).

The pore structure of permeable pavement porous surfaces consists on large interconnected voids with sizes ranging from 2 to 8 mm depending on the mix design, aggregates used and degreed of compaction (Kia, Wong, [20]).

Porosity (ϕ) can be defined as the fraction of the bulk density occupied by voids. Total or absolute porosity represented the fraction of the total void within the volume of the material while effective porosity considers only the fraction of pores that are interconnected. Effective porosity can be used as an indication of permeability (Collins, [124]). On porous surfaces for permeable pavement the porosity can be determined by direct methods as density methods (Tennis, Leming, [125]) (Montes, Valavala, [126]) ((CEN), [127]). XRT can be used to obtain effective porosity and other pore structure parameters otherwise difficult to obtain with traditional methods. Analyzing 21 pervious concrete specimens (Kuang, Ying, [128]) found out agreement between XRT and gravimetric methods. XRT results on total porosity, effective porosity, median diameter and tortuosity were nearly independent of image resolution (Kuang, Ying, [128]).

Consolidation and compaction influence porosity as observed on (Bonicelli, Crispino, [102]) while studying pervious concrete. On (Kia, Wong, [20]) it was notice that the porosity on porous concrete presents a stronger correlation with compressive strength than with permeability.

3.2.1.Permeability

Permeability is the property that characterizes the ease that which a fluid will flow through the material by an applied solid gradient, and is the hydraulic conductivity of the porous material when considering water as the fluid. It's a macroscopy property and has only significance when samples are sufficiently large to contain many pores (Collins, [124]). Permeability depends on pore structure, effective porosity, tortuosity, size distribution and shape of the pores and it can be affected by compaction and mechanical alterations of the structure (Kia, Wong, [20]) (Collins, [124]) (Kuang, Ying, [128]). The pore structure of the surface is critical to the permeability.

The coefficient of permeability (k) from Darcy's law (Equation 1) is often used to characterize the hydraulic conductivity under conditions of saturation, and non-turbulent flow and when volume and shape of pores remain independent of porewater pressure and time. It can be considered a measure of the ease with water flows through permeable materials and is used in permeable pavement evaluation.

$v = ki$ Equation 1

Where v is the discharge velocity, k is the hydraulic permeability and i is the hydraulic gradient. Discharge velocity can be defined as the quantity of water that percolates per unit of time across a unit area of section oriented normal to the flow lines (Terzaghi, Peck et al. 1996). Table 12 shows soils coefficient of permeability and drainage properties.

Table 12 - Permeability and drainage characteristics of soils (Terzaghi, Peck, [113]).

	Hydraulic conductivity k (m/s)											
	10^{0}	10^{-1}	10^{-2}	10^{-3}	10^{-4}	10^{-5}	10^{-6}	10^{-7}	10^{-8}	10^{-9}	10^{-10}	10^{-11}
Drainage	Good							Poor	Practically impervious			
Soil types	Clean gravel		Clean sands and gravel mixtures			Very fine sands, organic and inorganic silts, mixtures of sand silt and clay, glacial till, stratified clay deposits				"Impervious" soils, e.g., homogeneous clays below zone of weathering		
					"Impervious" soils modified by effects of vegetation and weathering							

Hydraulic conductivity can be measured with direct methods in laboratory, using falling head or constant head permeameters, or in situ, normally using infiltrometers that use the principle of the falling head permeameter (Ranieri, Colonna, [61]) (Terzaghi, Peck, [113]) (Collins, [124]). The falling head permeameter yields results that are qualitative and comparative instead of a quantitative permeability coefficient. It is preferable to use a constant head permeameter on laboratory that allows a better control of the flow (Ranieri, Colonna, [61]). The runoff coefficient can also be measured by indirect methods, analyzing the pore structure or the particle size distribution (Terzaghi, Peck, [113]).

The theory of Kozeny relates the pore structure with permeability by considering a porous media as a bundle of straight capillary tubes and then considering a solution using hydrodynamic equations for slow and steady flow. The equation was later modified to include the concept of tortuosity, considering that the tubes of flow are not straight (Collins, [124]). Using a modified Kozeny-Kovàv model (Equation 2) (Ranieri, Antonacci, [129]) compared measured and modeled hydraulic conductivity results.

$k_{sat} = \frac{1}{512}\frac{\gamma}{\eta}\emptyset_e D_e^2$ Equation 2

Where k_{sat} is saturated hydraulic conductivity coefficient, γ is the water specific weigh, η is the dynamic viscosity, Φe is the effective porosity and D_e is the characteristic diameter. Comparing the results of measured k_{sat} with modeled using different diameters D_e (D_5, D_{10}, D_{15}, D_{20}, D_{30}, D_{40}, D_{50} and D_{60}) found the best fit when using D_{30} (Ranieri, Antonacci, [129]). The k_{sat} measurement was held using a constant head permeameter.

Considering the difficult to estimate runoff coefficient the evaluation of permeable pavement is normally done through permeability related measurements, indicating such as the infiltration rate, which indicates the rate that water infiltrates into the soil (de Sousa Pinto, [111]). In soil classification, a soil that shows an infiltration rate above 10^{-6} m/s is considered having good permeability (Terzaghi, Peck, [113]) (Table 12). A permeable pavement should present a similar range during its lifespan in order to behave as a permeable soil (Marchioni and Silva, [114]).

Permeability measurement methods have been adapted for permeable pavement and are already mention in normative (ASTM, [115]), ((CEN), [118]), (ABNT, [112, (CEN), [121]). The (ASTM, [115]) the test method was applied on field tests with values ranging from 480 – 900 cm/h 1,9.10-5 – 8.9,10-6 (PA) 2.26-10^{-2} m/s (PICP new) (Borst, [119]) (Marchioni and Silva, [114, Jabur, [120]). (Brown and Borst, [60]) evaluated a parking lot in function since 2009 with pervious concrete, porous asphalt and permeable interlocking concrete pavement surfaces with the (ASTM, [115]) with values ranging from 2,0 cm/h to 147,0 cm/h observing a significantly difference between pavement surface types. On (Beeldens and Herrier, [80]) it was compared permeable interlocking concrete pavement sites using a double ring infiltrometer obtaining results ranging from 1,03.10^{-3} m/s – 7,6.10^{-5} m/s considering five different sites with different life use periods.

A guideline from FSGV (German Road and Transportation Research Association) requires that permeable pavements present an infiltration coefficient above 2,7 x10^{-5} m / s (Dierkes, Kuhlmann, [87]). The Brazilian standard (ABNT, [112]) requires a minimum value of 1.10^{-3} m/s for newly constructed permeable pavements and at least 80% of this value over its life use using a single ring falling head permeameter or a constant head permeameter for laboratory measurements. In U.S, porous asphalt mixtures should have, at least 100 mt/day of infiltration capacity when newly built (Andrés-Valeri, Marchioni, [1])

The ((CEN), [121]) and ((CEN), [118]) both mention permeability for bituminous porous mixtures, whereas the first proposes a laboratory test using a constant head permeameter and the second an in situ test using a falling head permeameter. A similar device to the *autostrade* falling head device, the LCS (Laboratorio de Caminos de Santander) permeameter have already been used to investigate the decaying of infiltration capacity on a parking lot with 5 years of heavy use obtaining results ranging from 0,26 – 0,79 cm/s for pervious concrete parking spaces and 0,18 – 0,30 cm/s for porous asphalt parking spaces finding statistically significantly difference between initial results and after five years but not significantly difference between materials (Sañudo-Fontaneda, Andrés-Valeri, [65]).

(Ranieri, Colonna, [61]) compared results between the field *autostrade* falling head permeameter and the laboratory constant head permeameter according the ((CEN), [121]) for a porous asphalt cored and molded specimens with porosity from 25% to 30% between results obtaining an average of 2,91.10-3 m/s for field test and 3,03.10-3 m/s for laboratory tests finding no correlation between results.

(Chandrappa and Biligiri, [130]) tested eighteen pervious concrete mixtures with porosities ranging from 15% - 37% with a laboratory falling head permeameter using different heads obtaining permeability from 0.076–3.5 cm/s observing that the permeability reduced as the head of water increase. (Ranieri, Colonna, [61]) affirmed that a head between Δh = 0,1 cm and Δh = 1,0 would reached a laminar flow regime during the test (Reynolds number bellow 10) and therefore approaches the Darcyan permeability coefficient. Runoff surface flow on urban pavement areas is very shallow and in fact a small head would be more representative of real case behavior, however in the case of test method the important is to maintain the same head to allow comparison between results (Chen, Geng, [131]).

(Batezini and JT, [99]) compared the results of three pervious concrete mix designs with twelve samples per mix using both laboratory falling head permeameter and constant head permeameter obtaining with the falling head permeameter average results from 0,57 – 0,70 m/s and for the constant head permeameter from 0,13 – 014 m/s where is possible to infer that permeability is strongly affect by test method.

The variability of permeability coefficient can be explained by the different ranges of hydraulic head (Δh) and degree of saturation. Same mix design cored on field or molded laboratory would yield different results due to compaction differences (Ranieri, Colonna, [61]).

Analyzing porous asphalt the permeable pore shows a good correlation with permeability, whereas total pore or air void shows a poor correlation with permeability (Tarefder and Ahmad, [132]).

3.3. Clogging

The clogging phenomena, i.e. the reduction of infiltration capacity due to sediments blocking pavement surface is the most discussed feature of permeable pavement and is direct connected with service life. Extensive research is held to understand this behavior, find solutions to regain infiltration capacity and model the phenomena to allow prediction.

Normally permeability measurement is used to asses clogging performing infiltration tests on field or laboratory using falling head or constant head permeameters. Reviewing several researches (Kia, Wong, [20]) found out permeabilities ranging from 0,003 to 3,3 cm/s, although it's important to notice that the results were not obtained with the same test method. Using the ASTM C1701 (ASTM, [115]) test method (Nichols and Lucke, [133]) found out permeabilities ranging from 134 to 13970 mm/h for three different locations of permeable interlocking concrete pavement. Analyzing pore structure through XRT tomography techniques can also be used to investigate clogging (Kayhanian, Anderson, [134]) (Teng and Sansalone, [58]) (Kuang, Ying, [128]) (Manahiloh, Muhunthan, [135]).

The first thing that can be related with clogging is pavement age, as noticed on (Borgwardt, [110]). Reviewing clogging research (Razzaghmanesh and Beecham, [136]) notice that permeabilities suffer an important reduction after two years of service life and without maintenance after 4 years permeability is below 1000 mm/h.

One of the earliest studies on permeable pavement, (Pratt, [56]) observed that the large part of sediments were trapped above the geotextile on the surface layer of the pavement. Other studies made the same observation (Yong, McCarthy, [137]) and (Kayhanian, Anderson, [134]).

The clogging material characteristics, especially particle size distribution, also influence on the clogging behavior as observed on several studies, where the coarser material normally is retain on the surface creating a "cake" or "schmutzdecke" while finer material tend to be trapped on the core of the specimen (Kia, Wong, [20]) (Sansalone, Kuang,

[98]) (Teng and Sansalone, [58]) (Hill and Beecham, [138]). (Kayhanian, Anderson, [134]) noticed that the particles less than 38 µm plays a significant role on pavement clogging. (Nichols and Lucke, [133]) observed that pavement with similar particle size distribution sediments showed different surface rates, therefore particle size distribution is not suitable as only parameter to infer clogging process.

The surface material will also influence on clogging. To confirm permeable pavement performance for municipality reasons (Bean, Hunt, [79]) analyzed the surface infiltration on 27 pavements sites with ages ranging from 6 months to 20 years, on initial conditions and after maintenance. For the tests it was applied an adaptation for a soil infiltration test, the double-ring infiltrometer. The average infiltration for permeable interlocking concrete pavement with enlarge joints was 8,0 cm/h and after maintenance it reached average of 2000 cm/h on sites without soil disturbance, while on the other case it reached average of 61 cm/h, punctuating the importance of the pavement adjacent. After 9 years of use (Jabur, [120]) conducted single-ring infiltrometer tests on the same pavement studied by (Acioli, [75]) in Porto Alegre, Brazil, finding out that the porous asphalt was almost fully clogged while the concrete grids was still fully function. A similar observation was done on (Sañudo-Fontaneda, Andres-Valeri, [67]) regarding a full scale experiment in Santander, Spain, where infiltration tests held after 10 years of operation without maintenance found the ICPI still functional while pervious concrete and porous asphalt were completely clogged.

On a full scale experiment in Calgary (Canada) (Van Duin, Brown, [139]) observed that after 10 months of use the porous asphalt was completely clogged, probably due to the use of winter sand and traffic loads and even maintenance using vacuum sweeping couldn't increase infiltration. On the other hand, the portion of the pavement with permeable interlocking concrete pavement showed improvement after maintenance by removing the clogged joint material. On this same study it was simulated on laboratory 20 years of runoff and winter sand over the pavement showing less clogging when compared with the field test, where the porous asphalt presented a better result than permeable interlocking concrete pavement, which can be explained by the lack of traffic. The author commented that modification on porous asphalt mix design could improve performance. On the USEPA headquarters parking lot on New Jersey after 5 years of use without maintenance the permeable interlocking concrete pavement and pervious concrete showed infiltration rates more than one order of magnitude largen than the porous asphalt when measured using the ASTM C1701 (ASTM, [115]) test method (Brown and Borst, [60]). Reviewing various researches (Razzaghmanesh and Beecham, [136]) observed largest infiltration rates on pervious concrete followed by permeable interlocking concrete pavement and then porous asphalt.

(Pratt, [56]) observed that after clogging the remedial works for permeable interlocking concrete pavement would consist on removing the bedding layers, while on porous asphalt it is necessary to reinstall the surface, concluding that this surface showed an advantage in maintenance routine. Also using a rainfall simulator (Gerritts and James, [140]) analyzed a parking lot an permeable interlocking concrete pavement with enlarge joints located on the University of Gelph, in Ontario, Canada measuring the infiltration rate initially and then after removing pre-determined layers of the joint material, showing considerable improvement.

On a field test conducted by (Dierkes, Kuhlmann, [87]) on a parking lot installed in 1996 the infiltration capacity was measured using a drip-infiltrometer before and after cleaning using a high pressure cleaner with direct vacuum suction. Before remedial works all points showed a infiltration capacity below 1mm/(s ha), therefore the pavement wouldn't be accepted by the demanded infiltration of 270 l/(s ha) accordingly to local law. After maintenance the infiltration capacity reached values between 1545 l/(s ha) and 5276 l/(s ha) therefore comprising legislation, attesting the suitability of cleaning method and reassuring the permeable pavement performance.

Table 13 brings the clogging mechanism, evidence of clogging rates and extends and rehabilitation mechanism for different permeable pavement surfaces:

Table 13 - Evidence of clogging on permeable pavements by surface type. Adapted from (Woods Ballard, Wilson, [27]).

Surface type	**Clogging mechanism**	**Evidence of likely clogging rates/extends**	**Rehabilitation mechanism**
Pervious asphalt	Dust and sediments trapped on the surface and core.	Clogging in the top 25 – 75 mm can occur rapidly without good design and maintenance where silt loads are significant. UK evidence show functional pavements after 8 years of use.	Rotating sweeper and jet wash use a surface layer with finer pores (i.e. smaller aggregates) and increasing aggregate size with depth.
Pervious concrete	Dust and sediments trapped on the surface and core.	Clogging in the top 25 – 75 mm can occur rapidly without good design and maintenance where silt loads are significant.	Rotating and oscillating truck sweeper. Use a surface layer with infer pores (i.e. smaller aggregates and increasing aggregate size with depth.
Permeable interlocking concrete pavement	Dust and sediments trapped between the joints and in the surface a core when used pervious concrete.	Penetration to 50 mm over six years, loss of 70% to 90% of initial infiltration rate over the first years and then rates maintain constant.	Brushing and suction sweeping on the surface, replacement of the top 20 mm of jointing material, weed removal programs.

To predict and reduce this process (Yong, McCarthy, [137]) analyze the physical mechanism of clogging, punctuating the need for further investigations and modeling of biological clogging both. (Yong, McCarthy, [137]) also affirm that the design has great relation with clogging comparing three surfaces being monolithic asphalt, monolithic aggregate and resign and interlocking concrete pavement. (Radfar and Rockaway, [141]) used artificial neural networks to model clogging progression to use as a prediction tool obtaining satisfactory results. A filtration mechanism model based on media and particle diameters was used on (Teng and Sansalone, [58]) and will be further discussed on Item 4.4.

4. Runoff pollutants load

Atmospheric dry deposition plays an important role in pollutants circulation and transportation in urban areas. Hetero-disperse dry deposition PM function as a vector for pollutants load transport into runoff. Pollutants from anthropogenic activities are removed from the atmosphere by settling on impervious surfaces accumulating until wash off by the rainfall-runoff event transferring the pollutant load to runoff (Ying and Sansalone, [142]). PM poses as a health risk, especially the finer fraction (<10 µm) ((USEPA), [143]). Vehicular traffic activities are a main source for dry deposition PM and can be correlated with indices such as average daily traffic (ADT), wind speed and direction and available surface load. Heavy metals (Cd, Cr, Cu Fe, Ni, Pb and Zn) are pollutants of main interest on dry deposition generates on paved roads (Item 1.3, Table 4 and Table 5). They can partition on the gradation of dry deposition PM or be dissolved (Sansalone, Ying, [144]). Research found out that most concentrations of metals are found on the finer gradations, but the coarser gradation contributes with the largest total metal mass (Ying and Sansalone, [142, Sansalone, Ying, [144, Sansalone and Ying, [145]) (Sansalone and Cristina, [21, Deletic and Orr, [146]). Permeable pavement can act as a filter reducing the pollutants load from runoff. The knowledge of particle size distribution of dry deposition PM is essential to design control strategies for separation.

4.1. Accumulation (build-up)

PM mass accumulation is a function of previous dry period expressed in days (PDD) or hours (PDH) (Ying and Sansalone, [142]), (Bolognesi, Maglionico, [147]) (Huber, Dickinson, [148]).

On (Ying and Sansalone, [142]) dry-deposition flux rates were modeled as first exponential function of previous dry hours (PHD) for PM and suspended, settleable (< ~25µ) and sediment fraction (> 75µm) for a paved area in Baton Rouge, Louisiana, United States.

The EPA SWMM code proposes an empirical exponential model for build-up accumulation according Equation 3 and 4 (Huber, Dickinson, [148]):

$M_a(t) = \frac{Accu}{Disp} \cdot \left(1 - e^{-Disp \cdot t_{se}}\right)$ Equation 3

$t_{se} = t_{sr} + \frac{1}{Disp} \cdot \ln\left(\frac{Accu}{Accu - Disp \cdot M_{ar}}\right)$ Equation 4

Where $M_a(t)$ is the accumulate mass on function of time [kg/ha], Accu is an accumulation coefficient rate express in [kg/(ha.d)], disp is the dispersion coefficient express in [d^{-1}] and t_{se} is the equivalent dry time expressed on days. The value of Accu is normally associated to land use (Table 14):

Table 14 - Accumulation rate (accu) in function of land use (Bolognesi, Maglionico, [147]).

Land use	Accu [kg/ (ha.d)
Highly occupied residential zone	10 – 25
Scarcely occupied residential zone	5 – 6
Commercial zone	15
Industrial zone	35

This rate can also vary with the surroundings characteristics, on (Chow, Yusop, [149]) it was observed similar rates for residential and commercial zones. The dispersion parameter is estimated on literature ranging from 0,08 to 0,4 d^{-1} and is normally used as calibration with experimental data (Bolognesi, Maglionico, [147]).

The equivalent dry time (Equation 4) considers a residual mass that remains on the watershed after a rainfall-runoff event and is calculated according Equation 3 where t_{sr} is the real previous dry period [days] and M_{ar} is the mass remained [kg].

4.2. Dry deposition PM characteristics

Dry deposition PM is a hetero-disperse non-uniform aggregate. The median diameter (d_{50}), where 50% of particles are finer by mass, for different studies ranges from 100 to 1100 µm (Table 15). The d_{50} obtained from runoff in (Zhang and Sansalone, [150]) and (Ying and Sansalone, [142]) was smaller than the obtained with dry deposition indicating that runoff did not deliver the coarser fraction (154 µm and 280 µm; 331 µm and 97 µm respectively). On (Deletic and Orr, [146]) it was used a wet method of sampling by washing and then vacuuming to avoid left behind the finer material. The average d_{50} and d_{10} on a year period was respectively 397 µm and 34 µm. The d_{50} varies also with the sample position where larger particles are found mainly on the road shoulders and present higher mobility on runoff.

Table 15 - Recorded on median diameter (D_{50}) of dry deposition.

Watershed / Country	Description	Type of surface	Sampling method	D_{50}	Reference
Abeerden, Scotland	One year average Salting period No salting period	Residential and commercial asphalt road	Washing and vacuuming	397 450 361	(Deletic and Orr, [146])
Bari, Italy	Cairoli Nov-2015 Cairoli Jan-2016 Dante Nov-2015 Dante Jan-2016	Residential asphalt road	Manual sweeping	111 236 268 158	(Ranieri, Berloco, [151])
	Napoli Mar-2014 Napoli Jan-2016	Commercial asphalt road		262 256	
	SanGiorgi Mar-2014			1455	

	SanGiorgi Jan-2016 Tatarella Mar-2014 Tatarella Jan-2016	Commercial porous asphalt road		216 351 449	
Taranto, Italy	Cannata Mar-2014 Cannata Dic-2015 Magna Grecia Mar-2014 Magna Grecia Dec-2015	Residential asphalt road		413 359 331 201	
	SS7 Mar-2014 SS7 Dec-2015	Industrial asphalt roadway		286 378	
New Orleans, United States	Jan-2001 to Apr-2004	Asphalt road	From runoff	216	(Sansalone, Ying, [144])
Baton Rouge, United States				633	
Little Rock, United States				248	
N. Little Rock United States				587	
Cincinnati, United States				425	
Gainesville, United States	Dry periods	Asphalt parking area	Manual sweeping and vacuuming	280	(Zhang and Sansalone, [150])
Baton Rouge, United States	17 dry deposition events from Jan-Jul-2014	Asphalt roadway	Samplers	304	(Ying and Sansalone, [142]) (Sansalone and Ying, [145])
Cincinnati, United States	West shoulder East shoulder Pavement	Asphalt roadway	Vacuuming	500(1) 600(1) 1100(1)	(Sansalone and Tribouillard, [152])

(1) D_{50} obtained graphically.

Dry deposition PM function as a vector and a source for pollutants load. Vehicular traffic plays an important role contributing pollutants especially heavy metals that settled on the road surface and during a rainfall-runoff event are transported into storm runoff. Metals can partition and distribute across PM gradation or remain dissolved (Sansalone and Cristina, [21]). Dry deposition PM finer fraction (< 75 μm) presents the highest heavy metals concentration however the highest heavy metal mass is present on the coarser fraction (> 75 µm) (Ying and Sansalone, [142, Sansalone, Ying, [144, Sansalone and Ying, [145]) (Sansalone and Cristina, [21, Deletic and Orr, [146]).

PM is a temporary repository for metals and can be physically separated through filtration acting on reducing their loads on runoff. A model linking metal mass and particle size distribution can be used to predict partitioning and then design a filter able to remove a given percentage of PM-bound metal mass based on the ability to remove a given PM size (Sansalone, Ying, [144]) (Sansalone and Cristina, [21]).

Other pollutants that are also present on stormwater can also partition on PM gradation, as nitrogen (N) and bacterial loadings (Zhang and Sansalone, [150, Dickenson and Sansalone, [153]). On (Zhang and Sansalone, [150]) analysis held on stormwater from a parking lot in Gainesville (United States) found out that dissolved N accounts for over 50% of on-site total nitrogen (TN) where on the particulate phase the suspended and sediment fractions showed higher N concentration (median value: 0.716 and 0.778 mg=L, respectively) than the settleable fraction (median value: 0.298 mg=L). Based on-site measures it was verified approximately a 7∶2∶1∶3 ratio of dissolved, suspended, settleable, and sediment fraction N.

(Dickenson and Sansalone, [153]) analyzed 25 rainfall-runoff events for bacterial loadings also in Gainesville (United States) where runoff exceeded the criteria of bacterial loadings and disinfection is needed to avoid health risk. Inactivation of PM-associated bacteria was effective for the suspended and settleable fractions in the applied hypochlorite doses (15,45 mg/L of HOCl), but that sediment PM associated coliforms are shielded by the host PM even at hypochlorite doses up to 45 mg/L.

4.3. Wash-off

Rainfall-runoff process promotes surface wash-off of the accumulated sediments during dry periods. The cumulative load on runoff is normally express as an exponential model with a peak concentration on the beginning on the rainfall event known as first flush, where the most part of the load would be washed off on the beginning of the event reaching an early peak (Woods Ballard, Wilson, [27]).This consideration motivates the inclusion of the first flush storage tanks that would retain the most polluted part of the runoff (Becciu and Paoletti, [26]).

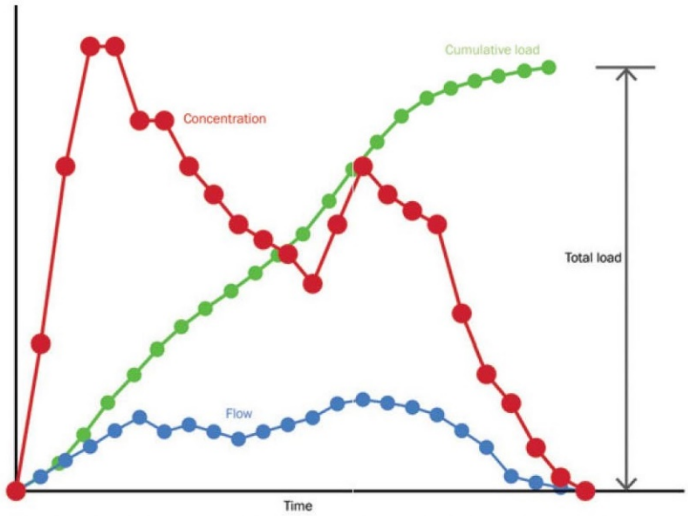

Figure 15 - Example of flow, pollutants load concentration and cumulative load during a rainfall-runoff event (Woods Ballard, Wilson, [27]).

However, analyzing pollutants load for rainfall-runoff events in Cincinnati (United States) (Sansalone, Koran, [33]) (Sansalone, Koran, [33]) observed a weak first flush event for low flow rate events . Also, the vehicular traffic occurring during the rainfall event will serve as a continues source (.

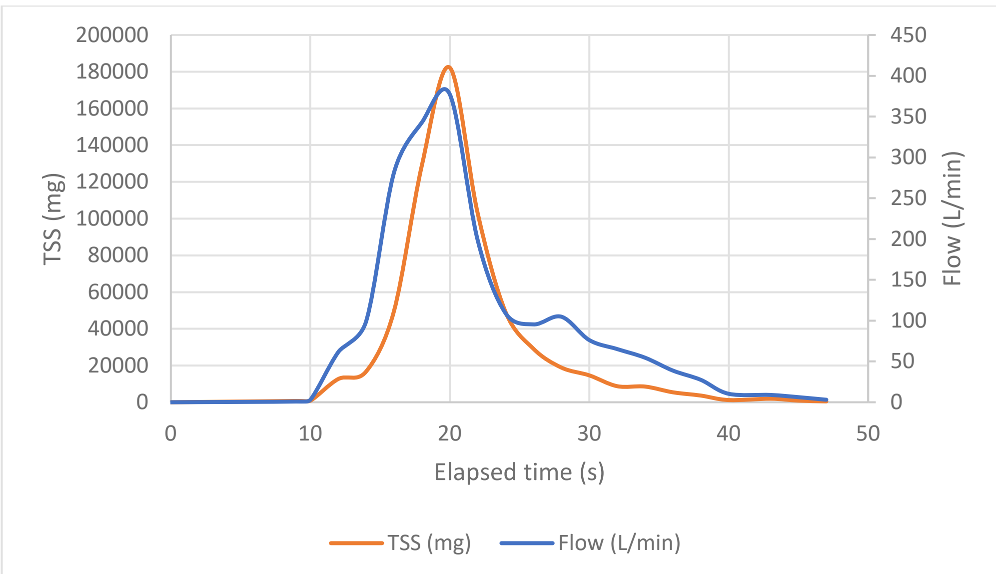

(a)

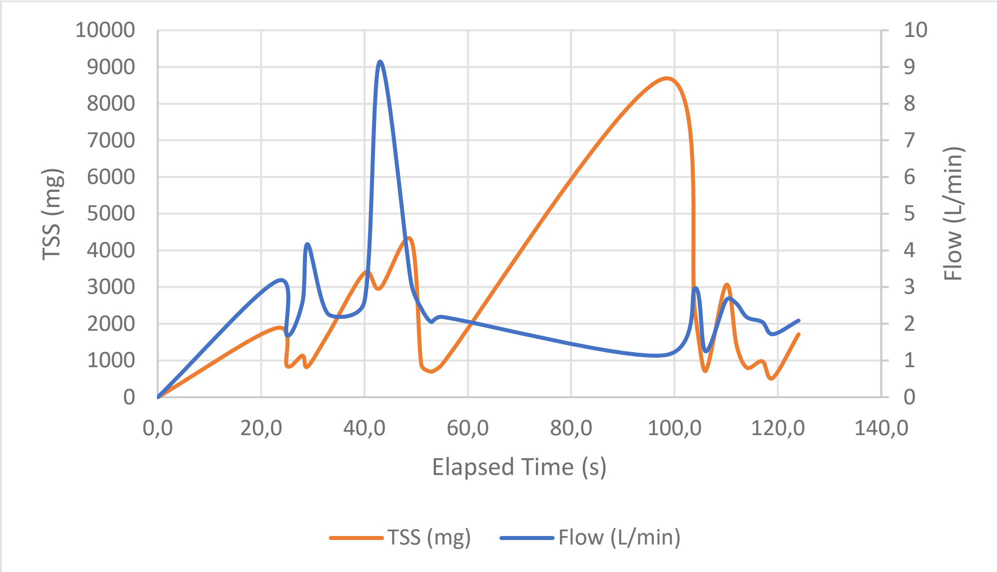

(b)

Figure 16 - Hydrograph and TSS mass for rainfall-runoff events measured on Cincinnati (United States). (a) – high intensity event measured on 08-08-1996; (b) – low intensity event measured on 25-11-1996 (Sansalone, Koran, [33])

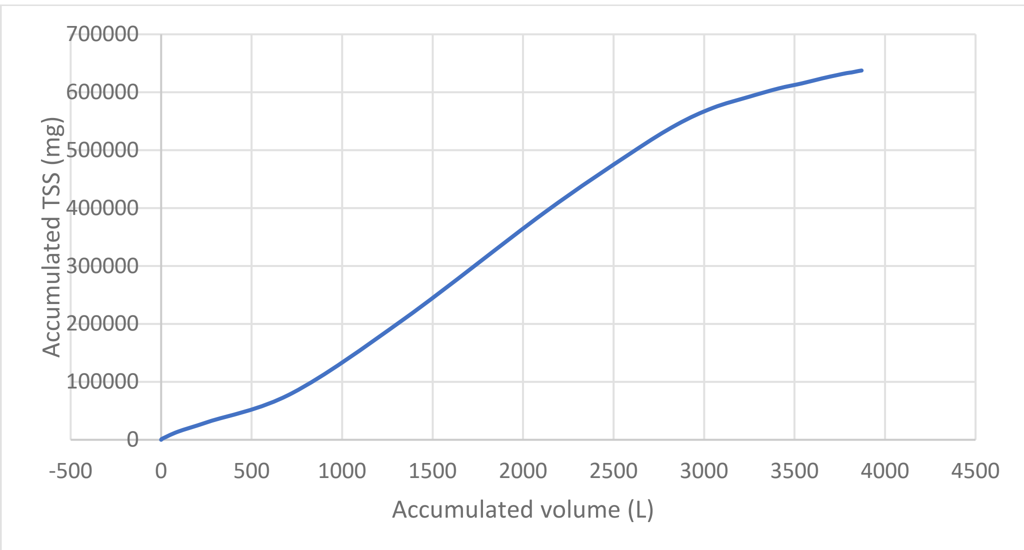

(a)

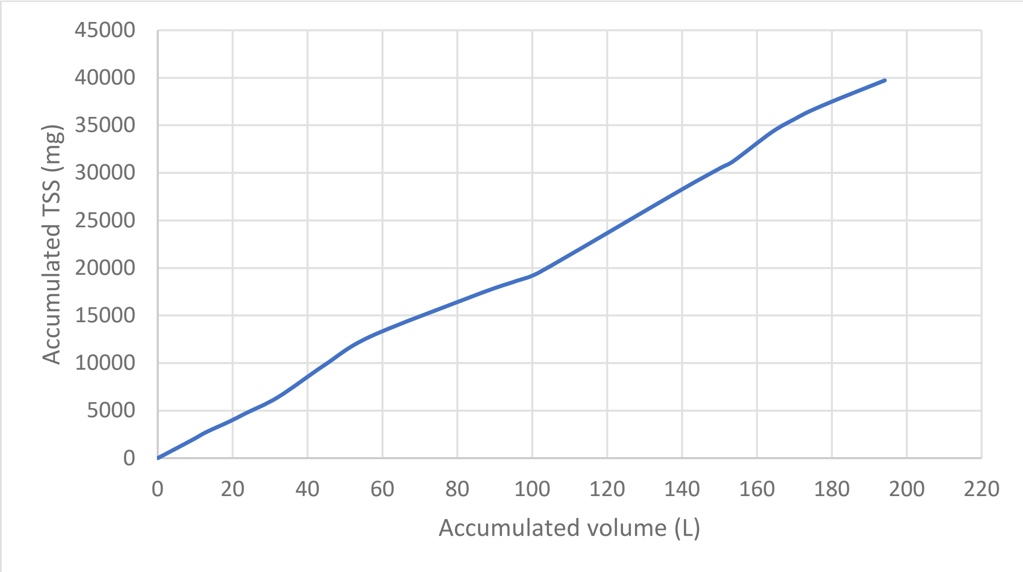

(b)

Figure 17 – Accumulated volume and accumulate TSS for rainfall-runoff events measured on Cincinnati (United States). (a) – high intensity event measured on 08-08-1996; (b) – low intensity event measured on 25-11-1996 (Sansalone, Koran, [33]).

4.4. Porous media filtration mechanisms

The pore average diameter (d_m) and particle diameter (d_p) are important parameters that govern the particle transport. Three main mechanisms of transport can be distinguished: surface (cake), straining filtration and physical-chemical filtration (Figure 18). When the particles are relatively larger as compared to the media the particles will not penetrate and will be retained on the surface, forming a "cake". That cake will increase in thickness over time and start behaving itself like a filter, reducing also the permeability of the media. That behavior is observed when $d_m/d_p < 10$ (McDowell-Boyer, Hunt, [32]).

The straining filtration, meaning the trapping of particles on pore throats that are too small to allow their passage, will likely happen on the narrow range of $10 < d_m/d_p < 20$ and plays an important role in pollutants removal (Auset and Keller, [154]) (McDowell-Boyer, Hunt, [32]). Smaller particles can only be removed by physical-chemical filtration mechanisms, normally when $d_m/d_p > 20$. In this case the mechanism will depend basically on the particle diameter, whereas particles with $d_p > 5$ µm will be under the effect of gravitational sedimentation and with $d_p < 5$ µm by the effect of Brownian motion. These mechanisms are also identified in pervious pavements (Teng and Sansalone, [58]).

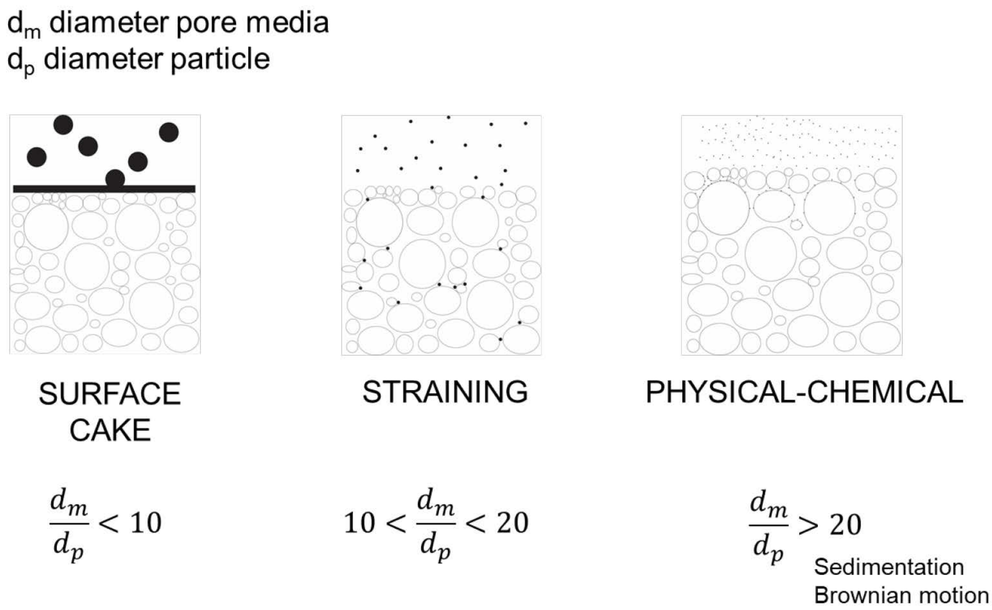

Figure 18 - Filtration mechanism on porous media.

5. Experimental plan

The experimental plan covers the two main aspects on permeable pavement: runoff quantity and pollutants load. Pervious concrete and porous asphalt specimens were produced using a mix design proposed on a previous research held on Politecnico di Milano (Bonicelli, Crispino, [102]) (Bonicelli, Giustozzi, [103]). A rainfall simulator was developed to measured runoff volume and sediments load. After the rainfall simulation tests samples of the asphalt specimens were analyzed using XRT to obtain pore structure data. Dry deposition PM was collect on four roads on Milan (Italy) obtaining the build-up accumulation rate and granulometric indices. The laboratory and field data was used to model permeability using Kozeny- Kovàcs and the filtration mechanism using a mechanistic model.

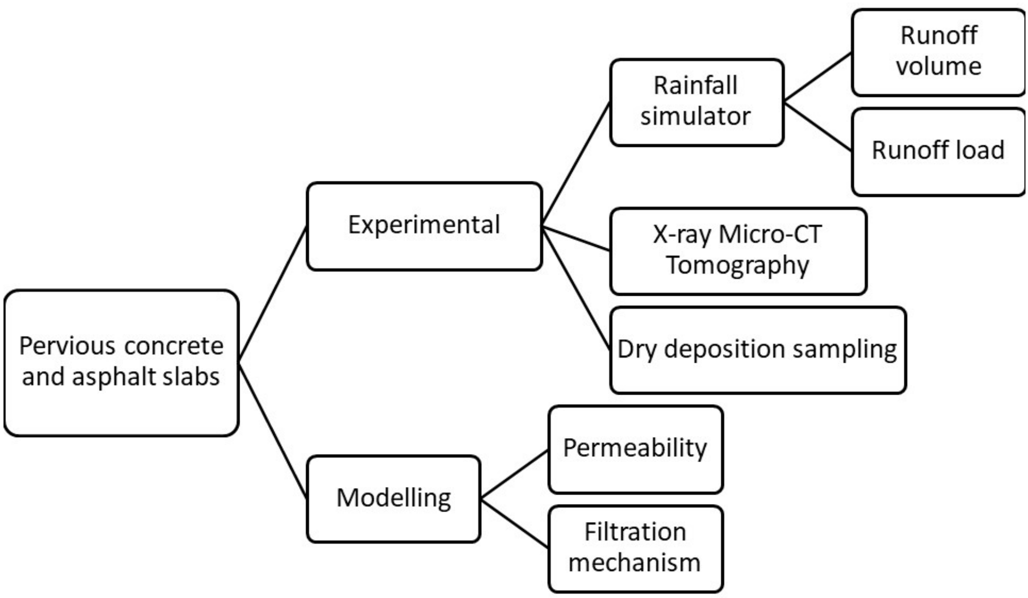

Figure 19 - Experimental plan.

5.1. Porous asphalt

It was produced nine samples of porous asphalt with 50 x 26 x 5 cm of dimension and 15%, 20% and 25% porosities. There porosities were achieved using bulk density data from (Bonicelli, Giustozzi, [103]). The porous asphalt mixture contained 4.1% by weight of mixture of SBS (Styrene-Butadiene-Styrene) modified bitumen and a mix of 80%/20% of limestone and basaltic aggregate, respectively, with particle size distribution according Figure 20. The samples were compacted with the help of a roller compactor.

5.2. Pervious concrete

Nine pervious concrete samples were produced with 50 x 26 x 5 cm of dimension and 15%, 20% and 25% porosity. There porosities were achieved using bulk density data from (Bonicelli, Giustozzi, [103]).The concrete mix design was obtained according to a previous study from (Bonicelli, Giustozzi, [103]). The mix design contained a 2-12 mm limestone coarse aggregate, and 5% by weight of finer aggregates of quarry sand and particle size distribution according Figure 20. It was used a type II CEM II 42.5R A-LL Portland cement with limestone addition with a water to cement ratio (w/c) of 0.27 and a cement to aggregate ratio (c/a) of 0.2. Three different admixtures were used: high range water reducer, air-entraining admixture and viscosity-modifying admixture with the dosages recommended by the manufacturers. The samples were manually compacted with the help of a Marshall test device.

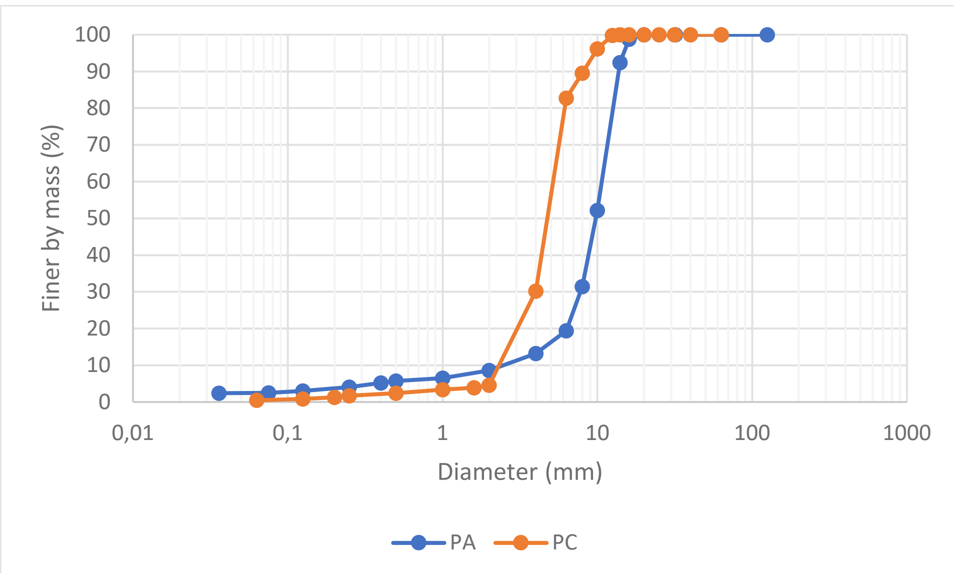

Figure 20 – Pervious concrete (PC) and porous asphalt (PA) aggregates particle size distribution.

5.3. Rainfall simulator

A rainfall simulator was designed and constructed to investigate the behavior over the porous surfaces under clogged conditions. The device consisted on a 3 m high steel structure with 30 droppers placed on top. The samples were placed 60 cm over the ground and in between the droppers and the samples were placed framed nets to distribute the raindrops. The droppers were feed by a plastic tube connected to a flow meter with 2-30 l/h capacity. The rainfall simulator allows to simulate rainfall intensities from 25 mm/h to 200 mm/h by adjusting the flow meter. The flour pellet method was used to measure the drop distribution and assure they respect the dimension of natural rainfall drops (Hudson and Rhodesia, [155]). The simulator allowed to collect infiltrate and superficial runoff.

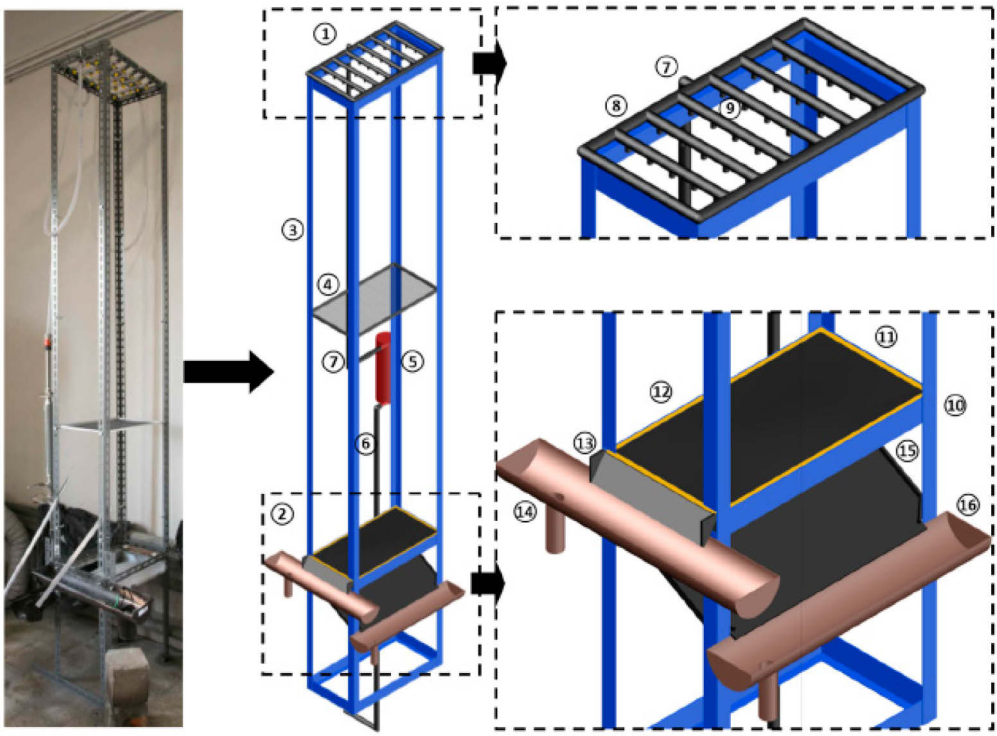

Figure 21 - Rainfall simulation. 1: dripper device; 2: testing area; 3: support structure; 4: framed net; 5: flowmeter; 6: flowmeter inlet pipe; 7: flowmeter outlet pipe; 8: flexible pipes; 9: drippers; 10: specimen support; 11: specimen; 12: waterproofing; 13: runoff conveyance ramp; 14: runoff collecting pipe; 15: infiltrated water conveyance ramp; 16: infiltrate water collecting pipe. Adapted from (Andrés-Valeri, Marchioni, [1]).

5.3.1.Sediment loadings

To proceed the tests with the rainfall simulation it was used a reference sediment assembled using quarry sand and recovery filler with a particle size distribution with maximum density according to particle size packing theories (Figure 22). This particle size distribution was them compare to dry deposition ones obtained on literature (Deletic and Orr, [146]) (Zafra, Temprano, [156]) (Bian and Zhu, [157]) to guarantee that fall within their limits.

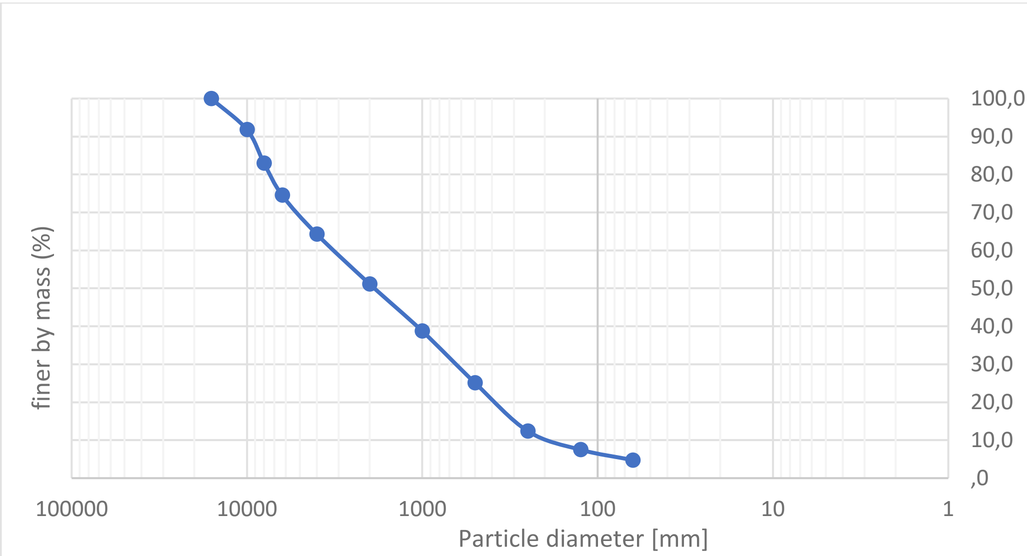

Figure 22 - Particle size distribution of sediments used on the rainfall simulation tests. D_{50} of 1906 µm.

5.3.2.Rainfall simulation test plan

Using the rainfall simulator, the 18 samples of pervious concrete and porous asphalt were tested applying an aerial loading of sediments of 0.5 kg/m^2, 1.0 kg/m^2 and 2.0 kg/m^2 and rainfall intensity of 50 mm/h, 100 mm/h,150 mm/h with 15 minutes duration and in a total of 162 tests. They were then submitted on a cleaning process using pressure water and air after being completely soaked on water for 24 hours. Then, on a second round of tests, it was applied an aerial loading of sediments of 0.5 kg/m^2, 2.0 kg/m^2, rainfall intensity of 100 mm/h with 30 minutes of duration, 150 mm/h with 15 minutes duration, and a variation of slope of 2.5% and 7,0% totalizing more 144 tests for an overall total of 306 tests. The flow chart with the tests in on Appendix 2.

Each test consisted in placing the sample on the rainfall simulator, manually adding the load of sediment over the sample compacting them by a steel roller and starting the chosen rainfall intensity. After the set time the rainfall stopped, the runoff mass was then collected on a small container and the discharge time was measured with the falling head permeameter.

5.3.3. Runoff coefficient

The runoff coefficient was obtained by the ratio of collect runoff water mass and the total rainfall mass.

5.3.4. Permeability

The permeability was measured using a falling head permeameter according to ((CEN), [118]). The test consisted on registering the discharge time, i.e., the time the falling water column falls 20 cm. When the discharge time reached 300 s the sample was considered fully clogged and the test stopped. All tests were conducted on three points of the samples. This type of in situ permeameter doesn't guarantee saturation and vertical flow on the material sample therefore do not yield the darcyan coefficient of permeability. The ((CEN), [118]) proposed the determination of a hydraulic conductivity (HC) according Equation 5:

$HC = \frac{1}{(t-r)}$ Equation 5

Where t is the discharge time (s) and r is the free discharge time, i.e. without a sample (s).

To obtain a reference of coefficient of permeability (k) it was used the Equation 6 for falling head permeameters (Neithalath, Weiss, [100]) (ABNT, [112]).

$k = \frac{A_1 l}{A_2 \mathrm{t}} log\left(\frac{h_2}{h_1}\right)$ Equation 6

Where A_1 and A_2 are the areas of the cross-section of the sample and the tube, l is the length of the sample, t is the discharge time, h_1 is the initial head and h_2 the final head.

5.3.5. Statistical methods

The obtained data was statistically analyzed to assess the influence of the parameters considered (porosity, aerial loadings, rainfall intensity, slope, cleaning methods, material) on the discharge time and runoff coefficient on a statistically significantly matter. Non-parametric tests were used considering the small samples sizes (less the 30) (Kottegoda and Rosso, [158]). Kruskal-Wallis were used for group analysis with a significance level of α = 0,01, Wilcoxon signed-rank test for two-sample paired observations with the exception for the case where the sample size is not equal and then it was used the Mann-Whitney U-test, both with a significance level of α = 0,05.

For correlation test it was used the Spearman coefficient for non-parametric correlation and calculated the p-values for testing the hypothesis of no correlation against the alternative that there is a nonzero correlation. The following guide was used to classified the strength of correlation: 00-0,19 “very weak”; 0,20-0,39 “weak”; 0,40-0,59 “moderate” ; 0,60-0,79 “strong” ; 0,80-1,0 “very strong”. All statistical tests were held using Matlab R2016a.

5.4. Pore structure

Three porous asphalt samples were scanned using the XRT NSI X25 system (NSI Inc., Rogers, MN, USA) available at Politecnico di Milano, equipped with a Dexela detector with 75 µm pixel pitch allowing for the acquisition of 1536 x 1944 pixel radiographies at full-binning with 16 bit encoding with a pore resolution of 61µm. The X-ray beam was set to 110 kVp and 48 µA, and a frame-rate of 6.6 Hz was adopted together with a 13 frame-averaging (to reduce noise), leading to 1800 angular projections. From the cone-beam geometry, the estimated voxel size resulted 61.88 µm with a zoom-factor equal to 1.21. 3D tomo-reconstruction was performed using a modified Feldkamp algorithm in the version provided by efX-CT commercial software (NSI Inc.). Approximately 2.5 hours were required on a Work STation HP Z820 with 8 CPUs INTEL XEON(R) E52630 @2.6 GHz, and NVIDIA GPU GeFOrce GTX 80 Ti. On Figure 24 is shown a slice imagine of a porous asphalt specimen and Figure 25 the 3D reconstruction of the specimen.

The approximately 800 slices obtained per slice (with 8 Gbyte storage) were processed using a code developed on Matlab R2016a. The images were first converted to binary (black and white), where the solid pixels would represent the pores (white color) (Figure 23).

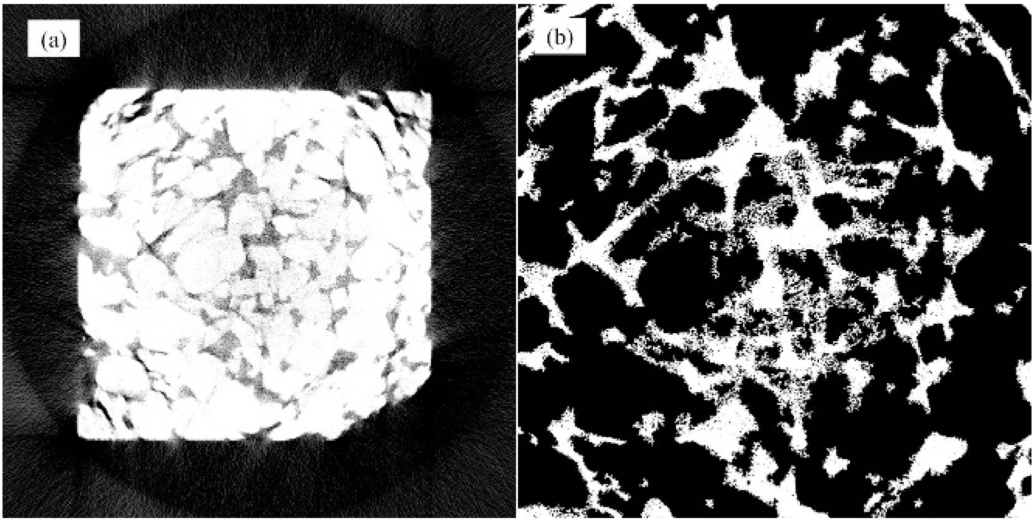

Figure 23 - (a) Original image acquired on the X-RAY μCT and (b) binary image used on the analysis.

The identification of the pores consisted in identifying a solid pixel *p* and use a flood-fill algorithm to label all the pixels connected to *p*. Each group of connections represented a pore.

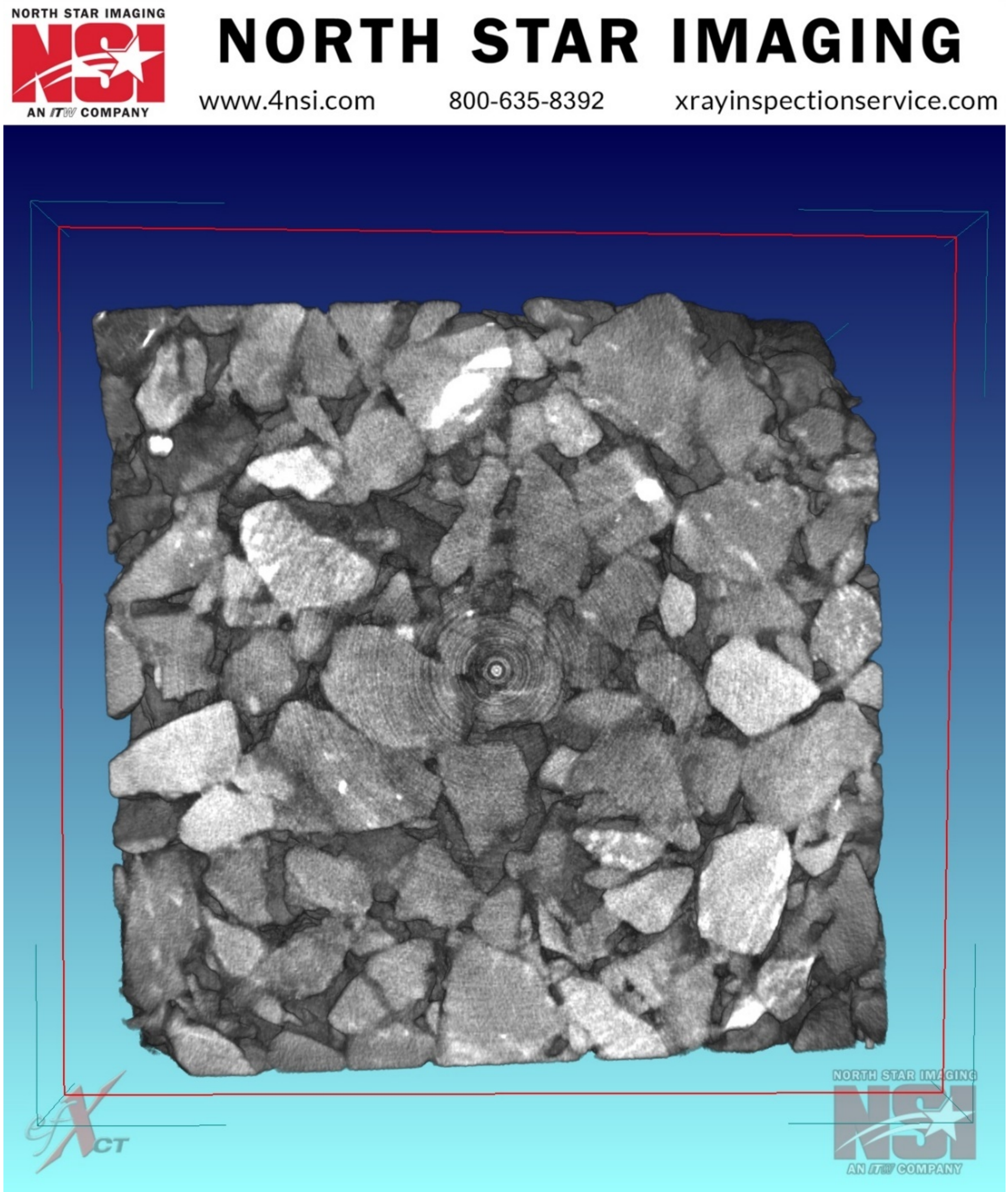

Figure 24 - Slice image of porous asphalt specimen obtained through XRT.

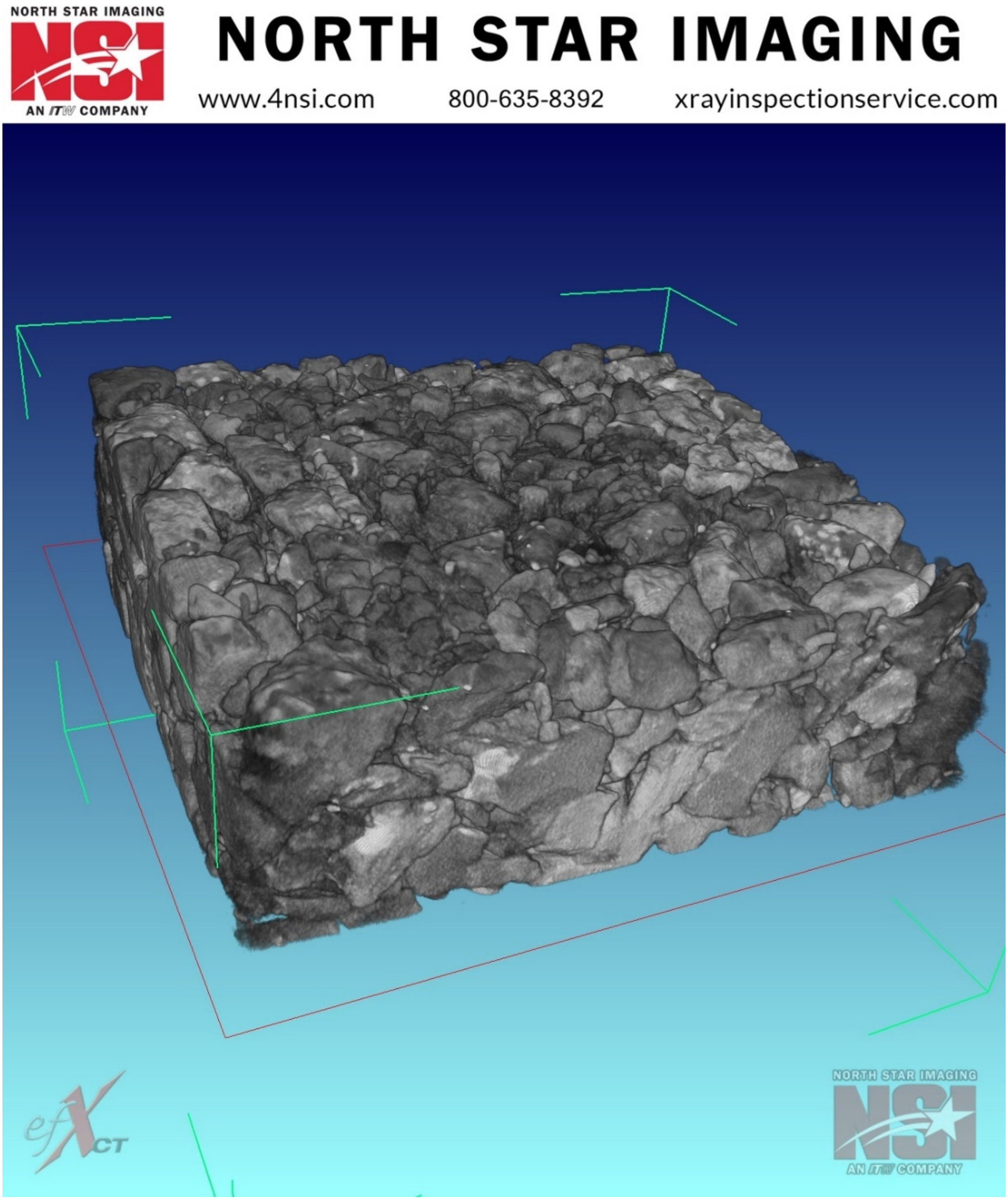

Figure 25 - 3D reconstruction of porous asphalt specimen obtained with XRT.

The total porosity (ϕ_t) was determined according Equation 7, where V_c indicates the volume for each connection, obtained by weighting all pores in each connections, V denotes the total volume and m is the total number of connections.

$$\emptyset_t = \frac{\sum_{i=1}^{m} V_{Ci}}{V}$$ Equation 7

To calculate the effective porosity (ϕ_e) all the connected components that didn't have pixels on the first layer (z=0) and on the last layers were excluded, and exclusively the connections that went all the way through the specimens were considered. Then the effective porosity was computed according to Equation 8.

$$\emptyset_e = \frac{\sum_{i=1}^{m} V_{ei}}{V}$$ Equation 8

Where V_e is the volume for each effective connections, obtained by weighting in all the connected pores, V is the total volume and m is the total number of connected connections

It was computed for each pore the area and the equivalent diameters, i.e. the diameter of a circumference covering the same area as the pore, and the pore size distribution [$PSD_{(pore)}$]. These parameters are essential to determine the behavior of the porous material in the presence of fluid, solute and PM loading (Kuang, Ying et al. 2015).

5.5. Modeled permeability

The permeability coefficient was calculated using the modified Kozeny-Kovàcs according 3.2.1. The pore diameter used was obtained with XRT according 5.4.

5.6. Dry deposition PM

5.6.1.Sampling

Traffic dry deposition PM samples were collected on four streets on Città Studi zone, Milan (Italy) on the surroundings of Politecnico di Milano (Figure 26). The method used was manual sweeping on the road shoulders to avoid fine particular loss that might happen with vacuuming.

Figure 26 - Location of the sampling area.

The area is a highly inhabited mostly residential zone and the samples were collected on October and November of 2016 (autumn season) on the evening before cleaning (Table 16).

Table 16 - Information about the sampling sites.

Sample ID[(1)]	Street	Date of sampling	Land use
MI_golgi_17_ott_2016	Via Golgi	17/10/2016	Residential
MI_pascoli_21_ott_2016	Via Pascoli	21/10/2016	Residential
MI_romagna_2_nov_2016	Viale Romagna	2/11/2016	Residential mostly
MI_zanoia_4_nov_2016	Via Zanoia	4/11/2016	Residential

(1) The samples ID follows the rule city_address_date_month_year. MI stands for Milan.

The four roads are constituted of impermeable asphalt. Aspects are presence of trees, traffic and others are gathered on Table 17.

Table 17 - Information of sampling area surroundings.

Sample ID	Vegetation	Traffic(1)	Others
MI_golgi_17_ott_2016	Absent	Mostly local	-
MI_pascoli_21_ott_2016	Trees above sampling area	Mostly local	Presence of TRAM
MI_romagna_2_nov_2016	Trees above sampling area	Collector	
MI_zanoia_4_nov_2016	Trees on the opposite side of the sampled stretch of the road	Local	Confines with a park

(1) qualitative

5.6.2.Build-up

The build-up accumulation rate was determined using the Equations 3 and 4 on Item 4.1. The rainfall data to asses the previous dry days was obtained with ARPA (*Azienda Regionale per la Protezione Ambientale*) Lombardia and the cleaning days with AMSA (*Azienda Milanese Servizi Ambientali*) (Table 18). Considering the high frequency of street cleaning on Milan the sampling date was set the night before cleaning.

Table 18 - Information about Previous Dry Day and the last day of road cleaning.

Sample ID	Day from last cleaning	Previous dry day
MI_golgi_17_ott_2016	5	7
MI_pascoli_21_ott_2016	5	11
MI_romagna_2_nov_2016	5	23
MI_zanoia_4_nov_2016	2	25

The sampling was held on the shoulder stretch of the road with length and width according Table 19. The mass of the collected samples were weight on laboratory (Table 19).

Table 19 – Mass of collected material and sampling area.

Sample ID	Mass of material sampled [kg]	Length of sampling [m]	Equivalent width [m]	$M_a(t)$ [kg/ha]	$M_{ar}(t) = 0,2 \cdot M_a(t)$ [kg/ha]
MI_golgi_17_ott_2016	1,791	≈ 94	≈ 3,2	59,5	11,9
MI_pascoli_21_ott_2016	1,452	≈ 72	≈ 1,4	144,0	28,8
MI_romagna_2_nov_2016	1,089	≈ 118	≈ 4,5	20,7	4,13
MI_zanoia_4_nov_2016	1,606	≈ 65	≈ 1,9	128,7	25,7

5.6.3. Particle size distribution (PSD)

The particle size distribution was obtained through mechanical sieve analysis according UNI EN 933-1. For each particle size distribution it was determined the indexes d_{10}, d_{50}, d_{60}, d_{90}, the percental of particles finer than 10%, 50%, 60% and 90% respectively and also the uniformity coefficient according Equation 7.

$$U = \frac{d_{60}}{d_{10}} \quad \text{Equation 9}$$

The mass cumulative particle size distribution was model as a gamma distribution. The goodness of fit was verified using the Kolmogorov-Smirnov (k-s) statistics test with p > 0,05. The Kruskal-Wallis test with α = 0,01 significance level was used to verified if the four different samples were statistically significantly different.

5.6.4. Particle number density (PND)

Particle number density is the number of particles for a given size fraction per volume of samples determined according Equation 8 (Sansalone and Cristina, [21, Ranieri, Berloco, [151]).

$$N_i = \frac{m_{i,norm}}{\rho_{s,i} . V_{s,i}} = \frac{m_{i,norm}}{\rho_{s,i} \frac{\pi}{6} d_{median}^3} \quad \text{Equation 10}$$

Where $\rho_{s,i}$ is the particle density, in this case assuming particle density of 2,65 g/cm^3, $V_{s,i}$ is the particle volume, assumed spherical with a median particle diameter (d_{median}), $m_{i,norm}$ is the dry mass normalized to 1000 g of the *i*th particle size according Equation 9:

$$m_{i,norm} = m_i \frac{1000\ g}{M_{total}} \quad \text{Equation 11}$$

The particle number density was model using power law distribution.

5.7. Filtration mechanism

The mechanistic model presented on Item 4.4 was used to estimate the sediments fate on the studied porous surfaces relating the pore structured obtained with XRT (Item 5.4) and the dry sediments PM particle size distribution. The same model was also applied with the rainfall simulation data for validation.

6. Results

6.1. Rainfall simulation

6.1.1. Initial permeability

Table 20 shows the permeability results without loadings and rainfall for all the samples. It is described the discharge time, the hydraulic conductivity (HC) and the coefficient of permeability (k) according 3.2.1. All k results are above the limit of good permeability established on Table 12 (Terzaghi, Peck, [113]).

Table 20 - Permeability on initial conditions.

id	Material	Porosity	Discharge time (s)	HC (s-1)	k (m/s)
PC11	PC	15%	21	0,05	1,07E-04
PC12	PC	15%	19	0,06	1,18E-04
PC13	PC	15%	16	0,07	1,40E-04
PC21	PC	15%	18	0,06	1,25E-04
PC22	PC	15%	15	0,07	1,50E-04
PC23	PC	15%	15	0,07	1,50E-04
PC31	PC	15%	18	0,06	1,25E-04
PC32	PC	15%	18	0,06	1,25E-04
PC33	PC	15%	21	0,05	1,07E-04
PC41	PC	20%	14	0,08	1,60E-04
PC42	PC	20%	11	0,10	2,04E-04
PC43	PC	20%	12	0,09	1,87E-04
PC51	PC	20%	11	0,10	2,04E-04
PC52	PC	20%	9	0,13	2,49E-04
PC53	PC	20%	11	0,10	2,04E-04
PC61	PC	20%	13	0,08	1,73E-04
PC62	PC	20%	12	0,09	1,87E-04
PC63	PC	20%	16	0,07	1,40E-04
PC71	PC	25%	10	0,11	2,24E-04
PC72	PC	25%	11	0,10	2,04E-04
PC73	PC	25%	10	0,11	2,24E-04
PC81	PC	25%	14	0,08	1,60E-04
PC82	PC	25%	14	0,08	1,60E-04
PC83	PC	25%	12	0,09	1,87E-04
PC91	PC	25%	7	0,17	3,21E-04
PC92	PC	25%	8	0,15	2,81E-04

id	Material	Porosity	Discharge time (s)	HC (s-1)	k (m/s)
PC93	PC	25%	5	0,26	4,49E-04
PA11	PA	15%	45	0,02	4,99E-05
PA12	PA	15%	49	0,02	4,58E-05
PA13	PA	15%	44	0,02	5,10E-05
PA21	PA	15%	20	0,05	1,12E-04
PA22	PA	15%	105	0,01	2,14E-05
PA23	PA	15%	74	0,01	3,03E-05
PA31	PA	15%	44	0,02	5,10E-05
PA32	PA	15%	43	0,02	5,22E-05
PA33	PA	15%	26	0,04	8,63E-05
PA41	PA	20%	18	0,06	1,25E-04
PA42	PA	20%	13	0,08	1,73E-04
PA43	PA	20%	17	0,06	1,32E-04
PA51	PA	20%	16	0,07	1,40E-04
PA52	PA	20%	19	0,06	1,18E-04
PA53	PA	20%	13	0,08	1,73E-04
PA61	PA	20%	14	0,08	1,60E-04
PA62	PA	20%	17	0,06	1,32E-04
PA63	PA	20%	10	0,11	2,24E-04
PA71	PA	25%	9	0,13	2,49E-04
PA72	PA	25%	18	0,06	1,25E-04
PA73	PA	25%	9	0,13	2,49E-04
PA81	PA	25%	8	0,15	2,81E-04
PA82	PA	25%	9	0,13	2,49E-04
PA83	PA	25%	10	0,11	2,24E-04
PA91	PA	25%	14	0,08	1,60E-04
PA92	PA	25%	11	0,10	2,04E-04
PA93	PA	25%	12	0,09	1,87E-04

Note: PA: porous asphalt, PC: pervious concrete.

6.1.2.Parameters influencing on permeability

Discharge time was used to investigate the parameters influencing on permeability. Table 21 gather the results of the statistical tests for discharge time comparing porosity, aerial loadings and rainfall intensities. Before using the rainfall simulator, the discharge time was obtained for the three porosities varying the aerial loadings (Figure 27). Both the variations of aerial loadings (0; 0,5; 1,0; 2,0) and porosity (0,15; 0,20; 0;25) resulted on statistical significantly difference for the discharge time. It was expected that a variation of porosity and aerial loading, that would ultimately result on reduction of porosity, would affect the discharge time, in this case related to permeability. It was confirmed a very strong correlation between aerial loadings and discharge time and porosity and discharge time using Spearman coefficient (Table 21).

The distribution from aerial loadings and discharge time follows an exponential trend, as mention on literature while the porosity follows a power law distribution (Table 22).

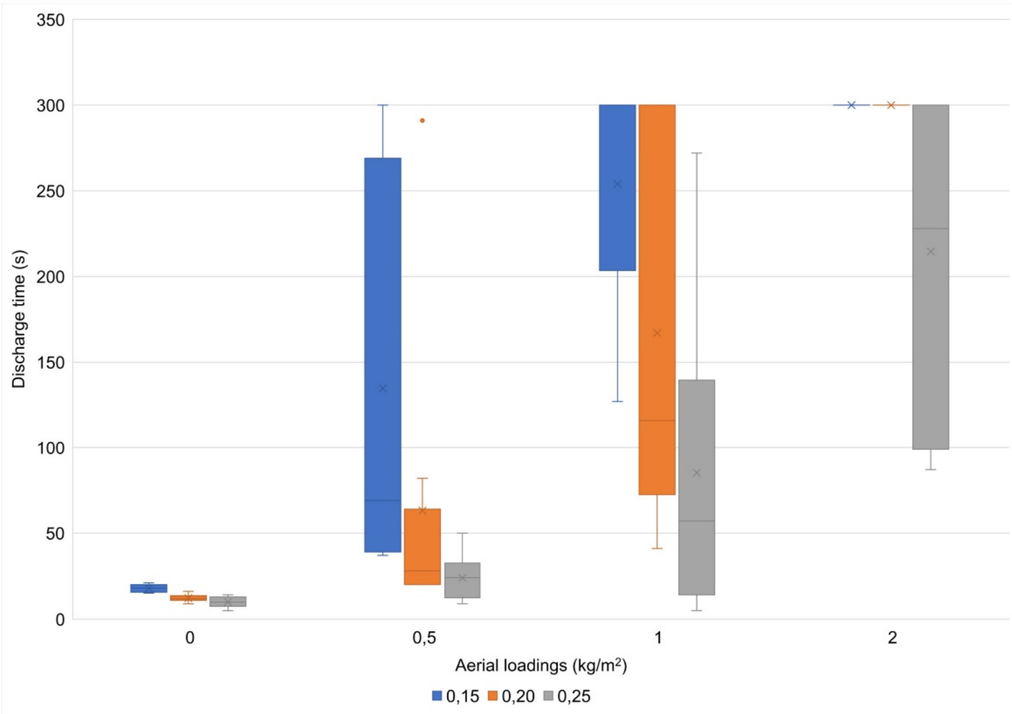

(a)

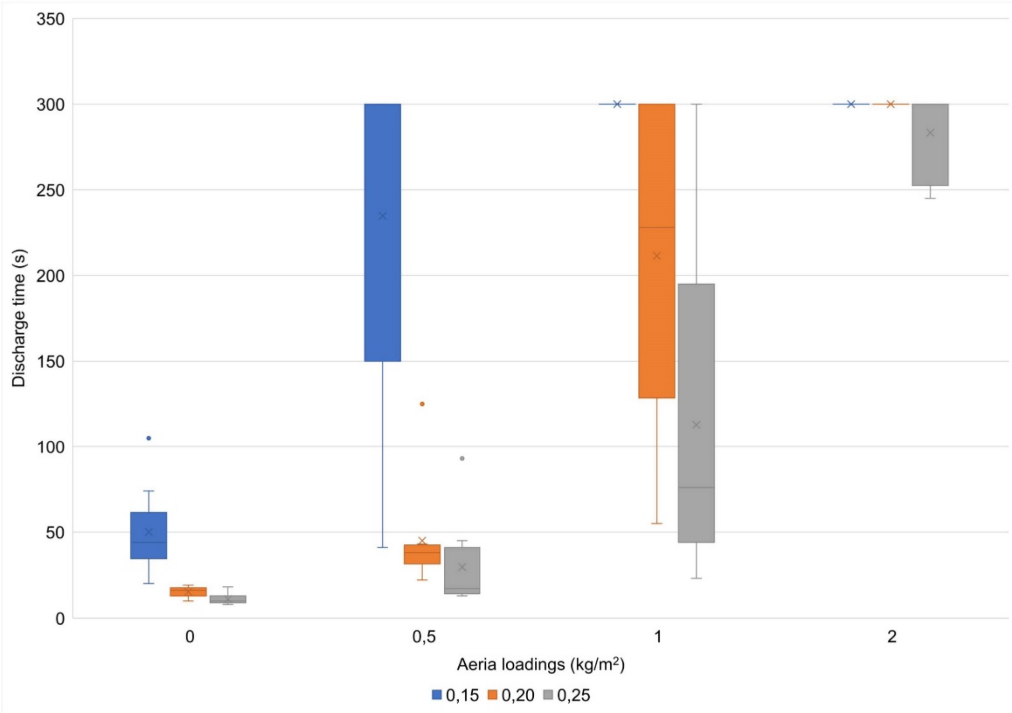

(b)

Figure 27 - Discharge time x aerial loadings for 0,15; 0,20 and 0,25 porosities without the effect of rainfall. (a) pervious concrete (b) porous asphalt.

Table 21 - Statistical tests for discharge time x aerial loadings, porosity and rainfall intensities.

	Rainfall intensity (mm/h)	Aerial loadings (kg^2/m)	Porosity	Slope (%)	p	p > 0,01
PC	0	0; 0,5; 1,0;2,0	0,15	2,5	4,29E-06	**false**
	0	0; 0,5; 1,0;2,0	0,2	2,5	1,01E-06	**false**
	0	0; 0,5; 1,0;2,0	0,25	2,5	3,29E-05	**false**
	0	0	0,15; 0,20; 0,25	2,5	1,59E-04	**false**
	50;100;150	0,5	15	2,5	0,005	**false**
	50;100;150	1	15	2,5	0,001	**false**
	50;100;150	2	15	2,5	0,003	**false**
	50;100;150	0,5	20	2,5	0,409	true
	50;100;150	1	20	2,5	0,048	true
	50;100;150	2	20	2,5	0,001	**false**
	50;100;150	0,5	25	2,5	0,121	true
	50;100;150	1	25	2,5	0,18	true
	50;100;150	2	25	2,5	0,003	**false**
PA	0	0; 0,5; 1,0;2,0	0,15	2,5	5,82E-06	**false**
	0	0; 0,5; 1,0;2,0	0,2	2,5	5,69E-07	**false**
	0	0; 0,5; 1,0;2,0	0,25	2,5	2,83E-06	**false**
	0	0	0,15; 0,20; 0,25	2,5	1,59E-04	**false**
	50;100;150	0,5	15	2,5	0,883	true
	50;100;150	1	15	2,5	0,392	true
	50;100;150	2	15	2,5	(2)	-
	50;100;150	0,5	20	2,5	0,022	true
	50;100;150	1	20	2,5	0,04	true
	50;100;150	2	20	2,5	0,457	true
	50;100;150	0,5	25	2,5	0,057	true
	50;100;150	1	25	2,5	0,371	true
	50;100;150	2	25	2,5	0,107	True

1) p-value for the null hypothesis that the tested data comes from the same distribution, using a Kruskal-Wallis test with α = 0,01 significance level. The alternative hypothesis is that not all samples come from the same distribution.
(2) For the 15% porosity with 2,0 kg/m^2 of sediments all the discharge times reached the maximum limit of 300 s.
Note: PA: porous asphalt, PC: pervious concrete.

Table 22 – Correlation and distribution for discharge time analysis without rainfall effect.

	Aerial loadings	Porosity	Spearman correlation RHO(1)	p(2)	p < 0,05	Distribution SSE	R-square	
PC	0; 0,5; 1,0;2,0	0,15	0,8704	5,32E-08	true	2,51E+05	0,56	exponential
	0; 0,5; 1,0;2,0	0,2	0,9327	1,27E-12	true	1,90E+05	0,6803	exponential
	0; 0,5; 1,0;2,0	0,25	0,8105	2,09E-05	true	1,44E+05	0,6146	exponential
	0	0,15; 0,20; 0,25	-0.7894	9,89E-03	true	1,53E+02	0,6546	power law
PA	0; 0,5; 1,0;2,0	0,15	0,8124	5,42E-09	true	2,56E+05	0,4266	exponential
	0; 0,5; 1,0;2,0	0,2	0,9477	1,96E-17	true	1,62E+05	0,6883	exponential
	0; 0,5; 1,0;2,0	0,25	0,8981	5,96E-13	true	1,14E+05	0,7547	exponential
	0	0,15; 0,20; 0,25	-0.8662	5,31E-09	true	5,52E+03	0,5776	power law

(1) pairwise Spearman correlation coefficient between each pair of data.
(2) p-value for the hypothesis of no correlation against the alternative that there is nonzero correlation.
Note: PA: porous asphalt, PC: pervious concrete.

Using then the rainfall simulator it was noticeable a reduction effect on discharge time when comparing the initial test without rainfall (“0”) and the test with 150 mm/h rainfall, which can be explained by a cleaning effect that will eventually result on lower discharge time and therefore a higher permeability (Figure 28). The Kruskal-Wallis in fact confirmed the statically significant difference for the groups with same porosity and aerial loading when varying the rainfall intensity (50 mm/h, 100 mm/h and 150 mm/h) for the pervious concrete samples, however that difference wasn’t significantly for the porous asphalt samples.

For the “false” results obtained on rainfall intensities tests on Table 21 it was applied the Wilcoxon Signed-Rank confirming the statistically significantly difference on discharge time when comparing the initial result without rainfall with the 150 mm/h rainfall intensity (Table 23). This intensity correspond to an event of 15 minutes duration with 50 years return period for the city of Milan (Italy) (Becciu and Paoletti, [26]).

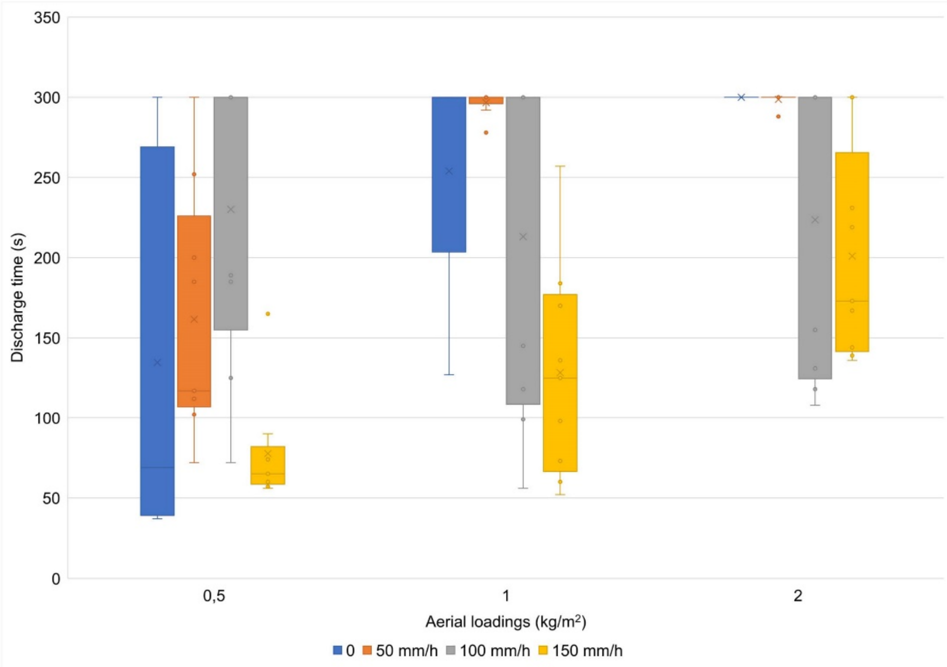
350
300
250
200
150
100
50
0
Discharge time (s)
0,5
1
2
Aerial loadings (kg/m2)
0
50 mm/h
100 mm/h
150 mm/h

(a)

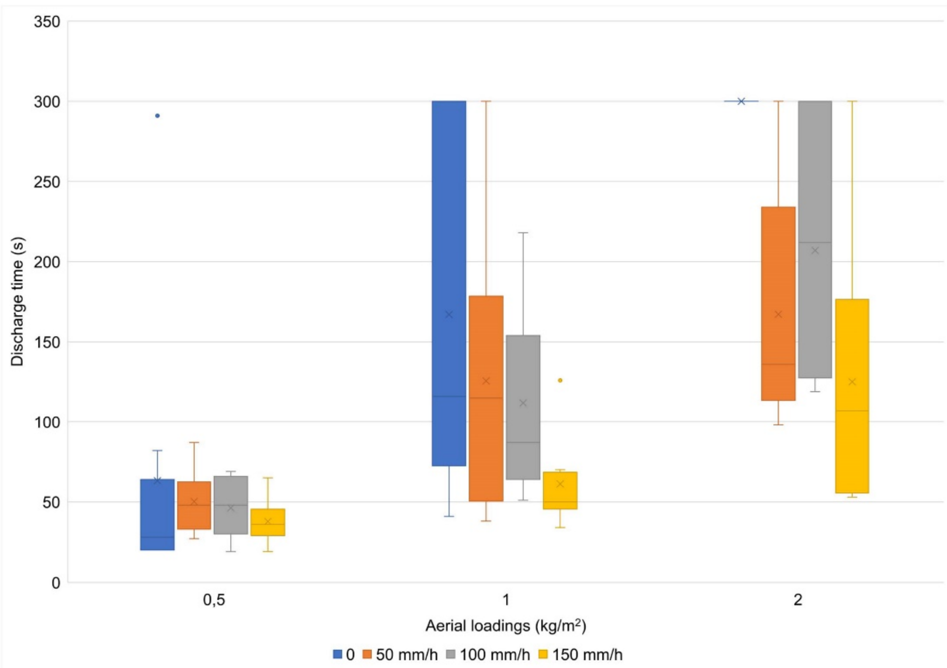
350
300
250
200
150
100
50
0
Discharge time (s)
0,5
1
2
Aerial loadings (kg/m2)
0
50 mm/h
100 mm/h
150 mm/h

(b)

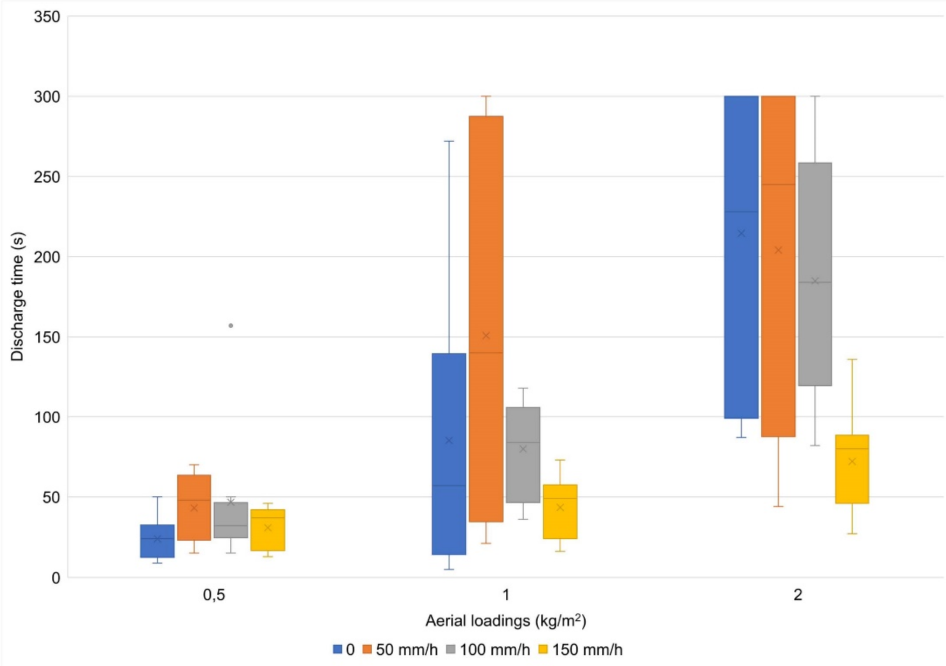
350
300
250
200
150
100
50
0
Discharge time (s)
0,5
1
2
Aerial loadings (kg/m2)
0
50 mm/h
100 mm/h
150 mm/h

(c)

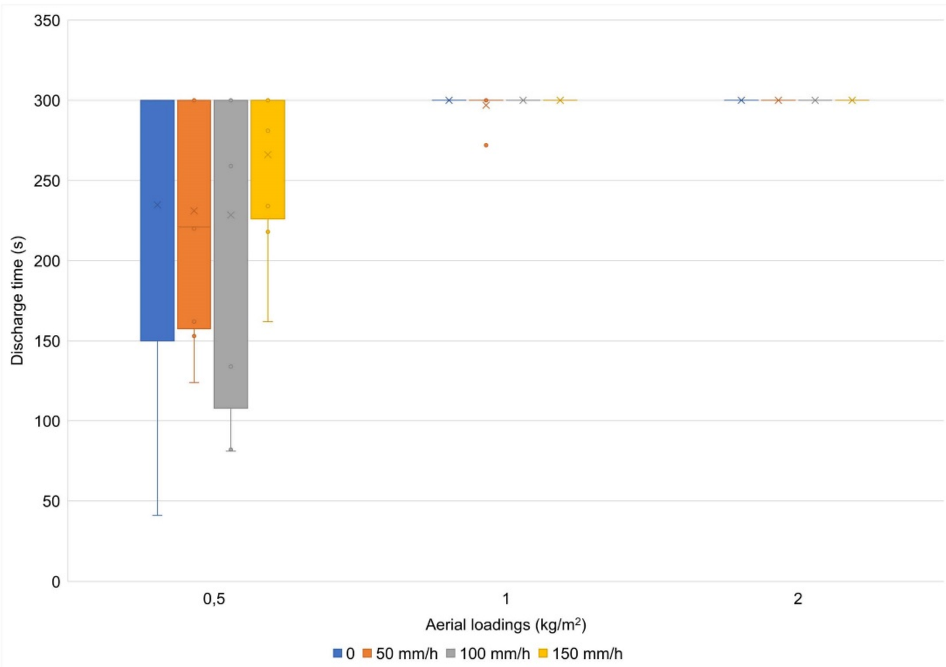
350
300
250
200
150
100
50
0
Discharge time (s)
0,5
1
2
Aerial loadings (kg/m2)
0
50 mm/h
100 mm/h
150 mm/h

(d)

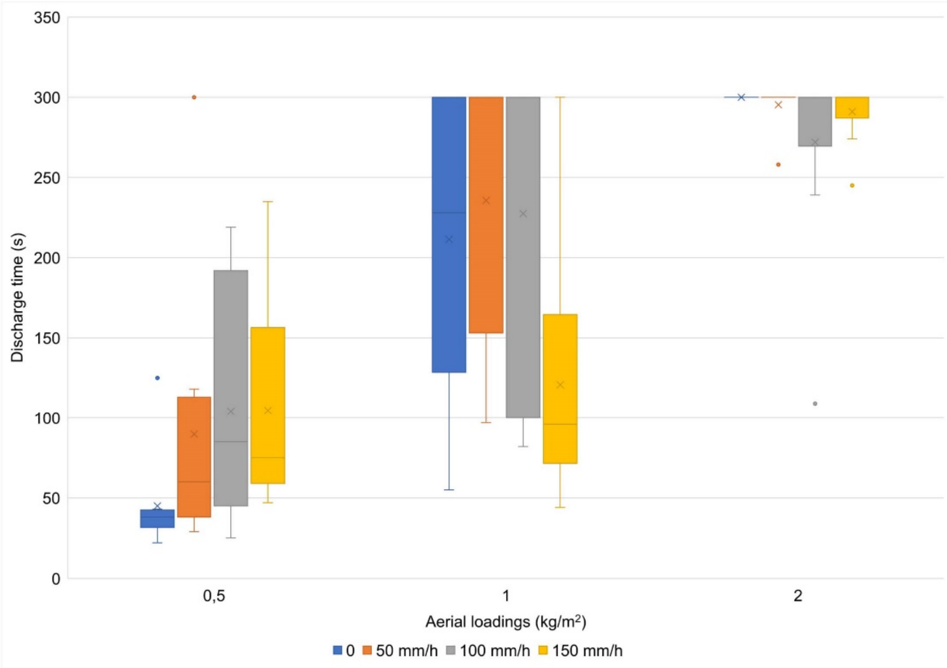
350
300
250
200
150
100
50
0
Discharge time (s)
0,5
1
2
Aerial loadings (kg/m2)
0
50 mm/h
100 mm/h
150 mm/h

(e)

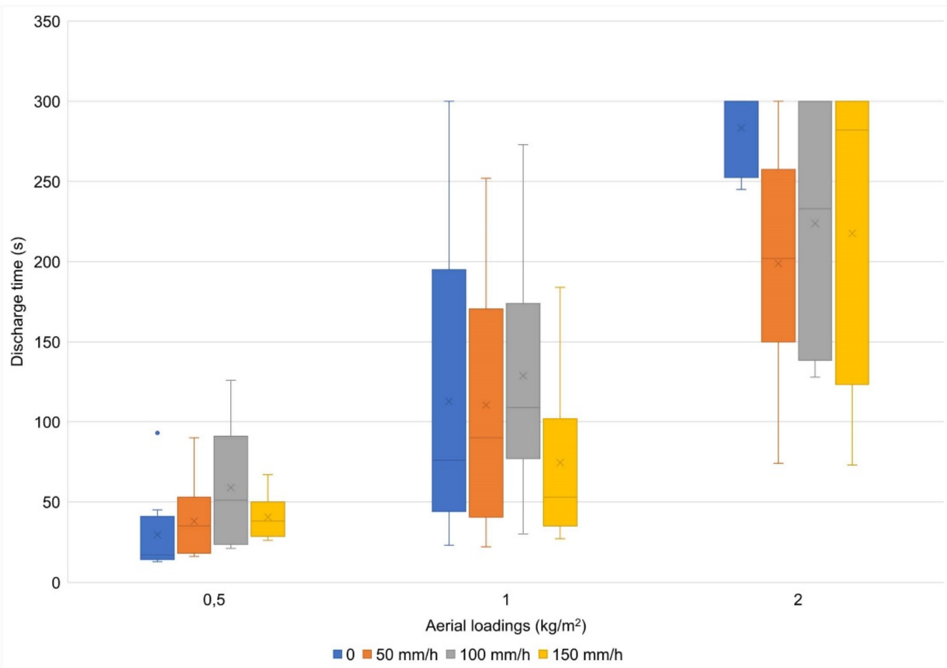
350
300
250
200
150
100
50
0
Discharge time (s)
0,5
1
2
Aerial loadings (kg/m2)
0
50 mm/h
100 mm/h
150 mm/h

(f)

Figure 28 - Discharge time x aerial loadings for different rainfall intensities. rainfall intensity. (a) pervious concrete porosity 0,15, (b) pervious concrete porosity 0,20, (c) pervious concrete porosity 0,25 (d) porous asphalt porosity 0,15, (e) porous asphalt porosity 0,20, (f) porous asphalt porosity 0,25.

Table 23 – Pervious concrete statistical analysis comparing discharge time for different rainfall intensities.

Porosity (%)	**Rainfall intensity (mm/h)**	**Aerial loading (kg/m2)**	**P(1)**	***p > 0,05***	**signedrank**
15	0 x 50	0,5	0,6523	true	18
15	0 x 100	0,5	0,0781	true	3
15	0 x 150	0,5	0,4961	true	29
15	0 x 50	1	0,125	true	1
15	0 x 100	1	0,3828	true	25
15	0 x 150	1	0,0078	**false**	44
15	0 x 50	2	1	true	1
15	0 x 100	2	0,125	true	10
15	0 x 150	2	0,0156	**false**	28
20	0 x 50	2	0,0156	**false**	28
20	0 x 100	2	0,0313	**false**	21
20	0 x 150	2	0,0078	**false**	36
25	0 x 50	2	0,8438	true	12
25	0 x 100	2	0,3828	true	25
25	0 x 150	2	0,0039	**false**	45

(1) p = p-value of a two-sided Wilcoxon signed rank test for the null hypothesis that x – y comes from a distribution with zero median with α = 0,05 significance level.

The discharge time was then investigate varying the slope (2,5%; 7,0%) on the rainfall simulation test, whereas wasn't observed a statistically significantly difference for both pervious concrete and porous asphalt samples (Table 24).

Table 24 - Statistical tests for discharge time x slope.

	Porosity (%)	**Rainfall intensity (mm/h)**	**Aerial loading (kg/m2)**	**P(1)**	***p > 0,05***	**signed-rank**
PC	15	100	0,5	0,25	true	0
	20	100	0,5	0,25	true	0
	25	100	0,5	0,25	true	0
	15	100	2	0,25	true	0
	20	100	2	0,25	true	0
	25	100	2	0,25	true	0
	15	150	0,5	0,25	true	0
	20	150	0,5	0,25	true	0
	25	150	0,5	0,25	true	0
	15	150	2	0,25	true	0
	20	150	2	0,25	true	0
	25	150	2	0,5	true	1
PA	15	100	0,5	1	true	2
	15	100	2	1	true	0
	20	100	0,5	0,875	true	6
	20	100	2	1	true	0
	25	100	0,5	0,25	true	1
	25	100	2	1	true	1
	15	150	0,5	1	true	2
	15	150	2	1	true	0
	20	150	0,5	0,156 3	true	18
	20	150	2	0,5	true	0
	25	150	0,5	0,5	true	5
	25	150	2	0,25	true	6

(1) p = p-value of a two-sided Wilcoxon signed rank test for the null hypothesis that x – y comes from a distribution with zero median with α = 0,05 significance level.
Note: PA: porous asphalt, PC: pervious concrete.

Comparing the results of discharge time for pervious concrete and porous asphalt, with a discharge average for porous asphalt of 145 s and standard deviation of 91 and for porous asphalt an average of 215 s and standard deviation of 93 s. The Mann-Whitney test reject the hypothesis that they came from the same distribution with p-value of $8{,}1071.10^{-10}$ confirming a statistically significant difference between material types.

After the first round of tests, when each sample was submitted to 9 rainfall events (225 mm) and a total loading of 1,82 kg, it was conducted deeper cleaning procedures and. The specimens were cleaned using pressure water, left soaked on water for 24 hours and they again cleaned with pressure water.

The initial discharge time was compared with the discharge time after cleaning obtaining 44% increase on discharge time for the 15% porosity samples, a 10% increase for the 20% porosity samples and 28% increase for the 25% samples, a variation considered statistically significantly (Table 25). Therefore, the cleaning procedures were not able to regain initial permeability.

Table 25 - Cleaning

	p	p > 0,01	p	*p > 0,05*	ranksum	p[(1)]	*p > 0,05*	signedrank
PC	0,3533	true	0,3743	true	75	0,0078	false	1
PA	0,2774	true	0,3176	true	44	0,0156	false	0

[(1)] p = p-value of a two-sided Wilcoxon signed rank test for the null hypothesis that x – y comes from a distribution with zero median with α = 0,05 significance level.
Note: PA: porous asphalt, PC: pervious concrete.

6.1.3. Runoff coefficient analysis

The overall results for runoff coefficient were considered low with an average of 0,07 and standard deviation of 0,11, where 47% of the tests present zero (0,00) runoff coefficient, not generating any measurable runoff. The maximum runoff measured was 0,67 for porous asphalt with 15% of porosity, 7% slope, 150 mm/h and 15 minutes rainfall and 2,0 kg/m^2 aerial loadings.

Considering the first round of tests, maintaining the rainfall intensity and considering the variation of porosity and aerial loadings it was observed a slightly higher runoff coefficient on the pervious concrete samples for the rainfall intensities of 100 mm/h and 150 mm/h for the 2,0 kg/m^2 aerial loadings. The porous asphalt samples showed results with higher variability and without a clear trend. It was observed statistically significant difference only when comparing rainfall intensities for the 15% porosity on pervious concrete and when comparing porosity for 15% porous asphalt, when the reduction on permeability ultimately leads to runoff quantity increase.

Table 26 – Statistical tests for runoff coefficient.

	Test	Rainfall intensity (mm/h)	Aerial loadings (kg^2/m)	Porosity	p[(1)]	p > 0,01
PC	Porosity	50	0,5; 1,0;2,0	0,15; 0,20;0,25	0,594	true
PC	Porosity	100	0,5; 1,0;2,0	0,15; 0,20;0,25	0,548	true
PC	Porosity	150	0,5; 1,0;2,0	0,15; 0,20;0,25	0,468	true
PC	Loading	50	0,5; 1,0;2,0	0,15; 0,20;0,25	0,594	true
PC	Loading	100	0,5; 1,0;2,0	0,15; 0,20;0,25	0,192	true

PC	Loading	150	0,5; 1,0;2,0	0,15; 0,20;0,25	0,091	true
PC	Rainfall	50;100;150	0,5; 1,0;2,0	15	0,006	**false**
PC	Rainfall	50;100;150	0,5; 1,0;2,0	20	0,028	true
PC	Rainfall	50;100;150	0,5; 1,0;2,0	25	0,122	true
PA	Void	50	0,5; 1,0;2,0	0,15; 0,20;0,25	0,263	true
PA	Void	100	0,5; 1,0;2,0	0,15; 0,20;0,25	0,227	true
PA	Void	150	0,5; 1,0;2,0	0,15; 0,20;0,25	0,003	**false**
PA	Loading	50	0,5; 1,0;2,0	0,15; 0,20;0,25	0,567	true
PA	Loading	100	0,5; 1,0;2,0	0,15; 0,20;0,25	0,365	true
PA	Loading	150	0,5; 1,0;2,0	0,15; 0,20;0,25	0,074	true
PA	Rainfall	50;100;150	0,5; 1,0;2,0	15	0,111	true
PA	Rainfall	50;100;150	0,5; 1,0;2,0	20	0,185	true
PA	Rainfall	50;100;150	0,5; 1,0;2,0	25	0,251	true

(1) p-value for the null hypothesis that the tested data comes from the same distribution, using a Kruskal-Wallis test with α = 0,01 significance level. The alternative hypothesis is that not all samples come from the same distribution.
Note: PA: porous asphalt, PC: pervious concrete.

On the second round of tests it's possible to observe an increase on runoff coefficient when varying the slope (2,5%; 7,0%) for the same rainfall intensity and duration for both pervious concrete and porous asphalt samples, especially for the 15% porosity.

The first round of tests (rainfall intensities of 50 mm/h, 100 mm/h, 150 mm/h and aerial loadings of 0,5 kg/m^2, 1,0 kg/m^2 and 2,0 kg/m^2) showed a runoff coefficient average of 0,00 for pervious concrete and 0.01 for porous asphalt while the second round (rainfall intensities of 100 mm/h 30 minutes duration, 150 mm/h 15 minutes duration, slope of 2,5%, 7,0% and aerial loadings of 0,5 kg/m2, 2,0 kg/m2) showed a runoff coefficient average of 0,10 for pervious concrete and 0.17 porous asphalt. By the fact that the cleaning between the tests wasn't completely efficient there was an accumulation and settling effect of loadings that ultimately resulted on the increase of runoff volume and then runoff coefficient on a statistically significantly matter (Table 27).

When comparing materials, pervious concrete showed and averaged runoff coefficient of 0,06 for pervious concrete and 0,07 for porous asphalt a difference not statistically significantly different (Table 27).

Table 27 – Statistical tests for runoff coefficient considering materials and slope.

	p(1)	p>0,05	ranksum
pc x pa	0,724	true	21637
pc slope	1,8292E-07	**false**	1
pa slope	1,23E-05	**false**	0

(1) p = p-value of a two-sided Wilcoxon signed rank test for the null hypothesis that x – y comes from a distribution with zero median with α = 0,05 significance level.
Note: PA: porous asphalt, PC: pervious concrete.

6.1.4. Correlation between runoff coefficient and discharge time

The results for discharge time and runoff coefficient for all experimental plan are plotted on Figure 29. The Spearman correlation coefficient resulted on a weak correlation significantly different from zero for discharge time and runoff coefficient for the entire experimental plan, for all PA and pervious concrete tests separately and excluding the tests that stopped at 300 s (Table 28).

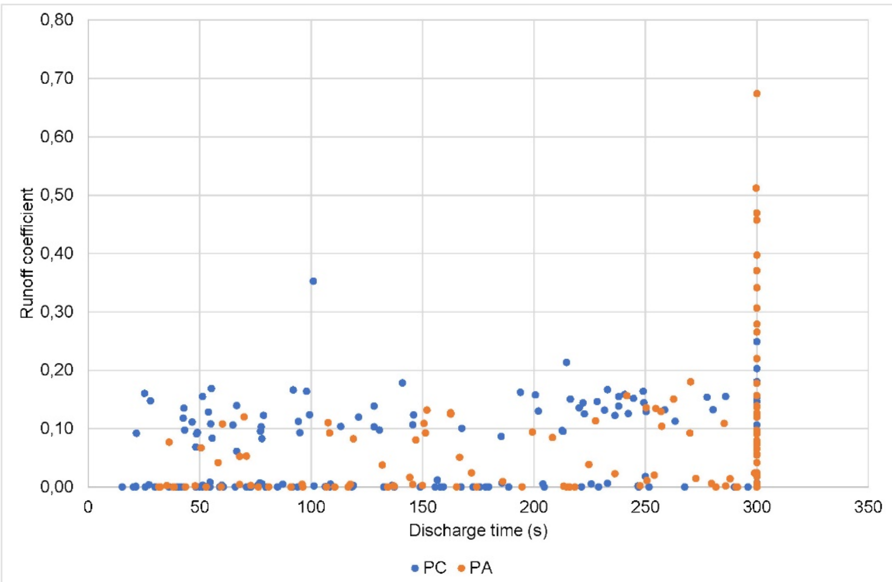

Figure 29 - Runoff coefficient x discharge time.

Table 28 – Spearman correlation coefficient

	RHO	p(1)	p < 0,05
all data	0,285	9,94E-07	true
PC	0,2679	8,14E-04	true
PA	0,3434	5,92E-05	true
without 300 s results	0,2578	4,06E-04	True

(1) p-values for testing the hypothesis of no correlation against the alternative that there is a nonzero correlation.
Note: PA: porous asphalt, PC: pervious concrete.

6.1.5.Filtration mechanism (laboratory)

Figure 30 shows the sediments fate for porous asphalt samples load with 0,5 kg/m^2 of sediments submitted to a 100 mm/h rainfall with 30 minutes duration and 2,5% slope. More than 90% of sediments mass were retained on the specimen creating a “cake” or on its core through straining mechanism. The amount of sediments that wash off on runoff was less than 1,0% by mass. The amount that pass through the specimen was between 8 – 10 and was compose visually mostly by fine material.

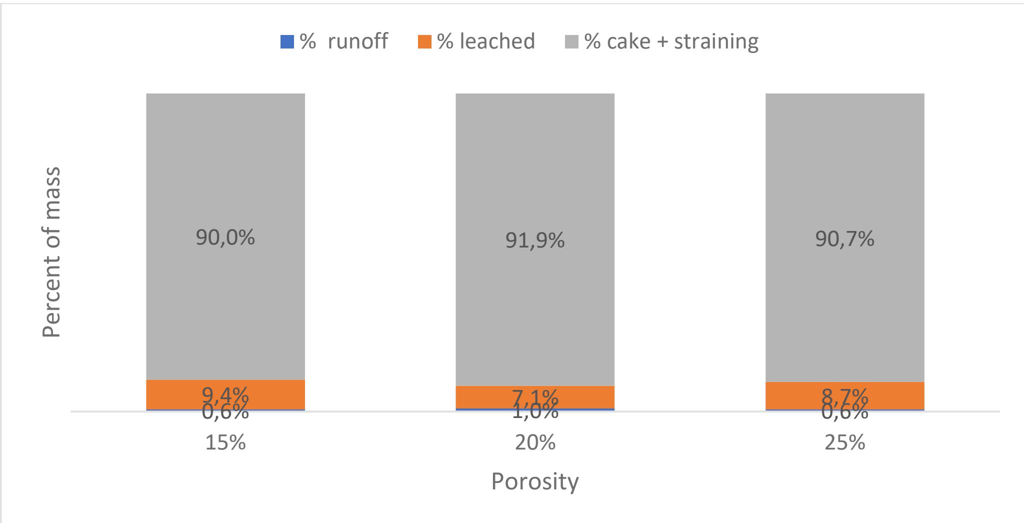

Figure 30 – Sediments fate on percent of sediments mass for porous asphalt with 100 mm/h rainfall intensity, 2,5% slope and 0,5 kg/m^2 aerial loadings.

The results for all tests are on Table 29 and the complete graphical analysis on Appendix 2. More than 85% of the sediments load remained on the specimen surface or core. It wasn’t observed a significative difference between different porosities.

By increasing the sediments load it was noticed an increase on the percent of material retained on the specimen. An explanation could be that the growing of the surface “cake” would retain more material on the surface, especially finer ones that would eluted on initial conditions. An interest fact is that there wasn’t a significative growth on the sediment share on runoff or on runoff volume meaning that the formation of the cake would improve the retaining of sediments and consequently pollution loads removal without affect the service life.

By increasing slope or rainfall intensity was observed a slight increase on runoff volume that wash off a part of the sediments that otherwise would be retained on the specimen.

Table 29 - Sediments fate by percent of mass on different conditions on rainfall simulation tests.

Material	Rainfall intensity	Slope	Aerial loading (kg/m^2)	Porosity	Sediments fate percent on mass		
					% runoff	% eluted	% cake + straining
PA	100 mm/h per 30 minuti	2,5%	0,5	15%	1%	9%	90%
				20%	1%	7%	92%
				25%	1%	9%	91%
			2	15%	1%	5%	94%
				20%	1%	4%	95%
				25%	1%	4%	96%
		7%	0,5	15%	1%	11%	88%
				20%	1%	11%	88%
				25%	1%	11%	88%
			2	15%	7%	3%	90%
				20%	2%	4%	94%
				25%	1%	5%	95%
	150 mm/h per 15 minuti	2,5%	0,5	15%	1%	8%	91%
				20%	1%	8%	91%
				25%	0%	9%	90%
			2	15%	5%	2%	93%
				20%	1%	4%	96%
				25%	1%	5%	94%
		7%	0,5	15%	1%	5%	94%
PC	100 mm/h per 30 minuti	2,5%	0,5	15%	1%	6%	93%
				20%	1%	6%	93%
				25%	1%	6%	93%
			2	15%	1%	3%	96%
				20%	1%	3%	96%
				25%	1%	2%	97%
		7%	0,5	15%	2%	6%	92%
				20%	1%	6%	93%
				25%	1%	6%	93%
			2	15%	2%	2%	95%
				20%	1%	2%	96%
				25%	1%	2%	97%
	150 mm/h per 15 minuti	2,5%	0,5	15%	0,7%	6,0%	93,3%
				20%	0,6%	5,0%	94,4%
				25%	0,7%	4,5%	94,8%
			2	15%	1,8%	1,9%	96,3%

	20%	0,8%	1,8%	97,4%
	25%	0,6%	1,2%	98,3%

Note: PA: porous asphalt, PC: pervious concrete.

The formation of a “cake” was visually observed during the tests (Figure 31).

Figure 31 - Sediments retained on the porous asphalt surface forming the "cake".

6.2. Pore structure

Three porous asphalt specimens (PA1, PA6 and PA7) were analyzed using XRT to obtain the pore structure parameters reunited on Table 30 and $PSD_{(pore)}$ on Figure 32. The analisis were held un sub-specimens of 80 x 80 mm extracted from the original ones to allow to fit then on the XRT equipment. Table 30 brings the average results for different samples taken for each specimen. Figure 32 brings the $PSD_{(pore)}$ for each sub-specimen analyzed.

There was a good accordance between total porosity obtained with bulk density and with the XRT. It was obtained analogous results of total porosity and effective porosity indicating a highly interconnected structure. This could be confirmed visually, where the pores showed a considerable dimension and connect all though the structure (Figure 24).

The pore diameter mean obtained present analogous results between samples and that could be explained by the fact that all three porosities have the same mix design and aggregates particle size distribution. This can also explain the similar results for filtration mechanisms presented on Item 6.1.5 since pore diameter governed filtration mechanism.

Table 30 - Pore structure obtained with XRT.

ID	total porosity[1]	total porosity	effective porosity	pore area mean (mm^2)	pore area median (mm^2)	pore diameter mean (mm)	pore diameter median (mm)	d_{50}	d_{30}
PA1	0,15	0,16	0,15	7,43	2,44	2,33	1,76	1,84	1,22
PA7	0,25	0,22	0,21	10,61	2,29	2,61	1,70	1,70	1,12
PA6	0,20	0,25	0,25	9,56	2,65	2,61	1,84	2,15	1,47

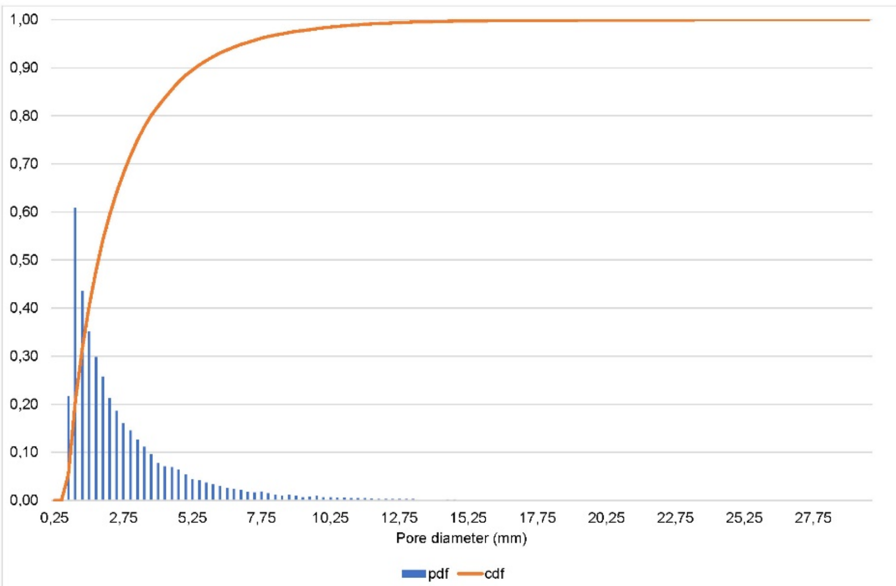

(a)

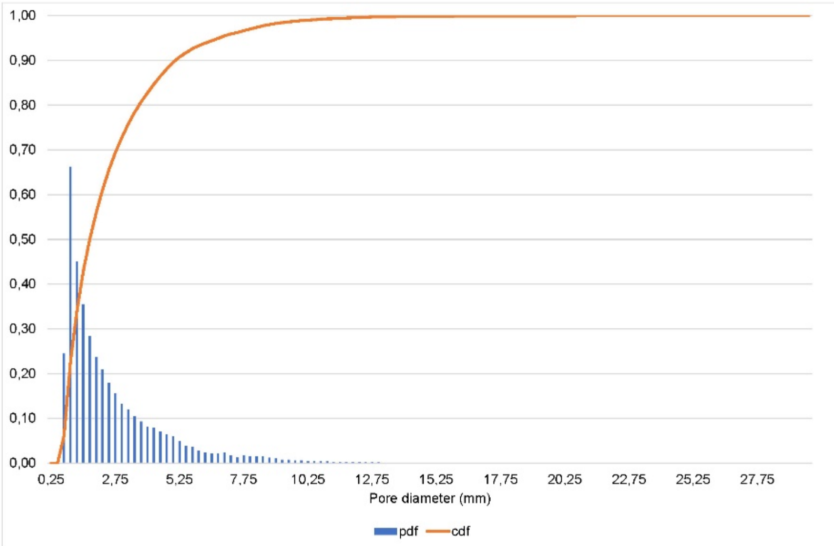
1,00
0,90
0,80
0,70
0,60
0,50
0,40
0,30
0,20
0,10
0,00
0,25 2,75 5,25 7,75 10,25 12,75 15,25 17,75 20,25 22,75 25,25 27,75
Pore diameter (mm)
pdf cdf

(b)

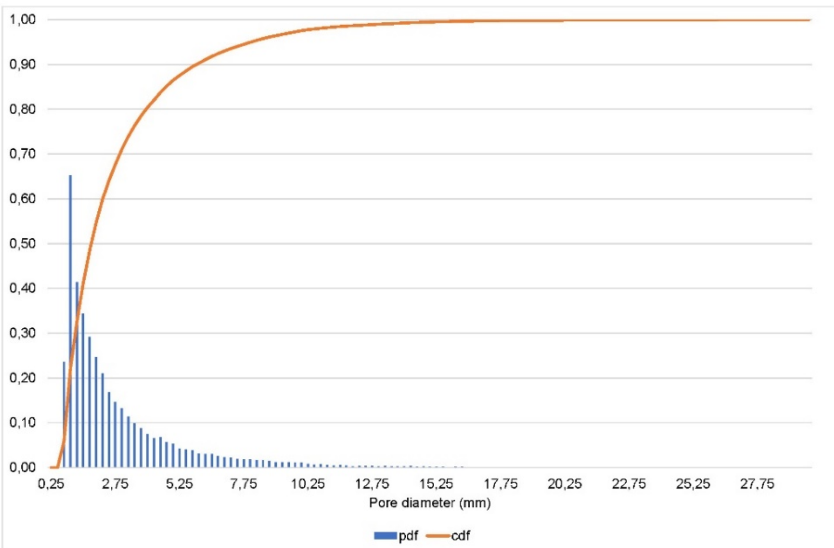
1,00
0,90
0,80
0,70
0,60
0,50
0,40
0,30
0,20
0,10
0,00
0,25 2,75 5,25 7,75 10,25 12,75 15,25 17,75 20,25 22,75 25,25 27,75
Pore diameter (mm)
pdf cdf

(c)

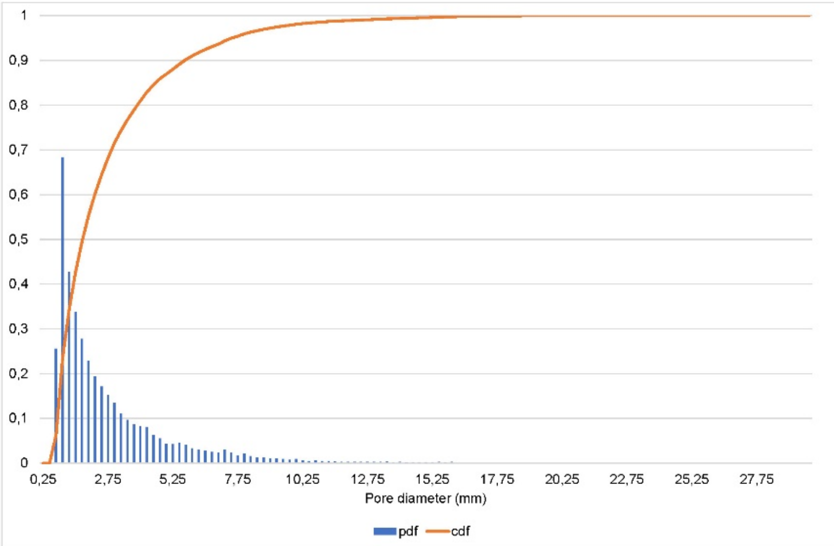
1
0,9
0,8
0,7
0,6
0,5
0,4
0,3
0,2
0,1
0
0,25
2,75
5,25
7,75
10,25
12,75
15,25
17,75
20,25
22,75
25,25
27,75
Pore diameter (mm)
pdf
cdf

(d)

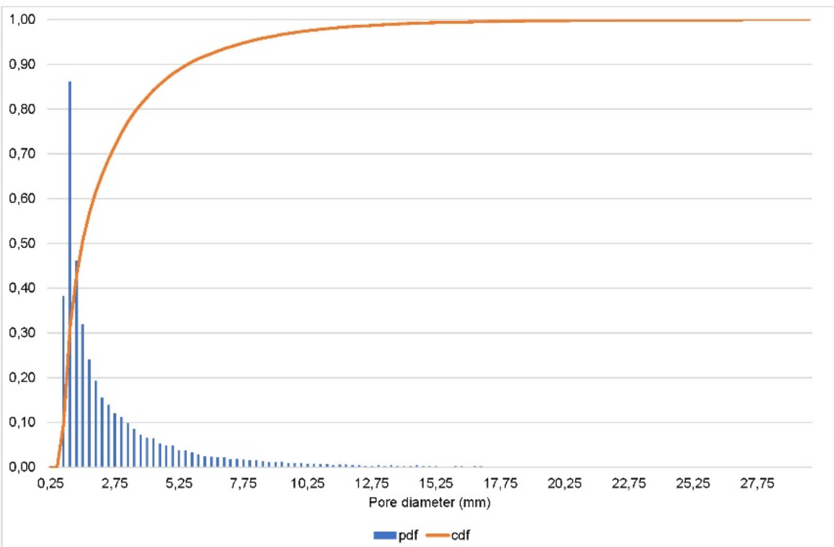
1,00
0,90
0,80
0,70
0,60
0,50
0,40
0,30
0,20
0,10
0,00
0,25
2,75
5,25
7,75
10,25
12,75
15,25
17,75
20,25
22,75
25,25
27,75
Pore diameter (mm)
pdf
cdf

(e)

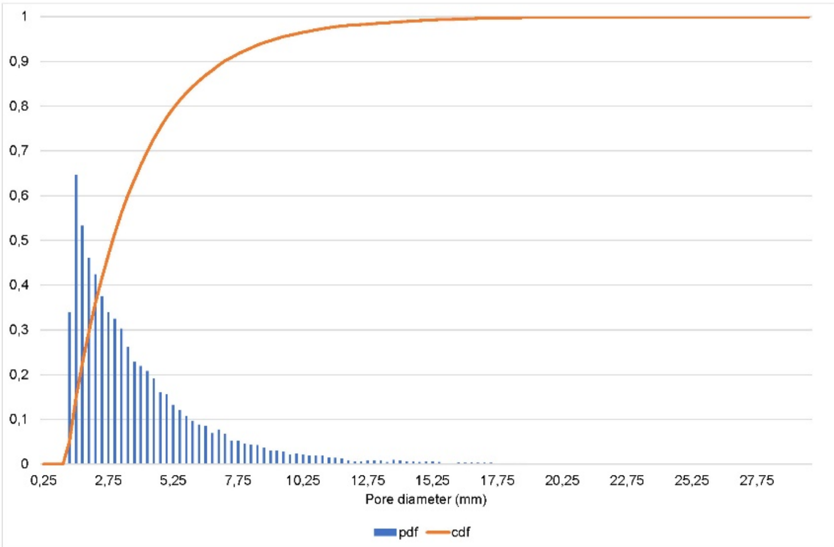
1
0,9
0,8
0,7
0,6
0,5
0,4
0,3
0,2
0,1
0
0,25
2,75
5,25
7,75
10,25
12,75
15,25
17,75
20,25
22,75
25,25
27,75
Pore diameter (mm)
pdf
cdf

(f)

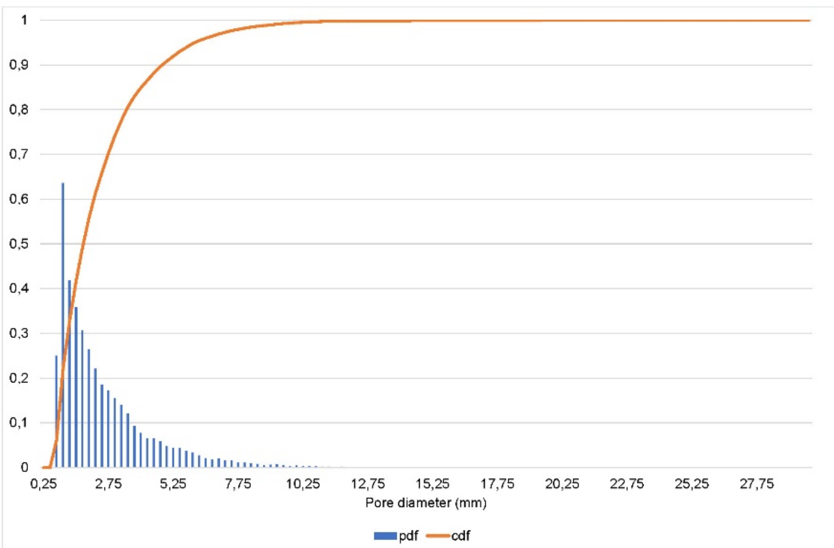
1
0,9
0,8
0,7
0,6
0,5
0,4
0,3
0,2
0,1
0
0,25
2,75
5,25
7,75
10,25
12,75
15,25
17,75
20,25
22,75
25,25
27,75
Pore diameter (mm)
pdf
cdf

(g)

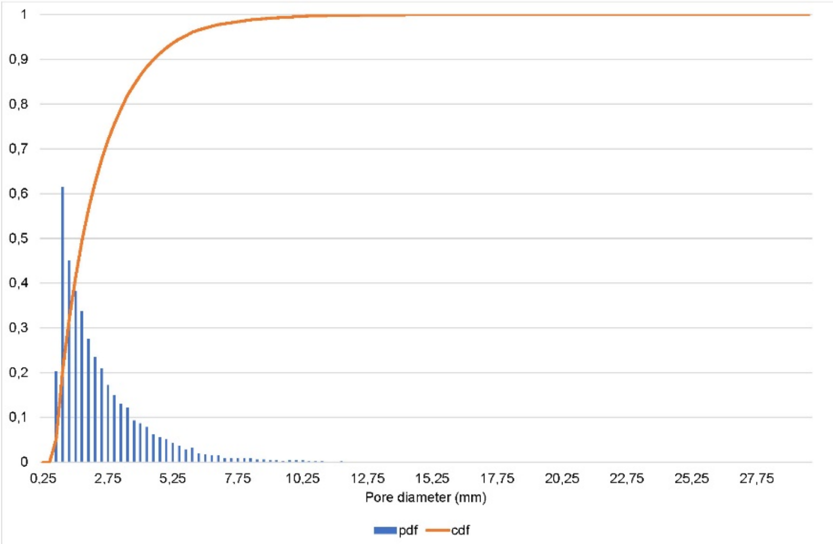

(h)

Figure 32 - Pore size distribution $(PSD)_{pore}$ obtained through XRT. 13 a – PA6 b – PA7A c – PA7B d – PA7C e – PA7D f – PA1A g – PA1B h – PA1C.

6.3. Modeled permeability

The Kozeny-Kovàv model was used to estimate the k_{sat} (Table 31). The results showed a significant difference between measured and modeled attesting that the falling head permeameter used does not yield a quantitative permeability coefficient.

Table 31 - Permeability coefficient measured and modeled.

ID	discharge time (s)	k measured (m/s)	effective porosity	d_{30}	k_{sat} modeled (m/s)	RPD[1]
PA1	47,00	4,78E-05	0,15	1,47	6,32E-04	1223%
PA6	14,00	1,60E-04	0,25	1,22	7,25E-04	352%
PA7	12,00	1,87E-04	0,21	1,12	5,13E-04	174%

[1] RPD: relative percent difference between measured and modeled results.

6.4. Dry deposition analysis

6.4.1. Build-up

The Equations 3 and 4 (Item 4.1) were used to determine the Accu coefficient for the sampled areas considering a cleaning efficient of 100% and 80%. Although the areas were on the same zone and with similar land use (highly inhabited residential) the Accu coefficients were distinct between samples.

On the [MI_zanoia_4_nov_2016] sample the accu was higher from the expect value (10 – 25 kg//(ha.day)) and higher from the industrial reference value (35 kg/ha-day). This can be explained by the fact that the street confines with a park that contribute with sediments. In fact, although it is a narrow street with mostly local traffic has a twice a week road cleaning frequency.

On the other hand, the [MI_romagna_2_nov_2016] sample showed a lower accumulation parameter even though it's a collectors highly traffic road. A possible explanation is the presence of trees above the sampled area function as filters for PM. That fact is already observed on literature (Nowak, Hirabayashi, [159]).

Table 32 - Parameter Accu calculated for the Build-up exponential law

	Accu	
Sample ID	**Efficient cleaning supposed to be 100% [kg/(ha · day)]**	**Efficient cleaning supposed to be 80% [kg/(ha · day)]**
MI_golgi_17_ott_2016	14	13
MI_pascoli_21_ott_2016	35	30
MI_romagna_2_nov_2016	5	4
MI_zanoia_4_nov_2016	70	58

6.4.2. Granulometric indices

The main granulometric indices of the samples are present on Table 33 and the particle size distribution on Figure 33. The d_{50} ranged from 524 to 1767 μm, coarser than obtained on literature (Table 15). The sampling on the shoulders could explain a coarser material, where the finer material remained on the center, also some finer material could be loss on the sampling process.

The uniformity coefficient confirm the dry deposition PM has non uniformity characteristics.

Table 33 - Descriptive index of the samples.

Sample ID	d_{10} [µm]	d_{50} [µm]	d_{60} [µm]	d_{90} [µm]	U [-]
MI_golgi_17_ott_2016	185	1767	2502	6794	13,5
MI_pascoli_21_ott_2016	75	1150	1732	5954	23,1
MI_romagna_2_nov_2016	75	738	1092	3862	14,6
MI_zanoia_4_nov_2016	89	524	715	1780	8,0

The curves can be summarized with gamma parameter of shape (α) and scale (β). The k-s tested attested with statistically significance that the gamma distribution represents the particle size distribution measured data.

Table 34 - Summary for particle size distribution and Kolmogorov-Smirnov goodness of fit test.

Sample ID	Gamma distribution			Goodness of fit(1)		
	α	β	SSE	p-value	k-s	Hp. Null(2)
MI_golgi_17_ott_2016	0,80	3,45	36,35	0,9448	0,1667	true
MI_pascoli_21_ott_2016	0,57	3,89	142,05	0,3874	0,2941	true
MI_romagna_2_nov_2016	0,56	2,57	284,39	0,3874	0,2941	true
MI_zanoia_4_nov_2016	1,09	0,66	307,97	0,3874	0,2941	True

(1) Fit of the cumulative gamma distribution.
(2) Null hypothesis that the samples are drawn for identical distribution ($p > 0,05$). True or false.

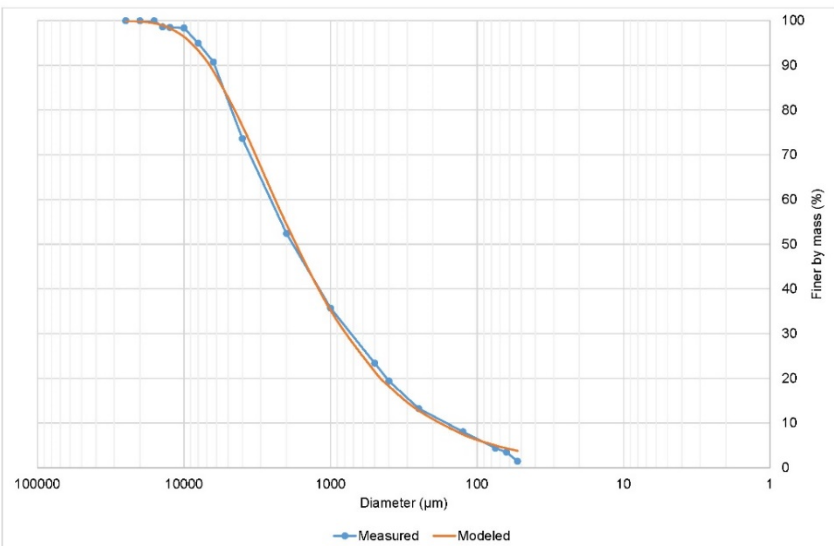

(a)

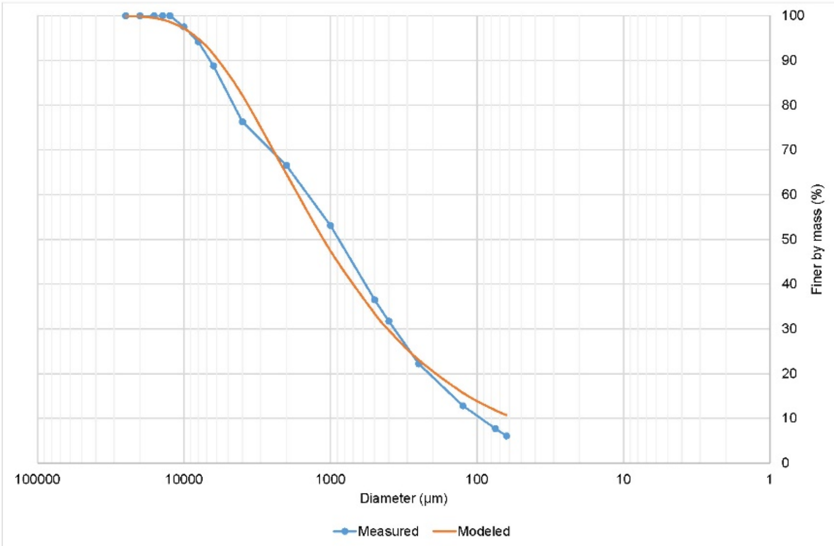
100
90
80
70
60
50
40
30
20
10
0
Finer by mass (%)
100000
10000
1000
100
10
1
Diameter (µm)
Measured
Modeled

(b)

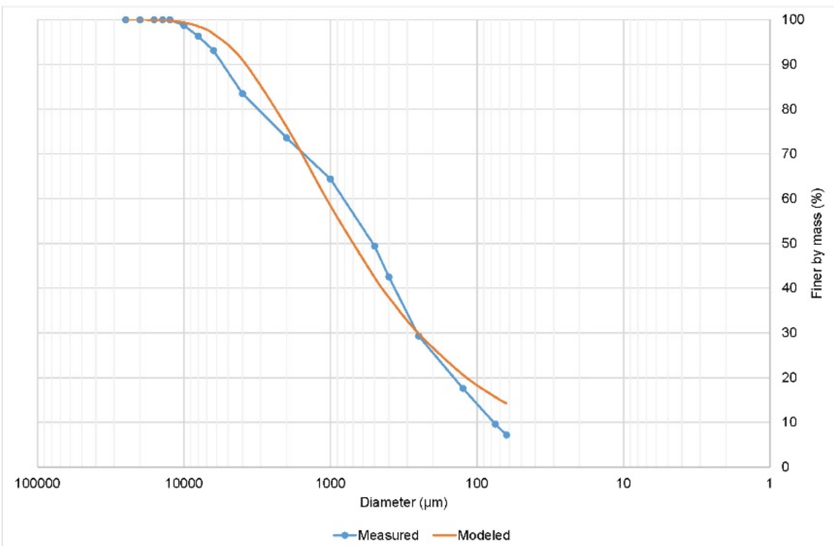
100
90
80
70
60
50
40
30
20
10
0
Finer by mass (%)
100000
10000
1000
100
10
1
Diameter (µm)
Measured
Modeled

(c)

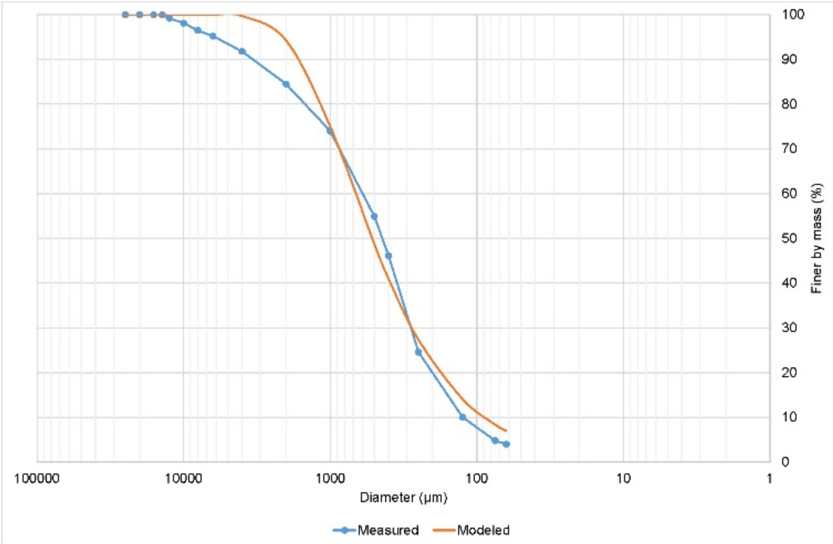

(d)

Figure 33 - Particle size distribution measured and modeled. a – MI_golgi_17_ott_2016 b – MI_pascoli_21_ott_2016 c – MI_romagna_2_nov_2016 d - MI_zanoia_4_nov_2016.

Kruskal-Wallis test verified that the four samples did not show a significantly statistically difference between particle size distributions (Table 35 and Figure 34).

Table 35 - Summary of Kruskal-Wallis test

sieve [µm]	% finer by mass			
	MI_golgi_17_ott_2016	MI_pascoli_21_ott_2016	MI_romagna_2_nov_2016	MI_zanoia_4_nov_2016
25000	100,00	100,0	100,0	100,0
20000	100,00	100,0	100,0	100,0
16000	100,00	100,0	100,0	100,0
14000	98,62	100,0	100,0	100,0
12500	98,48	100,0	100,0	99,2
10000	98,36	97,5	98,7	98,1
8000	94,96	94,2	96,3	96,5
6300	90,76	88,8	93,1	95,2
4000	73,64	76,3	83,5	91,8
2000	52,38	66,5	73,6	84,5
1000	35,74	53,1	64,4	74
500	23,38	36,5	49,4	54,9
400	19,4	31,7	42,5	46,1
250	13,24	22,2	29,3	24,6
125	8,06	12,8	17,6	10
75	4,38	7,7	9,6	4,8
63	4,92	6,1	7,2	4
Kruskal-Wallis test p-value = 0,8892				

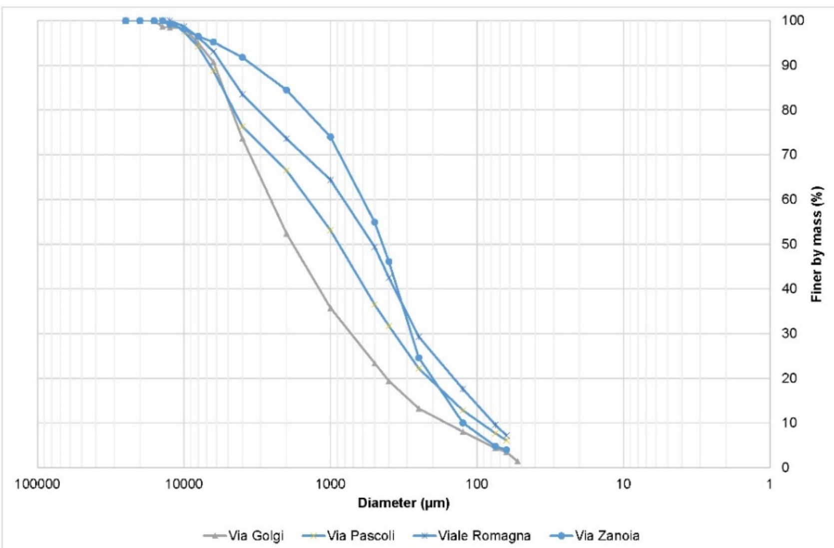

Figure 34 - Oarticle size distribution of four samples.

On Figure 35 is plotted the particle number density for the four samples on the means of log(Inv,it) and log(ni). Log(Inv,it) is equal the d_{median} for each sieve. The particle number density was well represented by a power law (Table 36).

Table 36 - Summary for PND (Particle Number Density) using the Power law and Kolmogorov-Smirnov goodness of fit test

Sample ID	**Power law:** $N_i = a \cdot (lnv, i)^{-\beta}$			**K-S test**		
	α	***β***	***r²***	**p-value**	**k-s**	**Hp. null**
MI_golgi_17_ott_2016	3,08E+16	3,78	0,984	0,869	0,200	True
MI_pascoli_21_ott_2016	2,89E+11	2,93	0,804	0,348	0,313	True
MI_romagna_2_nov_2016	2,98E+11	2,96	0,760	0,163	0,375	True
MI_zanoia_4_nov_2016	3,07E+11	2,97	0,739	0,163	0,375	true

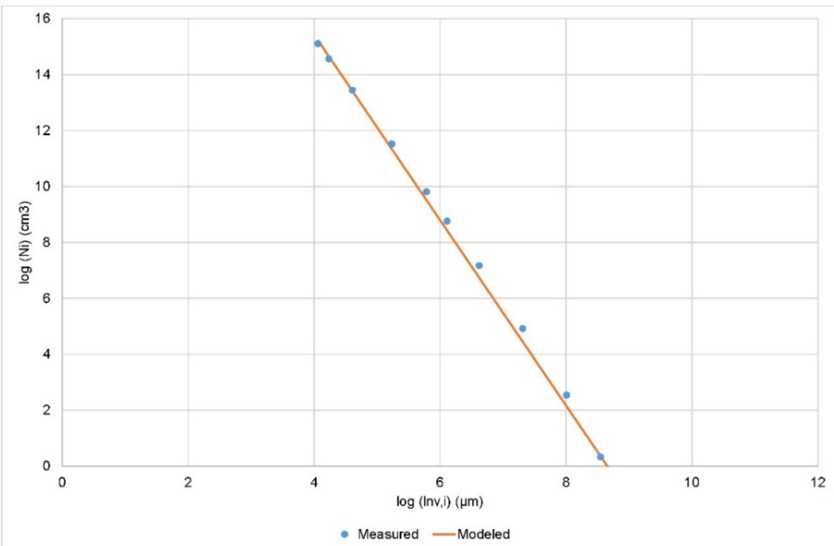

(a)

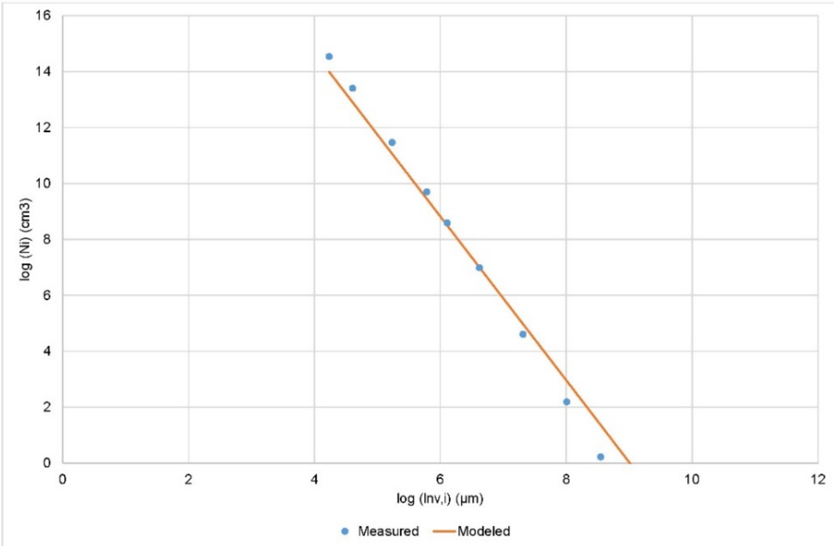
16
14
12
10
8
6
4
2
0
log (Ni) (cm3)
0
2
4
6
8
10
12
log (lnv,i) (μm)
Measured
Modeled

(b)

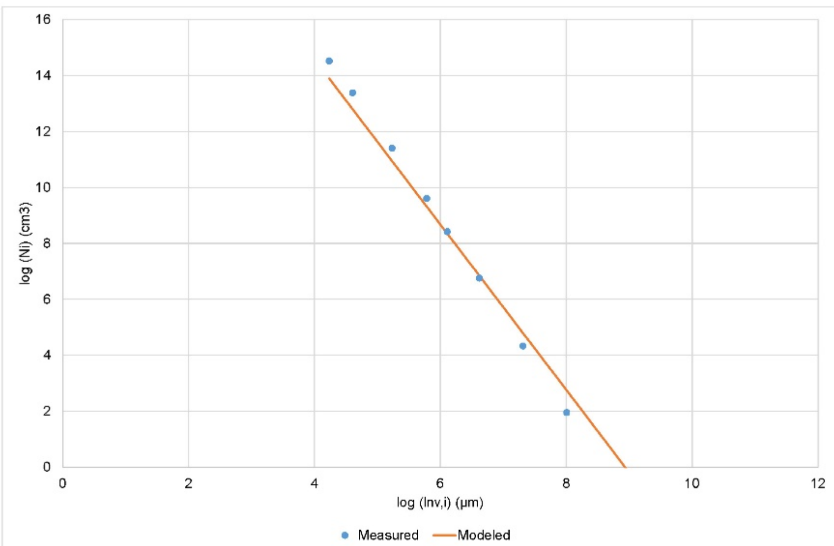
16
14
12
10
8
6
4
2
0
log (Ni) (cm3)
0
2
4
6
8
10
12
log (lnv,i) (μm)
Measured
Modeled

(c)

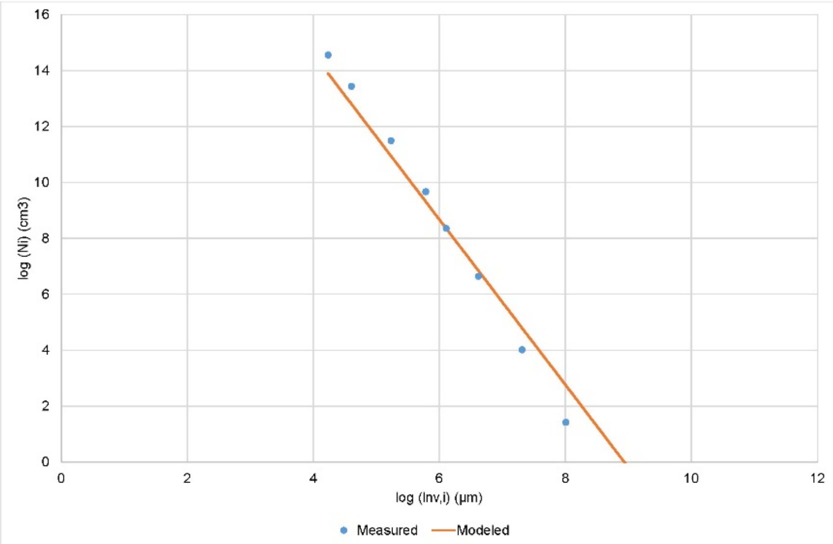

(d)

Figure 35 – Particle number distribution (PND) on the means of log(Lnv,i) and log(Ni) measured and modeled. a – MI_golgi_17_ott_2016 b – MI_pascoli_21_ott_2016 c – MI_romagna_2_nov_2016 d - MI_zanoia_4_nov_2016.

6.5. Filtration mechanism model

The mechanistic model proposed by (McDowell-Boyer, Hunt, [32]) and mentioned on 5.7 was applied for the laboratory sediment and compare with the laboratory data for validation. The results obtained for cake and straining were present together since the experimental data wouldn't allow measure then separately. The measured and modeled data presented a maximum of 8% of relative percent difference. Even though its simplicity the model presented accurate results under the test conditions.

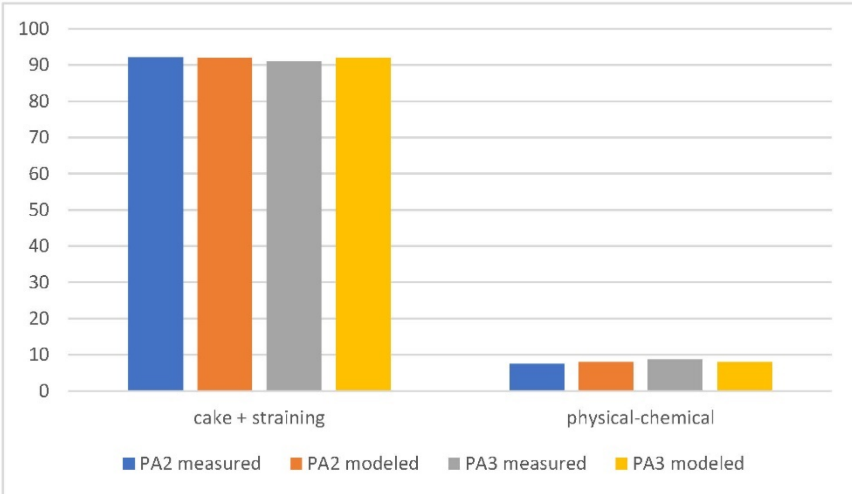

Figure 36 - Dominant filtration mechanism modeled and measured.

The model was then applied for the dry deposition PM samples. For all three porosities 87% of the sediments mass would be retained on the specimen surface creating a "cake".

The percent of sediment mass that would be most likely retained on the specimen core through the straining mechanism was 5% for the PA8 (20% porosity) 10% for the PA2 (25% porosity) and 9% for the PA2 (15% porosity).

The percent of sediment mass that would most likely pass through the specimen or be retained only by physical-chemical process was 8% for the PA8 (20% porosity) 3% for the PA2 (25% porosity) and 4% for the PA2 (15% porosity).

The results depend only on the pore diameter median and not on the porosity, which can explain equivalent results for different porosities and also less material passing through the 25 porosity specimen than the 15%.

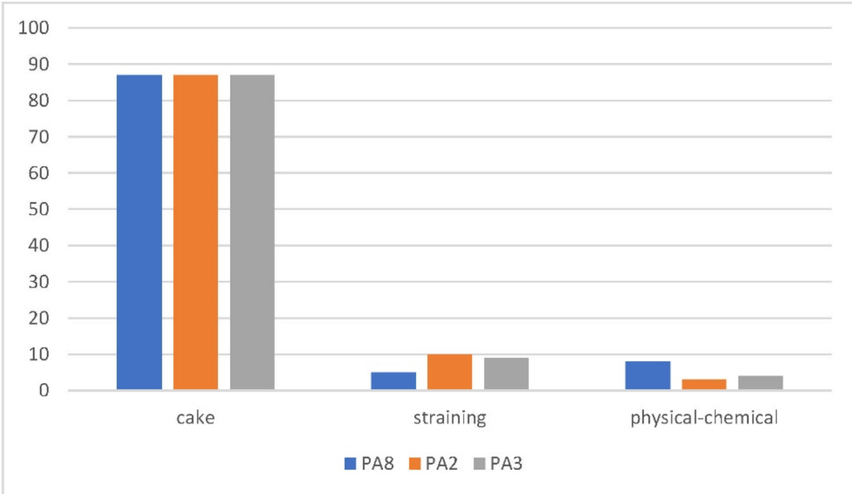

Figure 37 - Dominant filtration mechanism modeled with dry deposition PM sampled and porous asphalt specimens. PA8: 20% porosity; PA2: 25% porosity; PA3: 15% porosity.

7. Discussion of results

Porous asphalt and pervious concrete specimens were produced with a mix design obtained on previous studies. Permeability was measured on initial conditions using an in situ falling head permeameter according CEN EN 12697-40:2012 ((CEN), [118]). The discharge time ranged from 5 to 105 s, the hydraulic conductivity (HC) from 0,26 to 0,01s^{-1} and the coefficient of permeability (k) from 4,94.10^{-4} to 2,14.10^{-5} m/s. As expected, the lowest discharge time was measured on the 25% porosity specimen while the highest with the 15%.

The sediments load was then uniformly applied on the surface of the specimens and the permeability was measured again observing a reduction of discharge time on an exponential trend and a strong correlation between discharge time and loading. It was also observed a strong correlation between discharge time and porosity following a power law trend.

Rainfall simulation was used to investigate runoff and permeability response for different materials (PC and PA), porosities (15%, 20% and 25% bulk density) rainfall intensities (50 mm/h, 100 mm/h and 150 mm/h), rainfall duration (15 min and 30 min), slope (2,5% and 7,0%) and aerial loadings (0,5 kg/m^2, 1,0 kg/m^2 and 2,0 kg/m^2). Statistical analysis was performed to investigate the impact of each parameter. Rainfall intensities only produce statistically significant difference on discharge time for the 150 mm/h rainfall intensity on the pervious concrete specimens. The slope variation didn’t produce a statistically significant difference for discharge time. The discharge time between different materials produced a statistically significant difference.

After the first round of tests the specimens where cleaned and the permeability was measured, observing a reduction in comparation with the initial discharge from 28% to 44% depending on the specimen. This reduction was statistically significant and is concluded that it wasn’t possible to return to initial permeability. The material retained on the surface (cake) was easily removed, rather than the one on the core of the specimen. The 15% porosity specimen suffered the most decay on permeability.

The runoff coefficient results didn’t show a clear trend. The only parameters that result on a statistically significance impact on runoff coefficient were rainfall intensities for the pervious concrete 15% porosity specimen and slope for both pervious concrete and porous asphalt. Runoff volume increased only for high intensities, low porosity and higher slope. Results presented an average of 0,07 and 47% of tests presented zero (0,00) runoff volume, being considered generally low even for specimens considered clogged according to discharge time (> 300 s).

The rainfall-runoff transportation process depends on a series of watershed characteristics besides surface infiltration. That could explain that even with a low infiltration rate the specimen didn’t generate runoff on the test conditions. The roughness of the surface and the small slope allowed stormwater retention enough time to eventually infiltrate. In fact, the highest runoff coefficient was obtained when the slope increase to 7,0%.

A weak correlation was observed between discharge time and runoff coefficient, confirming that other factors have also influence. Considering that infiltration (permeability) is used to evaluate permeable pavement is important to take account of all parameters that impact the rainfall-runoff transformation, such as slope.

Still discussing rainfall simulation results, the majority (> 85%) of the sediments load was retained on the specimens surfaces ("cake") and on the core. Less than 15% leached through the specimens consisting mostly fine material. Just a small part of the sediments (< 2%) was washed off with runoff. The "cake" formed on the surface due to sediments trapping allow to retain finer materials that otherwise would pass through the porous material, increasing the pollutants load removal. On the test conditions the formation of the cake did not increase runoff volume at the point that the pavement would be considered not functional. The portion of sediments loads that pass though the specimen could potentially reach soil below the structure and a possible solution is to use a geotextile membrane that could retain the finer fraction of sediments.

Afterwards, three porous asphalt samples went through XRT analysis to obtain pore structure parameter (total and effective porosity, pore area and pore diameter). The total porosity and effective porosity presented analogous results confirming the visual observation that the pores highly interconnect. There was also good accordance with the bulk density porosity obtained with gravimetric method and the obtained through XRT. The pore diameter obtained was in accordance with the diameters mentioned on literature.

The Kozeny-Kovàv model was used to determine k_{sat} using the pore diameter (d_{30}) obtained with XRT. The results range from $5{,}88.10^{-4}$ to $6{,}49.10^{-4}$ m/s where the lowest k_{sat} was observed on the 15% porosity specimen as expected. The modeled showed a low accordance with the measured results obtained with the falling head permeameter, confirming that this device did not yield the darcyan k_{sat}. This method is able to provide a qualitative analysis of permeability on porous surfaces. In this case the use of discharge time, i.e., the time for a falling head of 20 cm, provides a simple parameter for porous surface efficiency analysis.

A sampling program collect dry deposition PM on four streets in a mostly residential zone in Milan (Italy). The accumulation rate (build-up) showed a wide range of results for the same zone (13 – 58 kg/ha.day for 80% of cleaning efficiency) inferring that the surroundings of the sample area have an impact on accumulation rate. The lowest accumulation rate was obtained when the sampling under a tree zone, suggesting a retention of PM effect of the trees. This highlights the importance of trees presence on urban area.

The particle size distribution of the collect material present a d_{50} ranging from 524 – 1767 µm. The coarser gradation comparing to literature may be a result of the sampling on the shoulder area of the pavement or loss of finer materials during the sampling process. The uniformity coefficient (U) ranged from 8,0 – 13,5 confirming a non-uniform gradation. The four samples did not shown statistically difference on particle size distribution and were satisfactory model using a gamma distribution.

The filtration mechanism between the porous asphalt specimens and the dry deposition PM samples were evaluated through a mechanistic model relating pore media diameter and particle diameter. Almost 90% of the loadings would be retained on the surface forming the “cake”, around 10% would remain on the core through straining mechanism and less than 10% would pass the porous media and could be only retained by physical-chemical process. This result was validate using the laboratory data with satisfactory accordance.

Results main points:

- No significant runoff observed under test conditions;
- Weak correlation between permeability and runoff;
- Low agreement between falling head permeameter measured and model permeability;
- Similar total and effective porosity;
- Importance of surroundings on sediments accumulation (build-up);
- “Cake” was the domination mechanism of filtration 90% retained material
- Satisfactory accordance between model and measured dry deposition PM fate.

8. Conclusion

The currently urbanization scenario demands a compressive stormwater management emphasizing source infiltration and pollutants load removal. Permeable pavement is among the measurements known as SuDS that acts on runoff water quantity, quality and provide biodiversity and amenities opportunities. Permeable pavement is an established technology already market available and mentioned on regulations and standards. Current research focus on clogging, materials characteristics and modelling.

This experimental research used rainfall simulation, x-ray micro-CT tomography (XRT) and field material sampling to investigate aspects of runoff quantity and load removal on porous surfaces (PC and PA) used on permeable pavement.

Infiltration measurements on initial conditions showed the permeability dependence on porosity and clogging. Rainfall simulation was then used to assess runoff volume and permeability response under different conditions. Permeability is normally measured on permeable pavement using falling head permeameter due to simplicity, especially on field, but this device does not yield darcyan hydraulic conductivity (k_{sat}) and should be used only on qualitative bases. Knowing also that k results are highly dependent of test method and test conditions it would be crucial to have a single test method to evaluate permeable pavement with a database of acceptable results to be used for acceptance/refusal.

Further on, specimens that were considered completely clogged through permeability standards, therefore showing a low infiltration rate, still functioned on runoff volume reduction. Although important, infiltration is not the only parameter impacting rainfall-runoff transformation and thus to evaluate permeable pavement a globally parameter analysis should be considered. The roughness and slope showed to be important factors on runoff volume. Permeable pavements guidelines in fact recommend a maximum 5% slope to facilitate water infiltration.

Pore structure parameters that are complex to obtain through conventional methods were obtained through XRT. Once established a code to obtain the parameters the test became simple and would allow to obtain results relatively easier and faster than the conventional methods. However, the method cost would be currently impractical outside research environment. The total porosity results were in accordance with the ones obtained through bulk density. The total porosity and effective porosity, both obtained through XRT, presented analogous results and confirmed visual observation of highly interconnected pores.

The second part focused on pollutants load present on runoff. Four dry deposition PM samples were collected on highly inhabited area in Milan (Italy) and was obtained the accumulation rate (build-up) and granulometric indices. The accumulation rate showed to be dependent on the surroundings conditions and was observed a positive aspect on PM retention on zones with tree presence. A broader sample program should be considered to include more roads with various surroundings conditions to confirm correlations between certain conditions and build-up and more sampling on different dates on the same area to confirm the accumulation rate.

The granulometric indices confirm dry deposition PM as a hetero-disperse non-uniform aggregate. The particle size distribution analysis provide a tool to design porous surface to remove a given percentage of aggregates. Research evidence of metals and other pollutants partitioning into fractions of PM could be used to predict the removal of certain PM-bound pollutants mass on a given PM size. Retaining the coarse material would mean to remove the largest part of the metal inventory.

The filtration mechanisms were investigated experimentally and using a mechanistic model based on pore media and particle diameter. For the studied specimens and loads the dominant mechanism was the accumulation on surface, namely “cake”. The majority part of the loads remained on the porous surface or core through straining. This “cake” results on permeability reduction while function on retaining finer material that otherwise would pass through, hence has an effect of reducing service life while improve pollutants load removal efficiency. The “cake” can be easily removed through maintenance but the process should be done with attention to avoid leach the contaminated material. Used to design separation and investigate the clogging mechanism.

In conclusion, this research investigates porous surfaces for permeable pavement runoff volume and pollutants load through an experimental program of rainfall simulation, XRT and dry deposition PM field sampling and permeability and filtration modelling. The results showed the efficiency of both type of tested materials (PC and PA) for runoff volume reduction and pollutants load removal under the tested conditions. The permeability model showed that the falling head permeameter did not yield a darcyan hydraulic conductivity. The filtration mechanism model showed good accordance between measured and modeled results.

9. Final considerations

On European context is still necessary to have a standard test method to evaluated permeable pavement performance. A database of results using this test method should provide a guidance to asses acceptance or refusal.

A broader sampling plan of dry deposition PM including more roads and more sampling on the same road could confirm the accumulation rate and surrounding influence observed on this research. Chemical analysis on the material fractions and toxicity analysis could be an important addition.

A computational fluid dynamics (CDF) model using the porous materials pore structure and granulometric indices could give more accurate view of filtration mechanism and pollutants load fate.

A combination of parameter studied on this research like permeability with infiltration tests, PM accumulation rate and filtration mechanism could be used to develop a model to predict clogging and define maintenance routines and could be a follow up of this research.

References

[1] Andrés-Valeri, V.C., et al., *Laboratory assessment of the infiltration capacity reduction in clogged porous mixture surfaces.* Sustainability, 2016. **8**(8): p. 751.

[2] Brugin, M., et al., *Clogging potential evaluation of porous mixture surfaces used in permeable pavement systems.* European Journal of Environmental and Civil Engineering, 2017: p. 1-11.

[3] Marchioni, M. and G. Becciu, *Experimental Results On Permeable Pavements In Urban Areas: A Synthetic Review.* International Journal of Sustainable Development and Planning, 2015. **10**(6): p. 806-817.

[4] 0 (ISTAT), I.n.d.s., *Forme, livelli e dinamiche dell'urbanizzazione in italia*. 2017.

[5] Alves Filho, A.P. and H. Ribeiro, *Configuração Espacial de eventos de precipitação extrema na Região Metropolitana de São Paulo: interações entre a ilha de calor e a entrada da brisa oceânica.* InterfacEHS, 2007. **2**: p. 1-8.

[6] Sansalone, J.J., et al., *Event-based stormwater quality and quantity loadings from elevated urban infrastructure affected by transportation.* Water Environment Research, 2005. **77**(4): p. 348-365.

[7] Becciu, G., M. Ghia, and S. Mambretti, *A Century Of Works On River Seveso: From Unregulated Development To Basin Reclamation.* International Journal of Environmental Impacts, 2018. **1**(4): p. 461-472.

[8] Lamera, C., et al., *Green roofs effects on the urban water cycle components.* Procedia Engineering, 2014. **70**: p. 988-997.

[9] Marchioni, M.L. and G. Becciu, *Permeable pavement used on sustainable drainage systems (SUDs): a synthetic review of recent literature.* WIT Press Urban Water II, 2014: p. 12.

[10] Field, R. and A.N. Tafuri, *The Use of Best Management Practices (BMPs) in Urban Watersheds*. 2006: DEStech Publications.

[11] Woods-Ballard, B., et al., *The SUDS manual (C697)*. 2007: CIRIA.

[12] Pratt, C.J., *Use of permeable, reservoir pavement constructions for stormwater treatment and storage for re-use.* Water Science and Technology, 1999. **39**(5): p. 145-151.

[13] Imran, H.M., S. Akib, and M.R. Karim, *Permeable pavement and stormwater management systems: a review.* Environmental Technology, 2013. **34**(18): p. 2649-2656.

[14] Sañudo-Fontaneda, L., et al. *Comparison of the Infiltration Capacity of Permeable Surfaces for Rainwater Energy Valorization*. in *Proceedings of the 12th International Conference on Urban Drainage (ICUD)*.

[15] Asaeda, T. and V.T. Ca, *Characteristics of permeable pavement during hot summer weather and impact on the thermal environment.* Building and Environment, 2000. **35**(4): p. 363-375.

[16] Smith, D.R. *Evaluations of concrete grid pavements in the United States*. in *Second International Conference on Concrete Block Paving*. 1984. Delft.

[17] Sarat, A.-A. and M.A. Eusuf, *Effects of pavement surface temperature on the modification of urban thermal environment.* DIMENSI (Jurnal Teknik Arsitektur), 2012. **39**(1): p. 1-4.

[18] de Melo, J.V.S., et al., *Development and evaluation of the efficiency of photocatalytic pavement blocks in the laboratory and after one year in the field.* Construction and Building Materials, 2012. **37**(0): p. 310-319.

[19] Scholz, M. and V.C. Uzomah, *Rapid decision support tool based on novel ecosystem service variables for retrofitting of permeable pavement systems in the presence of trees.* Science of The Total Environment, 2013. **458–460**(0): p. 486-498.

[20] Kia, A., H.S. Wong, and C.R. Cheeseman, *Clogging in permeable concrete: A review.* Journal of Environmental Management, 2017. **193**: p. 221-233.

[21] Sansalone, J. and C. Cristina, *Gradation-based metal mass prediction utilizing granulometry of snow particulate residuals.* J. Environ. Eng, 2004. **130**(12): p. 1488-1497.10.

[22] 0 United Nations, D.o.E.a.S.A.U., *World urbanization prospects: The 2014 revision, highlights. department of economic and social affairs*, in *Population Division, United Nations*. 2014.

[23] Gibelli, M. and E. Salzano, *No sprawl.* 2006.

[24] (FAO-UN), F.a.A.O.o.t.U.N., *Status of the World's Soil Resources (SWSR)–Main Report.* Food and Agriculture Organization of the United Nations and Intergovernmental Technical Panel on Soils, Rome, Italy, 2015. **650**.

[25] Chow, V.T., D.R. Maidment, and L.W. Mays, *Applied hydrology*. 1988.

[26] Becciu, G. and A. Paoletti, *Fondamenti di costruzioni idrauliche*. 2010: Utet Scienze tecniche.

[27] 0 Woods Ballard, B., et al., *The SuDS Manual, C753, CIRIA, London, UK*. 2015, ISBN 978-0-86017-760-9. http://www. susdrain. org/resources/SuDS_Manual. html.

[28] Water, U.S.E.P.A.O.o., *Urbanization and Streams: Studies of Hydrologic Impacts*. 1997: U.S. Environmental Protection Agency, Office of Water.

[29] (USEPA), O.o.W.U.S.E.P.A., *Urbanization and Streams: Studies of Hydrologic Impacts*. 1997: U.S. Environmental Protection Agency, Office of Water.

[30] Kertesz, R. and J. Sansalone, *Hydrologic Transport of Thermal Energy from Pavement.* Journal of Environmental Engineering, 2014. **140**(8).

[31] Sansalone, J., X. Kuang, and V. Ranieri, *Permeable pavement as a hydraulic and filtration interface for urban drainage.* Journal of irrigation and drainage engineering, 2008. **134**(5): p. 666-674.

[32] McDowell-Boyer, L.M., J.R. Hunt, and N. Sitar, *Particle transport through porous media.* Water Resources Research, 1986. **22**(13): p. 1901-1921.

[33] Sansalone, J.J., et al., *Physical characteristics of urban roadway solids transported during rain events.* Journal of Environmental Engineering, 1998. **124**(5): p. 427-440.

[34] (USEPA), U.E.P.A. *Seminar publications - EPA/625/R-95/003.* in *National Conference on Urban Runoff Management: Enhancing Urban Watershed Management at the Local, County, and State Levels*. 1993. Chicago.

[35] 0 (BR), S.P., *Manual de Drenagem e manejo de águas pluviais: gerenciamendo do sistema de drenagem urbana.*, S.M.d.D.U. (SMDU), Editor. 2012: São Paulo. p. 168.

[36] 0 (BR), S.P., *Manual de Drenagem e manejo de águas pluviais: aspectos tecnológicos, diretrizes para projetos.*, S.M.d.D.U. (SMDU), Editor. 2012: São Paulo. p. 128.

[37] Tucci, C.E., *Gestão de águas pluviais urbanas*. 2005: Programa de Modernização do Setor Saneamento, Secretaria Nacional de Saneamento Ambiental, Ministério das Cidades.
[38] Elliott, A.H. and S.A. Trowsdale, *A review of models for low impact urban stormwater drainage.* Environmental Modelling & Software, 2007. **22**(3): p. 394-405.
[39] Pyke, A. *Great Western Park, Didcot*. in *SuDS Conference*. 2012. Oxfordshire.
[40] Ahiablame, L.M., B.A. Engel, and I. Chaubey, *Effectiveness of low impact development practices in two urbanized watersheds: Retrofitting with rain barrel/cistern and porous pavement.* Journal of Environmental Management, 2013. **119**(0): p. 151-161.
[41] Gnecco, I. and A. Palla. *Analyzing the resilience of a sustainable urban catchment to climate change effects*. in *XXXV Convegno Nazionale di Idraulica e Costruzione Idrauliche Bologna*. 2016. Bologna.
[42] Sansalone, J., et al., *Retrofitting impervious urban infrastructure with green technology for rainfall-runoff restoration, indirect reuse and pollution load reduction.* Environmental Pollution, 2013. **183**(0): p. 204-212.
[43] 0 (EU), E.C., *Water framework directive 2000/60/EC*, T.E.P.A.T.C.O. THE and E. UNION, Editors. 2000.
[44] 0 Kingdom, U., *Flood and water management act.*, C. 29, Editor. 2010. p. 84.
[45] Act, C.W., *Federal Water Pollution Control Act.* As Amended Through PL, 2002: p. 107-133.
[46] (US), D.o.C.W.a.S.A. *Impervious Area Charge*. [cited 2018 13/04/2018]; Available from: https://www.dcwater.com/impervious-area-charge.
[47] (US), D.o.C.D.o.E.E. *Stormwater Fee Background*. [cited 2018 13/04/2018]; Available from: https://doee.dc.gov/service/stormwater-fee-background.
[48] (US), D.o.C.W.a.S.A. *Impervious Area Charge Incentive Program*. [cited 2018 13/04/2018]; Available from: https://www.dcwater.com/iac-incentive.
[49] (US), D.o.C.D.o.E.a.E. *RiverSmart Rewards and Clean Rivers IAC Incentive Programs*. [cited 2018 13/04/2018]; Available from: https://doee.dc.gov/riversmartrewards.
[50] Ferguson, B.K., *Porous Pavements*. 2005: Taylor & Francis.
[51] Weiss, P.T., et al., *Permeable pavement in northern North American urban areas: research review and knowledge gaps.* International Journal of Pavement Engineering, 2017: p. 1-20.
[52] Pratt, C.J., *Sustainable drainage: A review of published material on the performance of various SUDS components.* Prepared for the Environment Agency. SUDS Science Group/99705.015, 2004.
[53] Hogland, W., J. Niemczynowicz, and T. Wajlman, *The unit superstructure during the construction period.* Science of the Total Environment, 1987. **59**: p. 411-424.
[54] Fujita, S. *Experimental sewer system for reduction of urban storm runoff*. in *INTERNATIONAL CONFERENCE ON URBAN STORM DRAINAGE*. 1984.
[55] Suda, S., et al. *Development and application of permeable paving concrete block*. in *International Conference on Concrete Block Paving, 1988, 3rd, Rome, Italy*. 1988.
[56] Pratt, C.J. *Permeable pavements for stormwater quality enhancement*. in *Urban Stormwater Quality Enhancement@ sSource Control, Retrofitting, and Combined Sewer Technology*. 1990. ASCE.

[57] Pratt, C.J., J. Mantle, and P. Schofield, *UK research into the performance of permeable pavement, reservoir structures in controlling stormwater discharge quantity and quality.* Water science and technology, 1995. **32**(1): p. 63-69.

[58] Teng, Z. and J. Sansalone, *In situ partial exfiltration of rainfall runoff. II: Particle separation.* Journal of environmental engineering, 2004. **130**(9): p. 1008-1020.

[59] Sansalone, J.J. and Z. Teng, *Transient rainfall-runoff loadings to a partial exfiltration system: Implications for urban water quantity and quality.* Journal of Environmental Engineering, 2005. **131**(8): p. 1155-1167.

[60] Brown, R.A. and M. Borst, *Evaluation of surface infiltration testing procedures in permeable pavement systems.* Journal of Environmental Engineering, 2014. **140**(3): p. 04014001.

[61] Ranieri, V., et al., *Measurement of hydraulic conductivity in porous mixes.* Transportation Research Record: Journal of the Transportation Research Board, 2012(2295): p. 1-10.

[62] Casal-Campos, A., C. Jefferies, and S.P. Momparler, *Selecting SUDS in the Valencia region of Spain.* Water Practice and Technology, 2012. **7**(1): p. wpt2012001.

[63] Perales-Momparler, S., et al., *Inner-city SUDS retrofitted sites to promote sustainable stormwater management in the Mediterranean region of Valencia: AQUAVAL (Life+ EU Programme).* NOVATECH 2013, 2013.

[64] Castro-Fresno, D., et al., *Sustainable drainage practices in Spain, specially focused on pervious pavements.* Water, 2013. **5**(1): p. 67-93.

[65] Sañudo-Fontaneda, L.A., et al., *Field study of infiltration capacity reduction of porous mixture surfaces.* Water, 2014. **6**(3): p. 661-669.

[66] Gomez-Ullate, E., et al., *Design and construction of an experimental pervious paved parking area to harvest reusable rainwater.* Water Science and Technology, 2011. **64**(9): p. 1942-1950.

[67] Sañudo-Fontaneda, L., et al., *The Long-Term Hydrological Performance of Permeable Pavement Systems in Northern Spain: An Approach to the "End-of-Life" Concept.* Water, 2018. **10**(4): p. 497.

[68] Brunetti, G., J. Šimůnek, and P. Piro, *A comprehensive numerical analysis of the hydraulic behavior of a permeable pavement.* Journal of Hydrology, 2016. **540**: p. 1146-1161.

[69] Carbone, M., G. Brunetti, and P. Piro, *Hydrological performance of a permeable pavement in Mediterranean climate.* 14th SGEM geoconference on water resources. Forest, marine and ocean ecosystems, 2014: p. 381-388.

[70] (INTERPAVE), T.p.c.p.a.k.a., *Permeable pavements: guide to design, construction and maintenance of concrete block permeable pavements.* 2008, Leicester: INTERPAVE.

[71] Smith, D., *Permeable Interlocking Concrete Pavements: Selection, Design, Construction, Maintenance*. 2006: Interlocking Concrete Pavement Institute.

[72] Pilotti, M. and M. Tomirotti, *Linee Guida per la determinazione della capacità drenante delle pavimentazioni modulari in calcestruzzo*. 2011: ASSOBETON.

[73] Hansen, K., *Porous asphalt pavements for stormwater management.* Lanham, MD: National Asphalt Pavement Association.(Information Series 131), 2008.

[74] Pagotto, C., M. Legret, and P. Le Cloirec, *Comparison of the hydraulic behaviour and the quality of highway runoff water according to the type of pavement.* Water Research, 2000. **34**(18): p. 4446-4454.

[75] 0 Acioli, L.A., *Estudo experimental de pavimentos permeaveis para o controle de escoamento superficial na fonte*, in *Recursos Hidricos e Saneamento Ambiental*. 2005, Universidade Federeal do Rio Grande do Sul: Porto Alegre. p. 162.

[76] 0 Pinto, L.L.C.A., *O desempenho de pavimentos permeáveis como medida mitigadora da impermeabilização do solo urbano.*, in *Escola Politécnica - Engenharia de Transportes*. 2011, Universidade de São Paulo: São Paulo.

[77] 0 Virgiliis, A.L.C.d., *Procedimentos de projeto e execução de pavimentos permeáveis visando retenção e amortecimento de picos de cheias.*, in *Escola Politécnica - Engenharia de Transportes*. 2009, Universidade de São Paulo: São Paulo. p. 213.

[78] Dreelin, E.A., L. Fowler, and C. Ronald Carroll, *A test of porous pavement effectiveness on clay soils during natural storm events.* Water Research, 2006. **40**(4): p. 799-805.

[79] Bean, E.Z., et al., *Study on the surface infiltration rate of permeable pavements.* Proceedings of the American Society of Civil Engineers and EWRI 2004 world water and environmental resources congress, Salt Lake City, UT, USA, 2004. **27**.

[80] Beeldens, A. and G. Herrier. *Water pervious pavement blocks: the belgian experience*. in *8 th International conference on Block Paving materials*. 2006.

[81] 0 (USEPA), O.o.W.U.S.E.P.A., *Flood and Water Management Act 2010 (US)*, T.S. Office, Editor. 2010.

[82] Schlüter, W. and C. Jefferies, *Modelling the outflow from a porous pavement.* Urban Water, 2002. **4**(3): p. 245-253.

[83] Qin, H.-p., Z.-x. Li, and G. Fu, *The effects of low impact development on urban flooding under different rainfall characteristics.* Journal of Environmental Management, 2013. **129**(0): p. 577-585.

[84] Legret, M., V. Colandini, and C. Le Marc, *Effects of a porous pavement with reservoir structure on the quality of runoff water and soil.* Science of The Total Environment, 1996. **189–190**(0): p. 335-340.

[85] Legret, M. and V. Colandini, *Effects of a porous pavement with reservoir structure on runoff water: Water quality and fate of heavy metals.* Water Science and Technology, 1999. **39**(2): p. 111-117.

[86] Kirkpatrick, R., et al. *Improvement Of Water Quality By Coarse Graded Aggregates In Permeable Pavements*. in *Proceedings of the 9th International Conference on Concrete Block Paving. Buenos Aires, Argentina*. 2009.

[87] Dierkes, C., et al. *Pollution retention capability and maintenance of permeable pavements*. in *Global Solutions for Urban Drainage, Proc. of the Ninth Int. Conf. on Urban Drainage, Sept 8-13 2002, Portland, OR*. 2002.

[88] Mullaney, J., P. Rikalainen, and C. Jefferies, *Pollution profiling and particle size distribution within permeable paving units–with and without a geotextile.* Management of Environmental Quality: An International Journal, 2012. **23**(2): p. 150-162.

[89] Morgenroth, J., G. Buchan, and B.C. Scharenbroch, *Belowground effects of porous pavements—Soil moisture and chemical properties.* Ecological Engineering, 2013. **51**(0): p. 221-228.

[90] McCarthy, D.T., et al., *Intra-event variability of Escherichia coli and total suspended solids in urban stormwater runoff.* Water Research, 2012. **46**(20): p. 6661-6670.

[91] Tota-Maharaj, K. and M. Scholz, *Combined permeable pavement and photocatalytic titanium dioxide oxidation system for urban run-off treatment and disinfection.* Water and Environment Journal, 2013. **27**(3): p. 338-347.
[92] Imteaz, M.A., et al., *Modelling stormwater treatment systems using MUSIC: Accuracy.* Resources, Conservation and Recycling, 2013. **71**(0): p. 15-21.
[93] Kipkie, C., *Feasibility of a permeable pavement option in the storm water management model (SWMM) for long term continuous modelling.* Master of Science Thesis, University of Guelph, 1998.
[94] Smith, D.R., *Permeable Interlocking Concrete Pavements.* America: ICPI, 2000.
[95] Hein, D.K., D. Swan, and L. Schaus. *Structural and hydrological design of permeable pavements*. in *2010 Annual Conference of the Transportation Association of Canada, Halifax*. 2010. Nova Scotia.
[96] Suzuki, C.Y., A.M. Azevedo, and F.I.J. Kabbach, *Drenagem subsuperficial de pavimentos: conceitos e dimensionamento.* 1 ed. Vol. 1. 2013, São Paulo: Oficina de Textos. 240.
[97] 0 BSI, *Pavements constructed with clay, natural stone or concrete paversGuide for the design of permeable pavements constructed with concrete paving blocks and flags, natural stone slabs and setts and clay pavers*. 2009.
[98] Sansalone, J., et al., *Filtration and clogging of permeable pavement loaded by urban drainage.* Water Research, 2012. **46**(20): p. 6763-6774.
[99] Batezini, R. and B. JT, *Study on the hydraulic conductivity by constant and falling head methods for pervious concrete.* Revista IBRACON de Estruturas e Materiais, 2015. **8**(3): p. 248-259.
[100] Neithalath, N., J. Weiss, and J. Olek, *Characterizing Enhanced Porosity Concrete using electrical impedance to predict acoustic and hydraulic performance.* Cement and Concrete Research, 2006. **36**(11): p. 2074-2085.
[101] Zheng, M., S. Chen, and B. Wang. *Mixture Ratio Design Method for Porous Concrete Permeable Base*. in *9th International Conference on Concrete Pavements*. 2008.
[102] Bonicelli, A., et al., *Laboratory Analysis for Investigating the Impact of Compaction on the Properties of Pervious Concrete Mixtures for Road Pavements.* Advanced Materials Research, 2013. **723**: p. 409-419.
[103] Bonicelli, A., F. Giustozzi, and M. Crispino, *Experimental study on the effects of fine sand addition on differentially compacted pervious concrete.* Construction and Building Materials, 2015. **91**: p. 102-110.
[104] Chen, Y., et al., *Strength, fracture and fatigue of pervious concrete.* Construction and Building Materials, 2013. **42**(0): p. 97-104.
[105] Knappenberger, T., et al., *Monitoring Porous Asphalt Stormwater Infiltration and Outflow.* Journal of Irrigation and Drainage Engineering, 2017. **143**(8): p. 04017027.
[106] Knapton, J. and C. McBride. *Permeable pavements for heavily trafficked roads - a full scale trial*. in *9th International Conference on Concrete Block Paving*. 2009. Argentina.
[107] Jones, D., *Laboratory Testing and Modeling for Structural Performance of Fully Permeable Pavements Under Heavy Traffic: Final Report (Davis, CA: University of California Pavement Research Center).* 2010.
[108] (AASHTO), A.o.S.H.a.T.O., *AASHTO Guide for Design of Pavement Structures, 1993*. Vol. 1. 1993: AASHTO.

[109] Hansen, K., *Porous asphalt pavements for stormwater management.* National Asphalt Pavement Association (NAPA), Lanham, 2008.

[110] Borgwardt, S. *Long-term in-situ infiltration performance of permeable concrete block pavement*. in *Proceedings*. 2006.

[111] de Sousa Pinto, C., *Curso básico de mecânica dos solos: exercícios resolvidos*. 2001: Oficina de Textos.

[112] ABNT, *NBR 16416: Pavimentos permeáveis de concreto: requisitos e procedimentos.* 2015.

[113] Terzaghi, K., R.B. Peck, and G. Mesri, *Soil mechanics in engineering practice*. 1996: John Wiley & Sons.

[114] Marchioni, M.L. and C.O. Silva. *Método de ensaio para avaliação de pavimento permeável executado*. in *55o Congresso Brasileiro do Concreto CBC2013*. 2013. Gramado: IBRACON.

[115] 0 ASTM, *Standard Test Method for Infiltration Rate of In Place Pervious Concrete*. 2009.

[116] Smith, D.R., K. Earley, and J.P.E. Lia. *Potential application of ASTM C1701 for evaluating surface infiltration of permeable interlocking concrete pavements.* in *10th International Conference on Concrete Block Paving*. 2012. Shanghai.

[117] Li, H., M. Kayhanian, and J.T. Harvey, *Comparative field permeability measurement of permeable pavements using ASTM C1701 and NCAT permeameter methods.* Journal of Environmental Management, 2013. **118**(0): p. 144-152.

[118] 0 (CEN), E.C.f.S., *Bituminous Mixtures-Test method for hot mix asphalt Part 40: In situ drainability*, in *BS EN 12697-40:2012*. 2012.

[119] Borst, M., *Surface infiltration rates of permeable surfaces: Six month update (November 2009 through April 2010)*. 2010: National Risk Management Research Laboratory, Water Supply and Water Resources Division, US Environmental Protection Agency.

[120] 0 Jabur, A.S., *Relatório final de pós-doutorado* 2013, Universidade Federal do Rio Grande do Sul. p. 42.

[121] 0 (CEN), E.C.f.S., *Bituminous Mixtures-Test method for hot mix asphalt Part 19: Permeability of specimen.*, in *BS EN 12697-19:2012*. 2012.

[122] Maidment, D.R., *Handbook of hydrology*. Vol. 1. 1993: McGraw-Hill New York.

[123] de Araújo, P.R., C.E. Tucci, and J.A. Goldenfum, *Avaliação da eficiência dos pavimentos permeáveis na redução de escoamento superficial.* 2000.

[124] Collins, R.E., *Flow of fluids through porous materials.* 1976.

[125] Tennis, P.D., et al., *Pervious concrete pavements*. 2004: Portland Cement Association Skokie, IL.

[126] Montes, F., S. Valavala, and L.M. Haselbach, *A new test method for porosity measurements of Portland cement pervious concrete.* Journal of ASTM International, 2005. **2**(1): p. 1-13.

[127] 0 (CEN), E.C.f.S., *Bituminous Mixtures-Test method for hot mix asphalt Part 6: Test methods for hot mix asphalt. Determination of bulk density of bituminous specimens*, in *BS EN 12697-6:2012*. 2012.

[128] Kuang, X., et al., *Examination of Pervious Pavement Pore Parameters with X-Ray Tomography.* Journal of Environmental Engineering, 2015. **141**(10): p. 04015021.

[129] Ranieri, V., et al., *Application of Kozeny-Kovàcs model to predict the hydraulic conductivity of permeable pavements.* Transportation Research Record: Journal of the Transportation Research Board, 2010(2195): p. 168-176.

[130] Chandrappa, A.K. and K.P. Biligiri, *Comprehensive investigation of permeability characteristics of pervious concrete: A hydrodynamic approach.* Construction and Building Materials, 2016. **123**: p. 627-637.
[131] Chen, X., et al., *Innovative Approach for Pavement Runoff Characterization.* Journal of Performance of Constructed Facilities, 2017: p. 04017047.
[132] Tarefder, R. and M. Ahmad, *Evaluation of pore structure and its influence on permeability and moisture damage in asphalt concrete.* International Journal of Pavement Engineering, 2017. **18**(3): p. 274-283.
[133] Nichols, P.W. and T. Lucke, *A Detailed Analysis of Sediment Particle Sizes and Clogging in Permeable Pavements.* CLEAN–Soil, Air, Water, 2017. **45**(4).
[134] Kayhanian, M., et al., *Permeability measurement and scan imaging to assess clogging of pervious concrete pavements in parking lots.* Journal of Environmental management, 2012. **95**(1): p. 114-123.
[135] Manahiloh, K.N., et al., *X-ray computed tomography and nondestructive evaluation of clogging in porous concrete field samples.* Journal of Materials in Civil Engineering, 2012. **24**(8): p. 1103-1109.
[136] Razzaghmanesh, M. and S. Beecham, *A review of permeable pavement clogging investigations and recommended maintenance regimes.* Water, 2018. **10**(3): p. 337.
[137] Yong, C.F., D.T. McCarthy, and A. Deletic, *Predicting physical clogging of porous and permeable pavements.* Journal of Hydrology, 2013. **481**(0): p. 48-55.
[138] Hill, K.D. and S. Beecham, *The Effect of Particle Size on Sediment Accumulation in Permeable Pavements.* Water, 2018. **10**(4): p. 403.
[139] Van Duin, B., et al. *Characterization of long-term solids removal and clogging processes in two types of permeable pavement under cold climate conditions*. in *11th International Conference on Urban Drainage*. 2008.
[140] Gerritts, C. and W. James. *Restoration of infiltration capacity of permeable pavers*. in *Proceedings of 9th International Conference on Urban Drainage. ASCE. Portland, OR*. 2002.
[141] Radfar, A. and T.D. Rockaway, *Clogging prediction of permeable pavement.* Journal of Irrigation and Drainage Engineering, 2016. **142**(4): p. 04015069.
[142] Ying, G. and J. Sansalone, *Transport and solubility of Hetero-disperse dry deposition particulate matter subject to urban source area rainfall–runoff processes.* Journal of hydrology, 2010. **383**(3-4): p. 156-166.
[143] 0 (USEPA), U.S.E.P.A., *Particle Pollution and Your Health*
[144] Sansalone, J., G. Ying, and H. Lin, *Distribution of metals for particulate matter transported in source area rainfall-runoff.* Journal of Environmental Engineering, 2009. **136**(2): p. 172-184.
[145] Sansalone, J. and G. Ying, *Partitioning and granulometric distribution of metal leachate from urban traffic dry deposition particulate matter subject to acidic rainfall and runoff retention.* Water research, 2008. **42**(15): p. 4146-4162.
[146] Deletic, A. and D.W. Orr, *Pollution buildup on road surfaces.* Journal of Environmental Engineering, 2005. **131**(1): p. 49-59.
[147] Bolognesi, A., M. Maglionico, and S. Artina. *Un supporto alla gestione delle caditoie stradali mediante simulazione numeriche di lungo periodo*. in *Acqua e Città '09 - Convegno Nazionale di Idraulica Urbana*. 2009. Milano.
[148] Huber, W.C., et al., *Storm water management model; version 4.* Environmental Protection Agency, United States, 1988.

[149] Chow, M.F., Z. Yusop, and I. Abustan, *Relationship between sediment build-up characteristics and antecedent dry days on different urban road surfaces in Malaysia.* Urban Water Journal, 2015. **12**(3): p. 240-247.

[150] Zhang, H. and J. Sansalone, *Partitioning and first-flush of nitrogen in rainfall-runoff from an urban source area.* Journal of Environmental Engineering, 2014. **140**(8): p. 04014027.

[151] 0 Ranieri, V., et al., *Granulometry of Particulate Matter Recovered from Roadway Systems in Apulia*, in *Transportation Research Board 96th Annual Meeting*, T.R.B. (TRB), Editor. 2017: Washington DC, United States.

[152] Sansalone, J. and T. Tribouillard, *Variation in characteristics of abraded roadway particles as a function of particle size: implications for water quality and drainage.* Transportation Research Record: Journal of the Transportation Research Board, 1999(1690): p. 153-163.

[153] Dickenson, J.A. and J.J. Sansalone, *Distribution and disinfection of bacterial loadings associated with particulate matter fractions transported in urban wet weather flows.* Water research, 2012. **46**(20): p. 6704-6714.

[154] Auset, M. and A.A. Keller, *Pore-scale visualization of colloid straining and filtration in saturated porous media using micromodels.* Water resources research, 2006. **42**(12).

[155] Hudson, N.W. and S. Rhodesia, *The flour pellet method for measuring the size of raindrops*. 1964: Department of Conservation and Extension.

[156] Zafra, C., J. Temprano, and I. Tejero, *Particle size distribution of accumulated sediments on an urban road in rainy weather.* Environmental technology, 2008. **29**(5): p. 571-582.

[157] Bian, B. and W. Zhu, *Particle size distribution and pollutants in road-deposited sediments in different areas of Zhenjiang, China.* Environmental geochemistry and health, 2009. **31**(4): p. 511-520.

[158] Kottegoda, N.T. and R. Rosso, *Applied statistics for civil and environmental engineers*. 2008: Blackwell Chichester, UK.

[159] Nowak, D.J., et al., *Tree and forest effects on air quality and human health in the United States.* Environmental Pollution, 2014. **193**: p. 119-129.

Appendix 1

From Figure 38 to Figure 53 a few examples of permeable pavement sites. Table 37 gathers general information about the sites. All images are from the author's personal collection.

Table 37 - Permeable pavement sites information.

Figure ID	Site location City	Site location Country	Land use	Traffic	Surface material	Observations
Figure 38	São Paulo	Brazil	Road	Local traffic	PICP	One of the first permeable pavement constructed in Brazil
Figure 39	São Paulo	Brazil	Park	Pedestrian	PICP	-
Figure 40	São Paulo	Brazil	Park	Pedestrian	PC slabs	-
Figure 41	Washington	United States	Parking lot	Automobiles and buses	PICP	Highschool overflow parking lot
Figure 42	Washington	United States	Parking lot	Automobile	PICP	Fire station parking lot
Figure 43	New Jersey	United States	Parking lot	Automobile	PA, PC, PICP	(Borst, [34]) (Brown and Borst, [60])
Figure 44	Oxfordshire	England	Local road and sidewalks	Local traffic and pedestrian	PICP	House condo
Figure 45	Oxforshire	England	Local road	Local traffic	PICP	House condo. Part of a SuDS compreensive design.
Figure 46	Sao Paulo	Brazil	Parking spaces	Automobile	PICP	Supermarket
Figure 47	Sao Paulo	Brazil	Parking lot	Automobile	PA and PICP	Mention on
Figure 48	Sao Paulo	Brazil	Parking lot	Automobile	PICP	Shopping mall. Parking lot used to attend construction drainage regulations.
Figure 49	Benaguasil	Spain	Parking lot	Automobile	PA	
Figure 50	Vipiteno	Italy	Parking lot	Automobile	PICP	-
Figure 51	Pesantina	Italy	Parking lot	Automobile	PICP	-
Figure 52	Milan	Italy	Park	Pedestrian	PICP	-
Figure 53	Milan	Italy	Parking lot	Automobile	PICP	-

Note: PA: porous asphalt, PC: pervious concrete.

Figure 38 – Local traffic road. São Paulo (Brazil).


Figure 39 - Park Ibirapuera. São Paulo (Brazil).

Figure 40 - Park Ibirapuera. São Paulo (Brazil).

Figure 41 - Highschool parking lot. Washington, D.C. (United States).

Figure 42 - Fire Station parking lot. Washington, D.C. (United States).

Figure 43 - USEPA parking lot. New Jersey (United States).

Figure 44 - House condo. Oxfordshire (England).


Figure 45 - House condo. Oxfordshire (England).

Figure 46 - Supermarket parking spaces. São Paulo (Brazil).


Figure 47 - University of São Paulo - hydraulic department parking lot. São Paulo (Brazil).

Figure 48 - Shopping mall parking lot. São Paulo (Brazil).

Figure 49 – Youth center parking lot. Benaguasil (Spain).

Figure 50 - Supermarket parking spaces. Vipiteno (Italy).

Figure 51 - Aquardens springs park parking lot. Pesantina (Italy).

Figure 52 – Giardinetto via Gaetano di Castillia. Milan (Italy).

Figure 53 – Parking lot Via Gaetano di Castillia. Milan, Italy.

Appendix 2

This appendix gathers the complete collection of graphical analysis of the rainfall simulation tests on Figure 55 to Figure 87. Figure 54 shows the rainfall simulation tests flow chart.

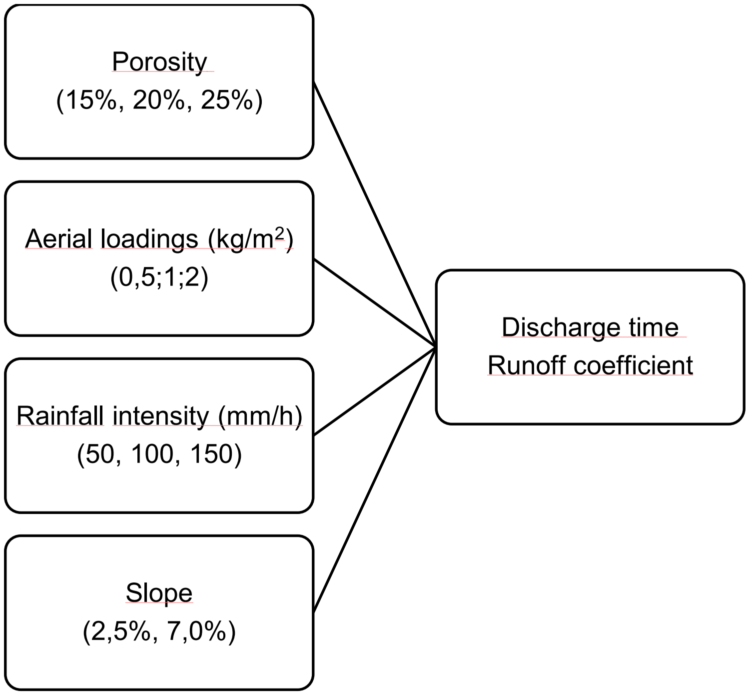

Figure 54 - Flow chart of rainfall simulation tests.

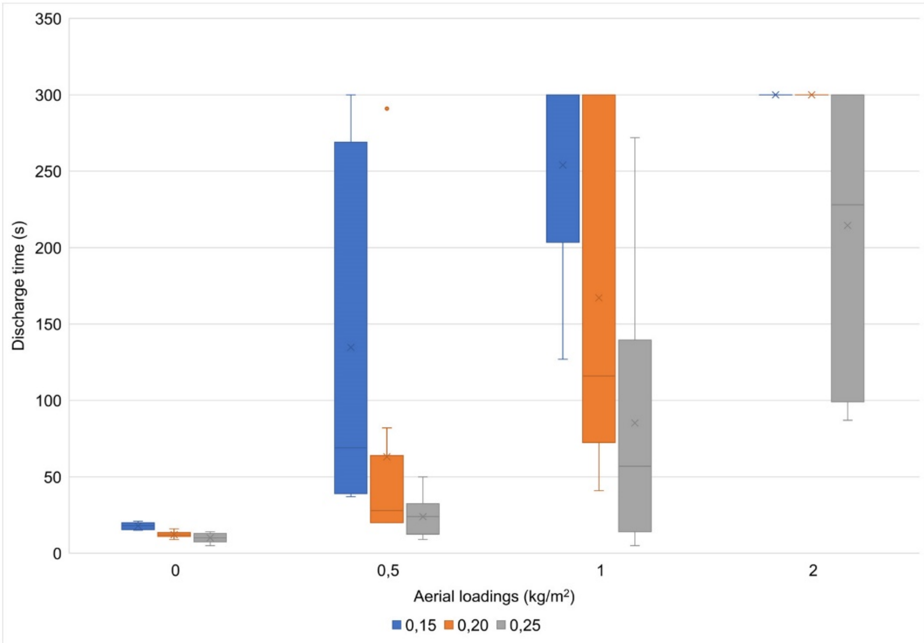

Figure 55 – Pervious concrete discharge time x aerial loadings initial tests.

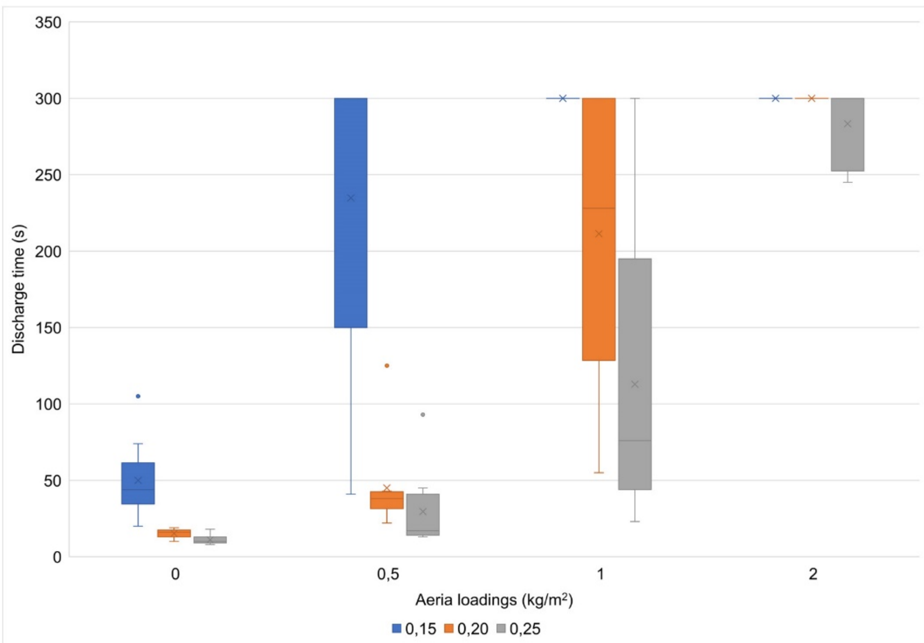

Figure 56 – Porous asphalt discharge time x aerial loadings initial tests.

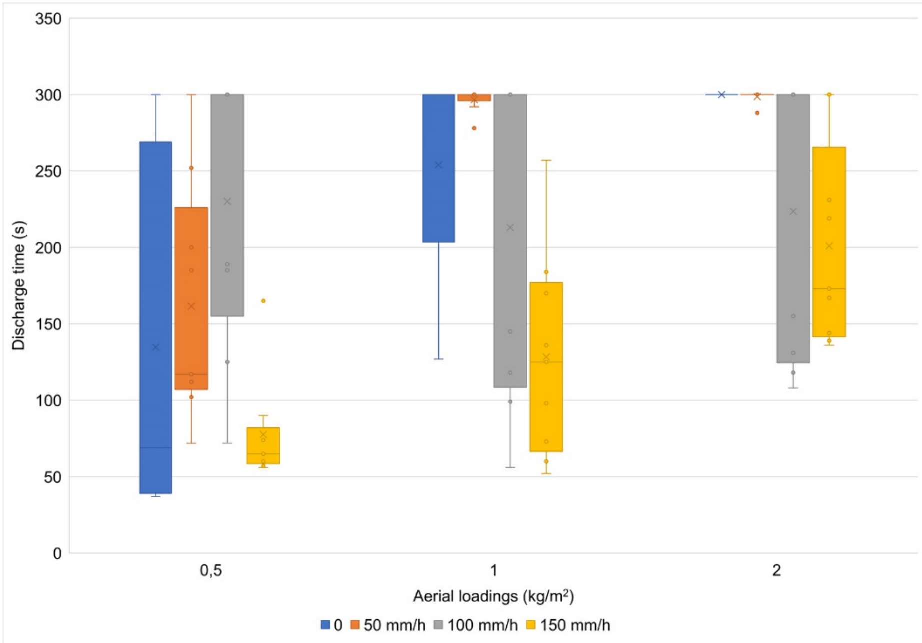

Figure 57 – Pervious concrete with 15% porosity discharge time x aerial loadings.

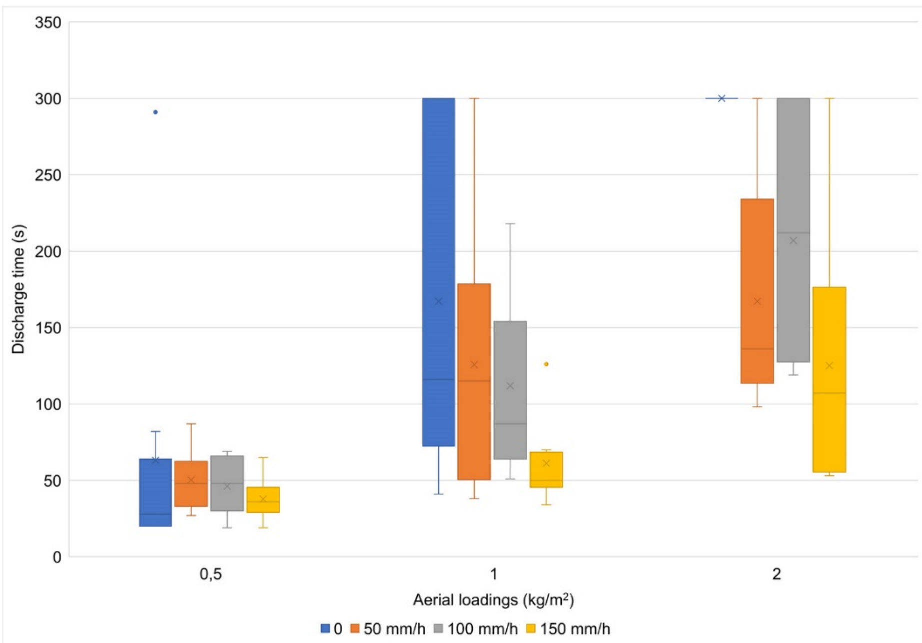

Figure 58 - Pervious concrete with 20% porosity discharge time x aerial loadings.

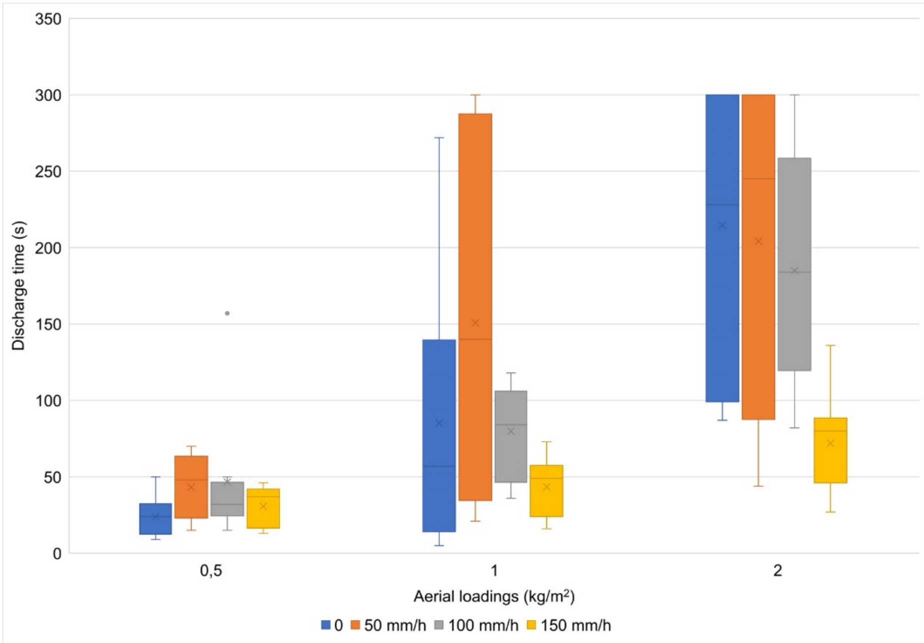

Figure 59 - Pervious concrete with 20% porosity discharge time x aerial loadings.

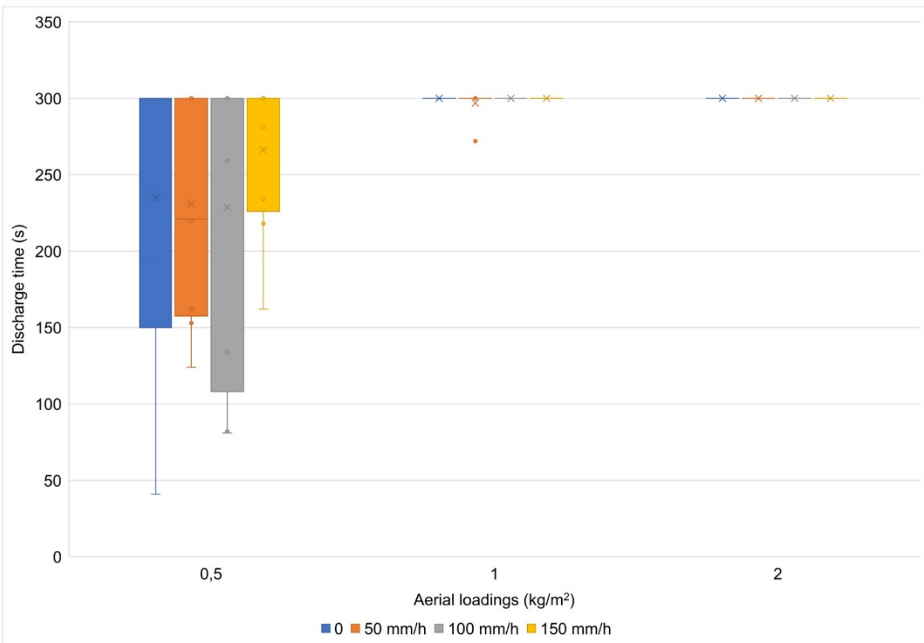

Figure 60 – Porous asphalt with 15% porosity discharge time x aerial loadings.

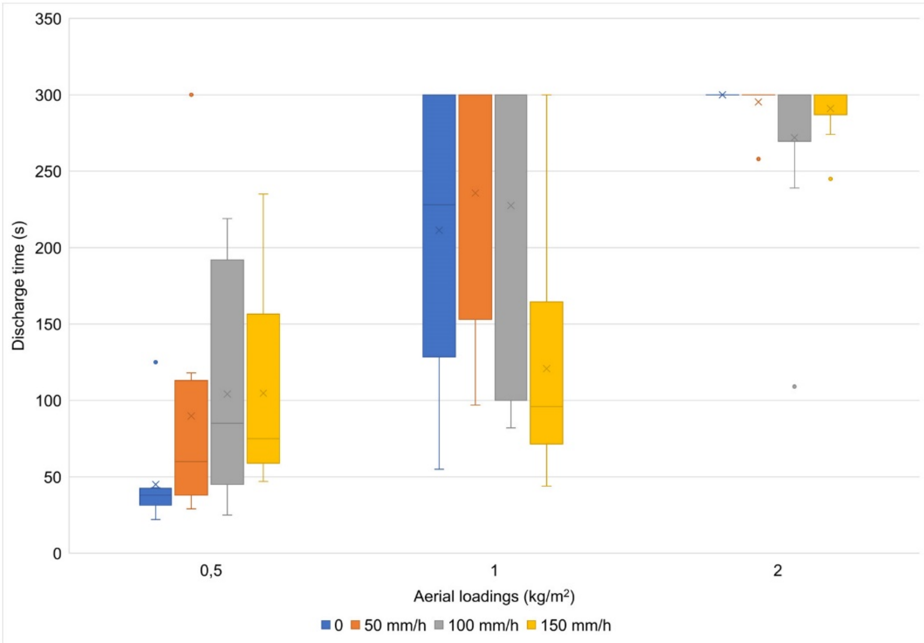

Figure 61 - Porous asphalt with 20% porosity discharge time x aerial loadings.

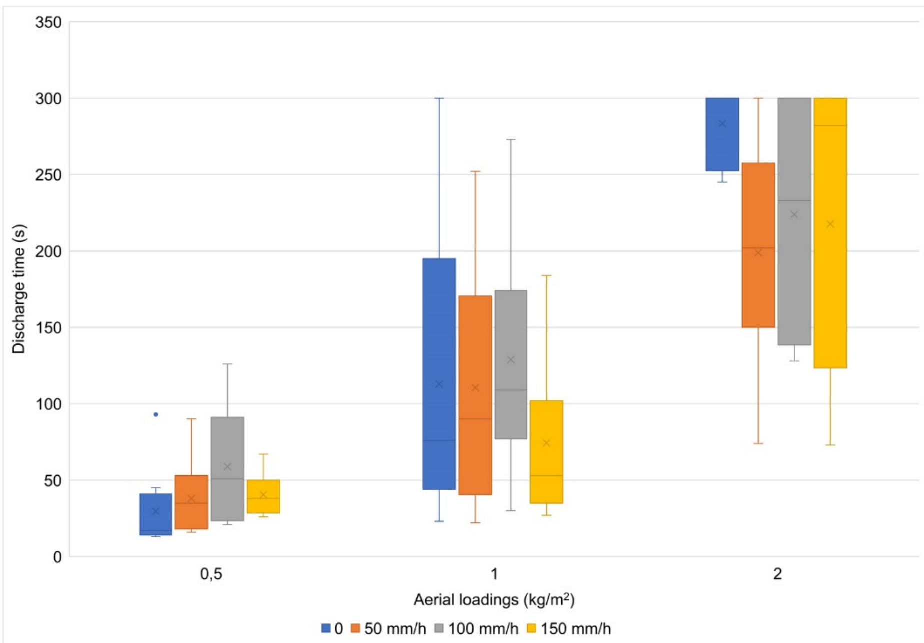

Figure 62 - Porous asphalt with 25% porosity discharge time x aerial loadings.

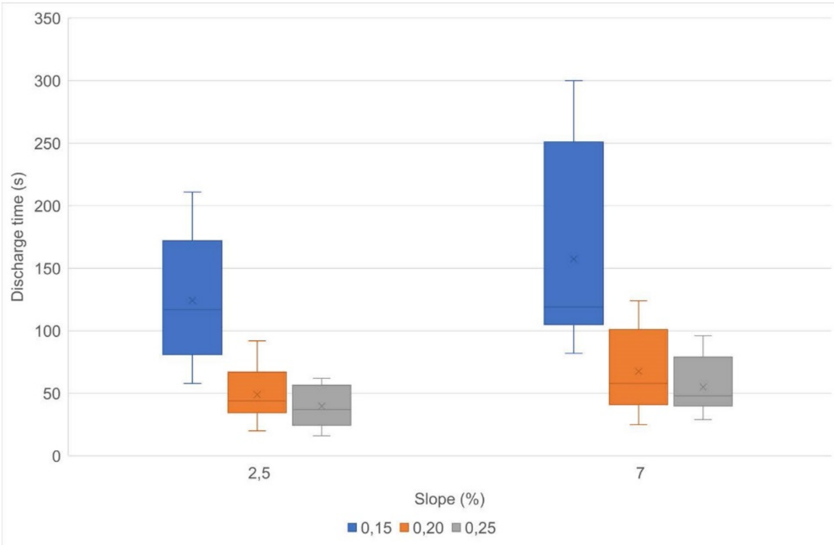

Figure 63 – Pervious concrete discharge time x slope for 100 mm/h rainfall intensity and 0,5 kg/m^2 aerial loadings.

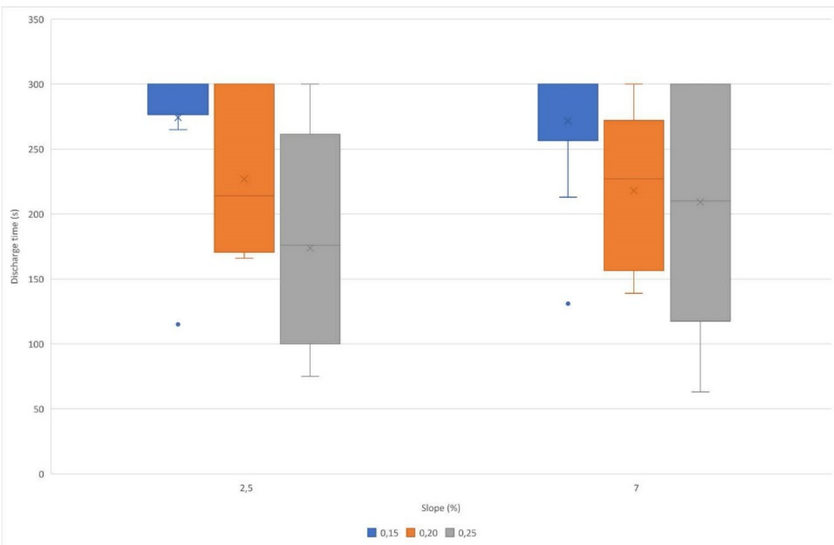

Figure 64 - Pervious concrete discharge time x slope for 100 mm/h rainfall intensity and 2,0 kg/m^2 aerial loadings.

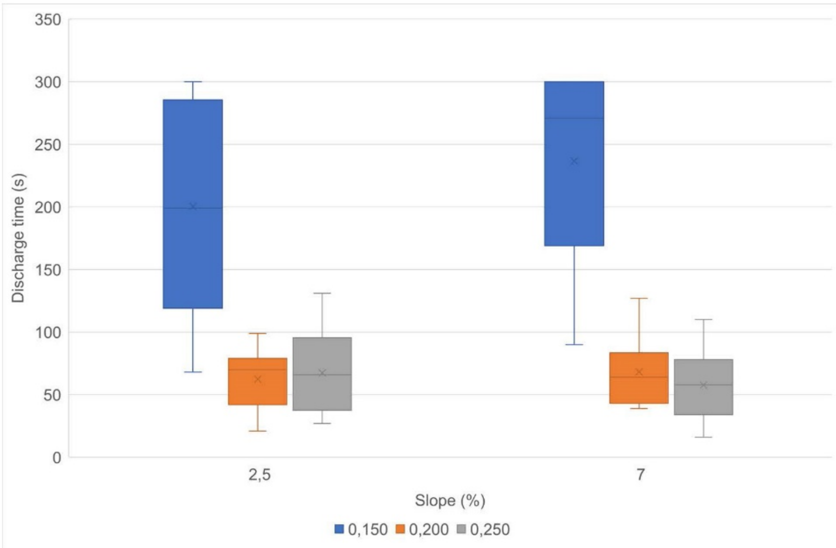

Figure 65 - Pervious concrete discharge time x slope for 150 mm/h rainfall intensity and 0,5 kg/m^2 aerial loadings.

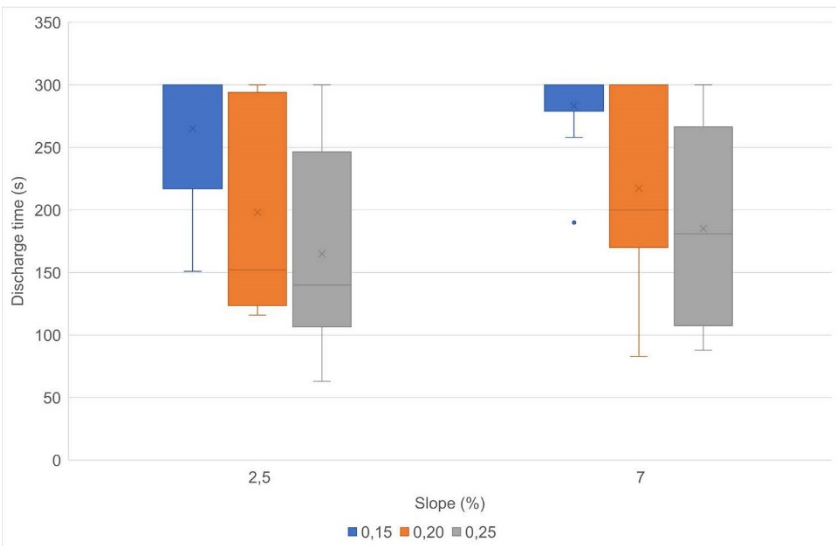

Figure 66 - Pervious concrete discharge time x slope for 150 mm/h rainfall intensity and 2,0 kg/m^2 aerial loadings.

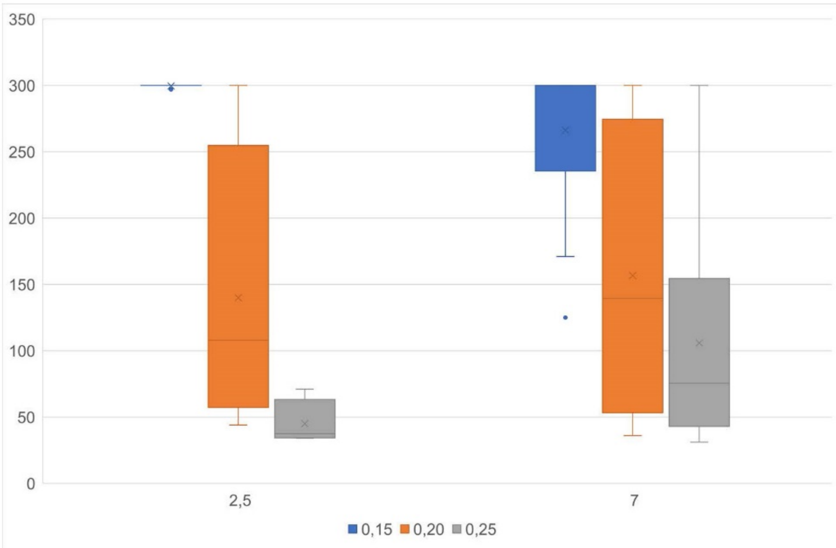

Figure 67 – Porous asphalt discharge time x slope for 100 mm/h rainfall intensity and 0,5 kg/m^2 aerial loadings.

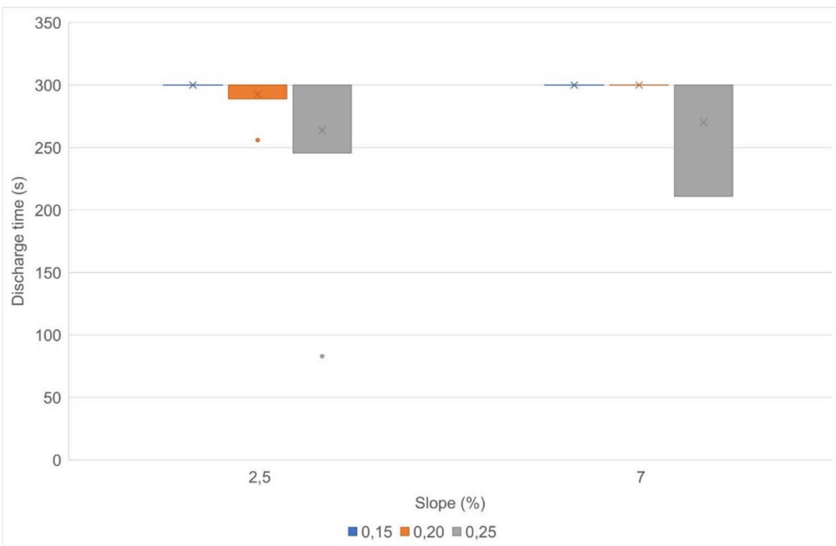

Figure 68 - Porous asphalt discharge time x slope for 100 mm/h rainfall intensity and 2,0 kg/m^2 aerial loadings.

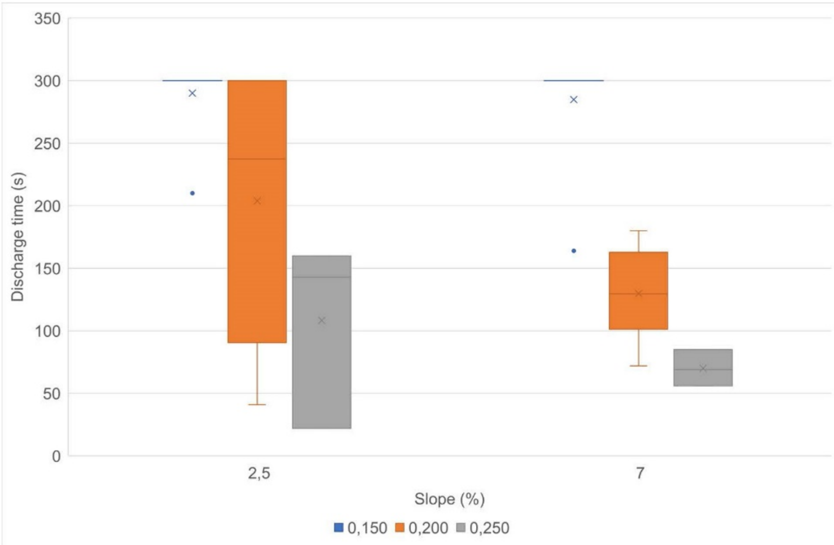

Figure 69 - Porous asphalt discharge time x slope for 150 mm/h rainfall intensity and 0,5 kg/m^2 aerial loadings.

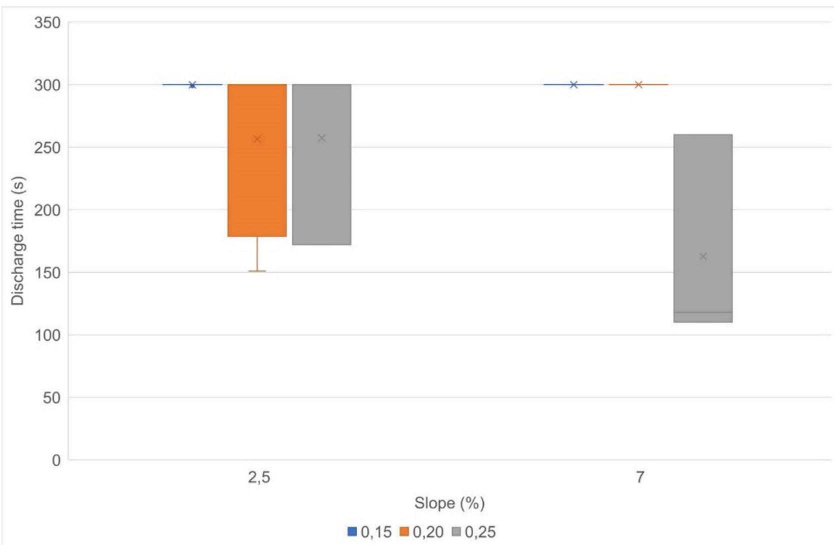

Figure 70 - Porous asphalt discharge time x slope for 150 mm/h rainfall intensity and 2,0 kg/m^2 aerial loadings.

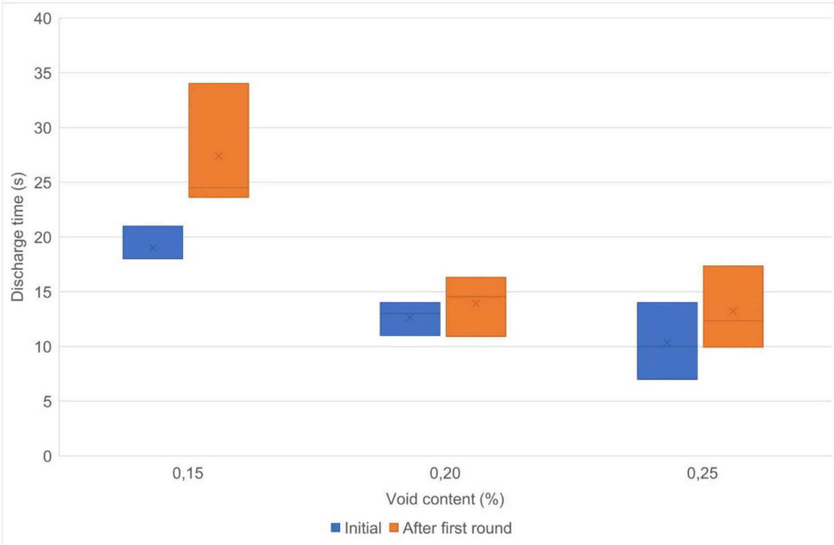

Figure 71 – Cleaning efficiency. Discharge time x porosity on initial conditions and after first round of tests with deeper cleaning procedures for pervious concrete.

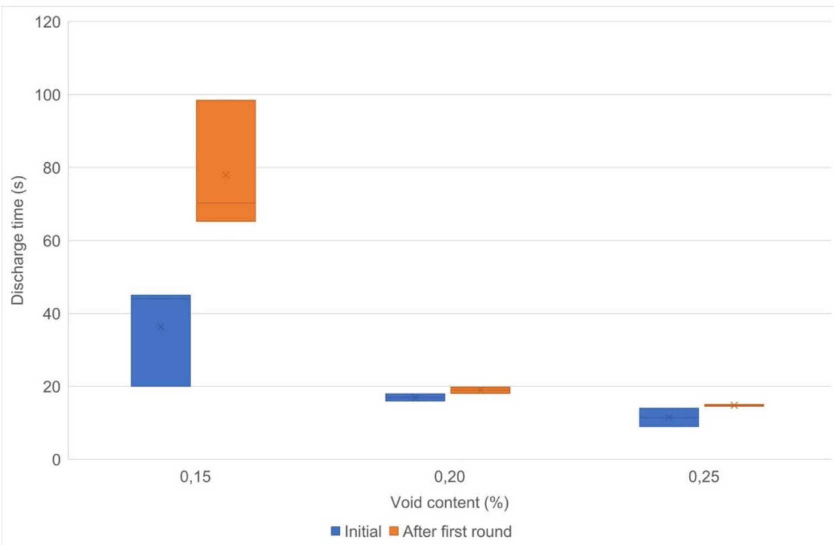

Figure 72 - Cleaning efficiency. Discharge time x porosity on initial conditions and after first round of tests with deeper cleaning procedures for porous asphalt.

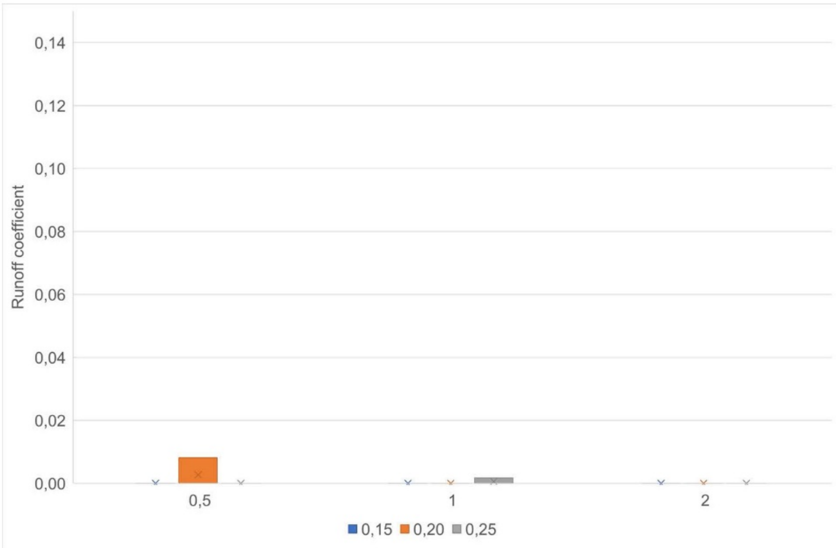

Figure 73 – Pervious concrete runoff coefficient x porosities for 50 mm/h rainfall intensity.

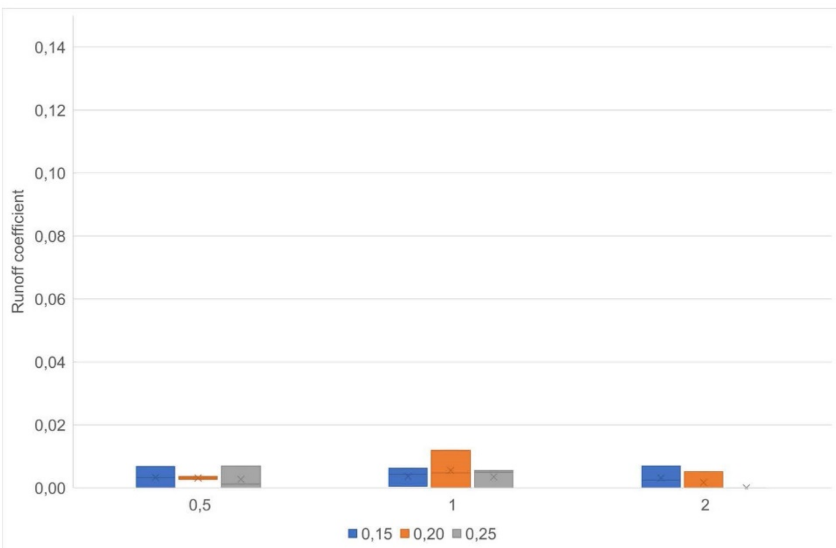

Figure 74 - Pervious concrete runoff coefficient x porosities for 100 mm/h rainfall intensity.

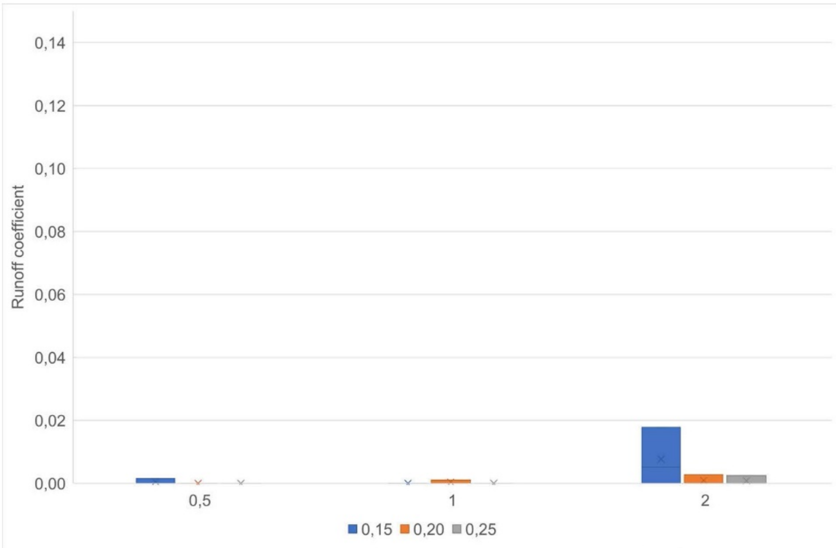

Figure 75 - Pervious concrete runoff coefficient x porosities for 150 mm/h rainfall intensity.

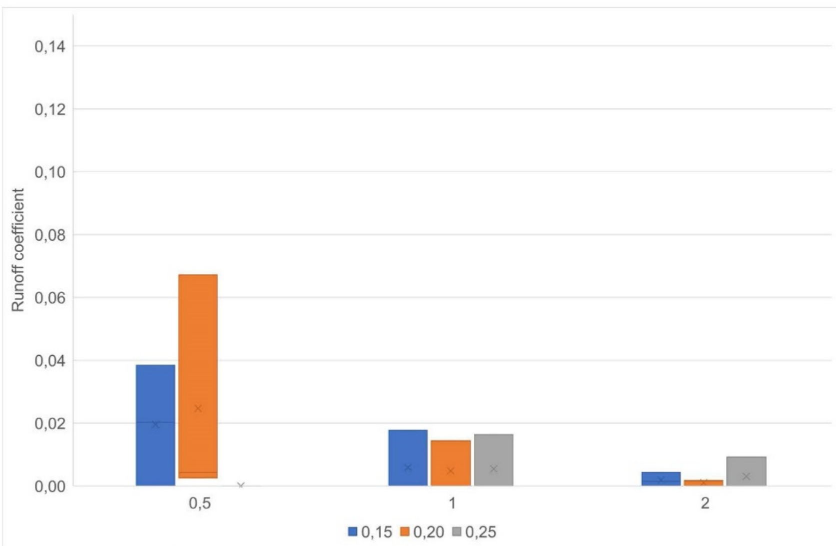

Figure 76 - Porous asphalt runoff coefficient x porosities for 50 mm/h rainfall intensity.

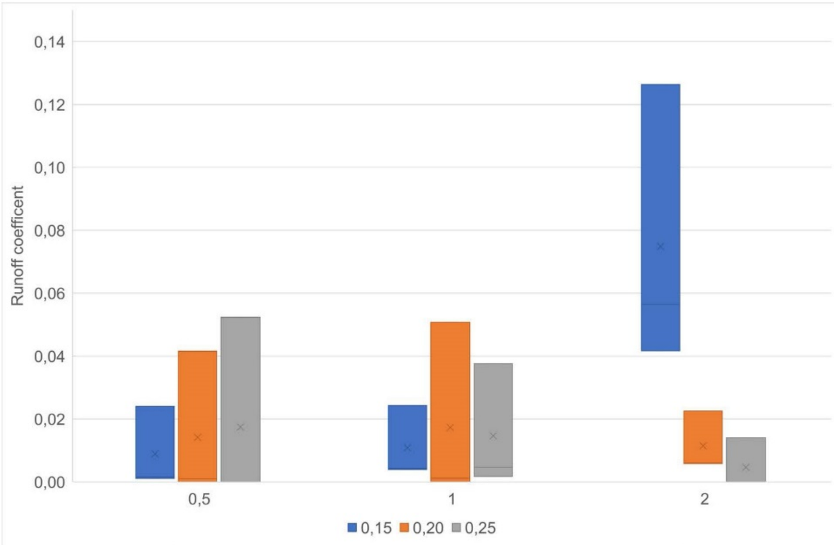

Figure 77 - Porous asphalt runoff coefficient x porosities for 100 mm/h rainfall intensity.

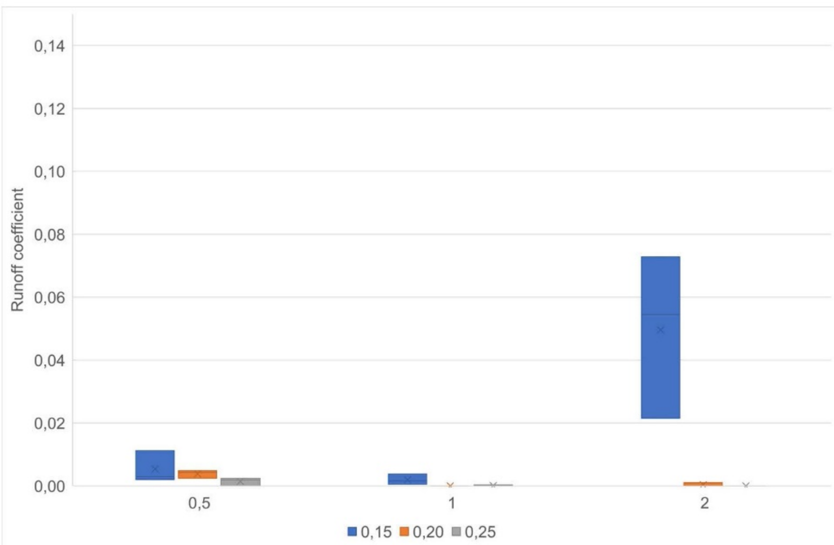

Figure 78 - Porous asphalt runoff coefficient x porosities for 150 mm/h rainfall intensity.

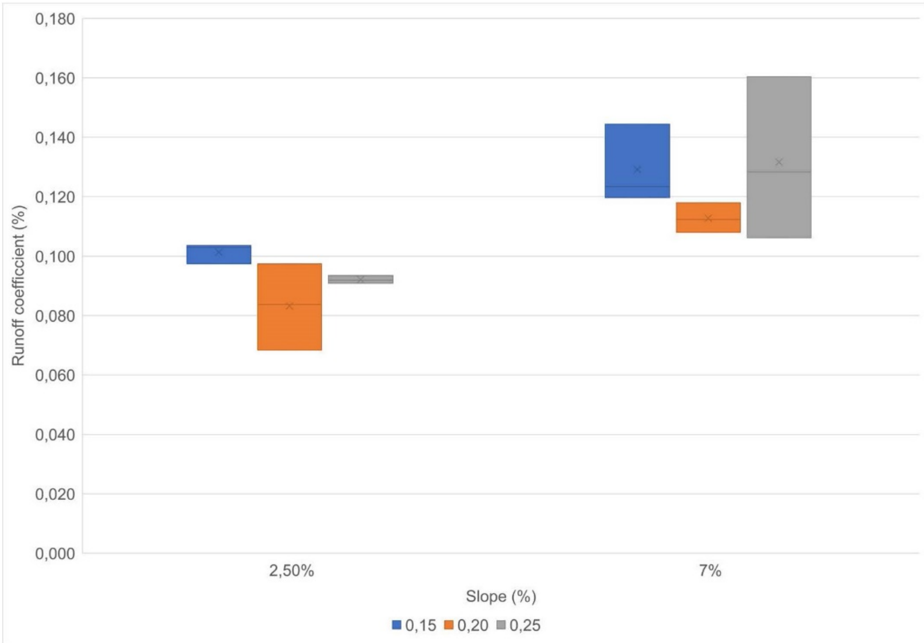

Figure 79 – Pervious concrete runoff coefficient x slope for 100 mm/h rainfall intensity and 0,5 kg/m^2 aerial loadings.

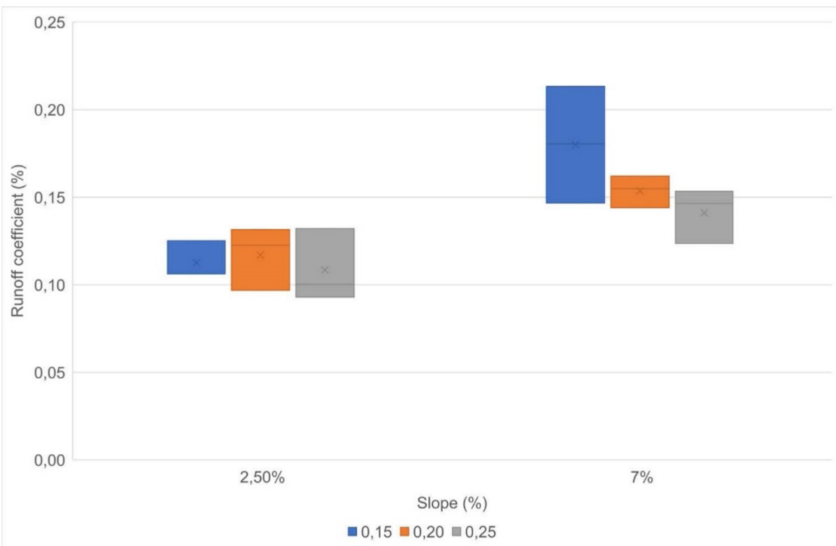

Figure 80 - Pervious concrete runoff coefficient x slope for 100 mm/h rainfall intensity and 2,0 kg/m^2 aerial loadings.

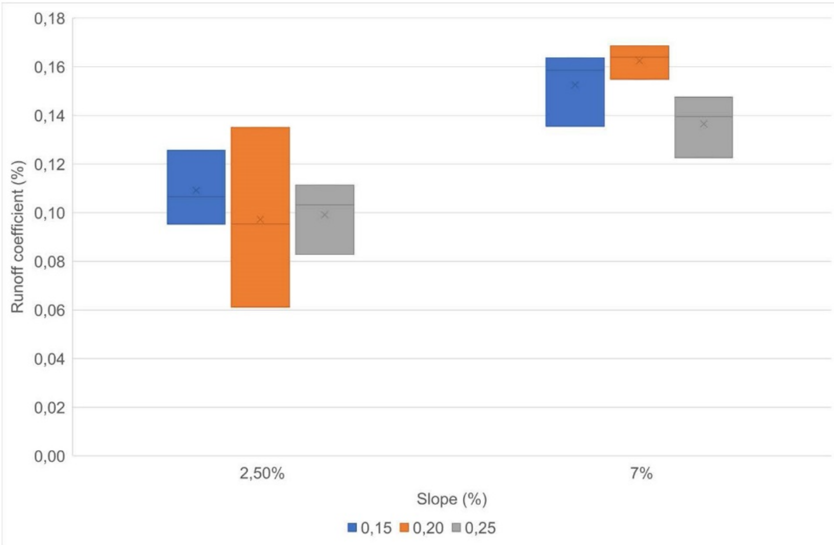

Figure 81 - Pervious concrete runoff coefficient x slope for 150 mm/h rainfall intensity and 0,5 kg/m^2 aerial loadings.

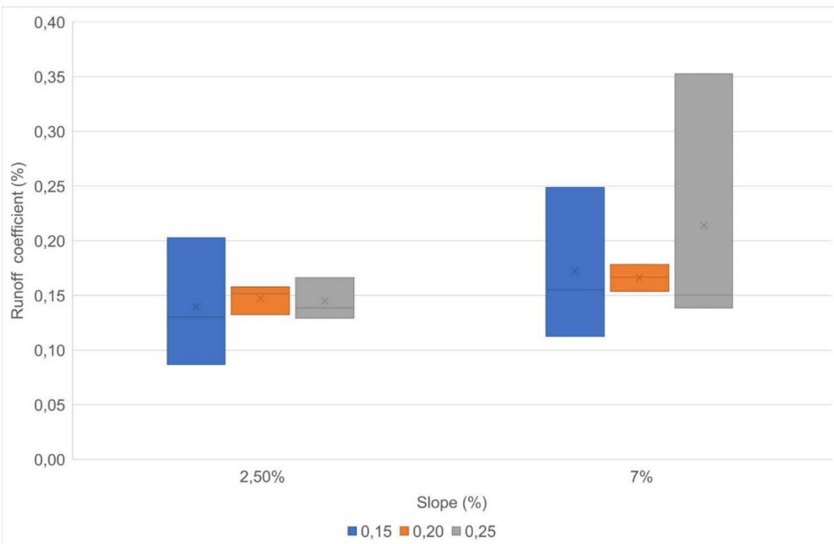

Figure 82 - Pervious concrete runoff coefficient x slope for 150 mm/h rainfall intensity and 2,0 kg/m^2 aerial loadings.

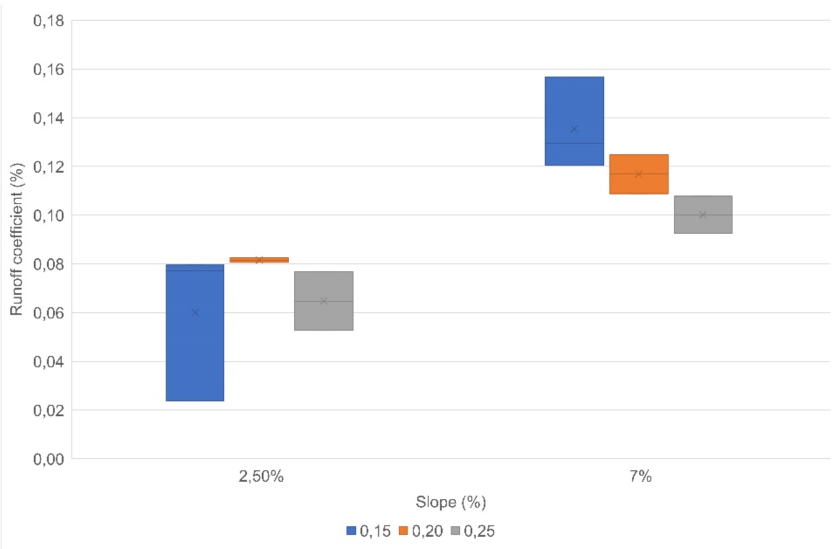

Figure 83 – Porous asphalt runoff coefficient x slope for 100 mm/h rainfall intensity and 0,5 kg/m^2 aerial loadings.

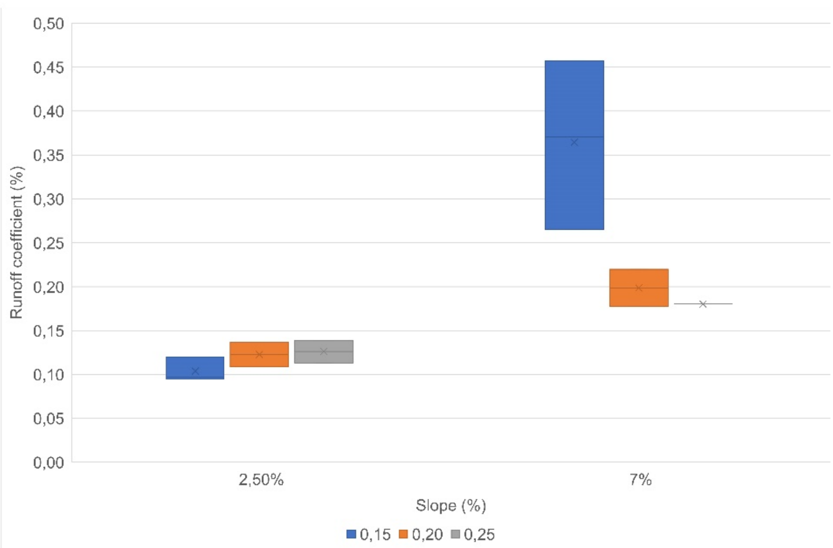

Figure 84 - Porous asphalt runoff coefficient x slope for 100 mm/h rainfall intensity and 2,0 kg/m^2 aerial loadings.

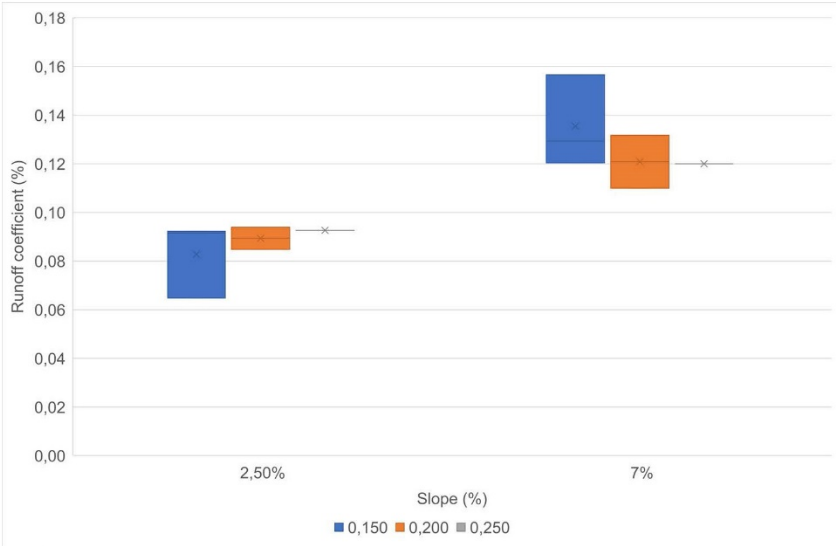

Figure 85 - Porous asphalt runoff coefficient x slope for 150 mm/h rainfall intensity and 0,5 kg/m^2 aerial loadings.

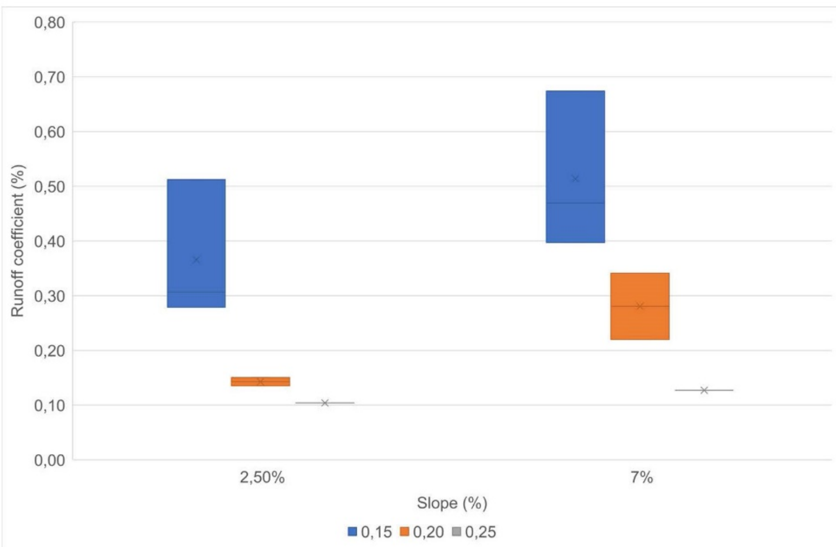

Figure 86 - Porous asphalt runoff coefficient x slope for 150 mm/h rainfall intensity and 2,0 kg/m^2 aerial loadings.

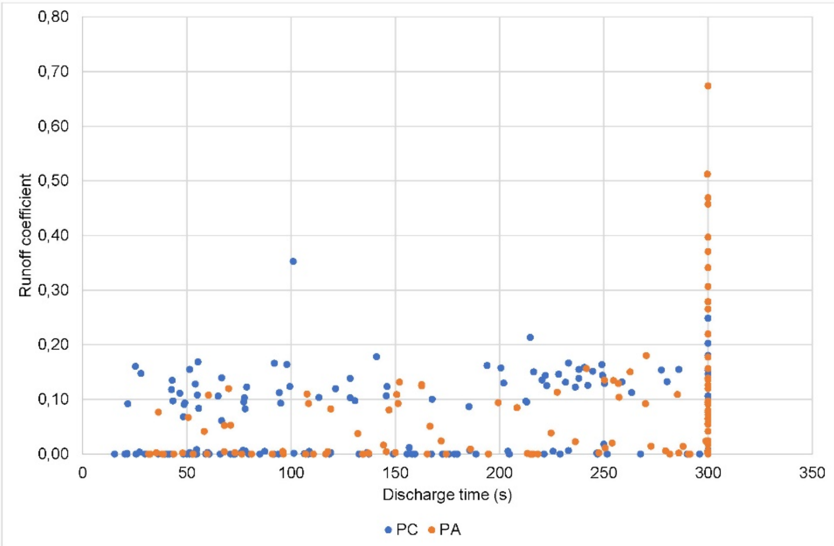

Figure 87 – Runoff coefficient x discharge time.

Acknowledgments

I would like to thank my supervisor Prof. Gianfranco Becciu for guiding me through this work with precious advises and a lot of support, and my co-supervisor Prof. John Sansalone for giving an important contribution and a priceless experience by welcoming me on University of Florida (United States). I also appreciate the contribution of Prof. Emanuele Toraldo and Prof. Roberto Fedele on the experimental program, Prof. Valerio Andres-Valeri for participating on the design and development of the rainfall simulator, Alessandra Bonicelli to share her thesis results to use as a start for this research, the laboratory technicians (Giuseppe Milleo and Edoardo Mariani) and the graduation students that participated on the experiments (Matteo Brugin, Martina Ceriani, Paolo Rota, Pietro Nicolello).

I specially acknowledge the support from Prof. Claudio Oliveira that encouraged me to follow this path, without him I would not be here today, all my colleagues and friends of the Brazilian Cement Association (ABCP) to introduce me to the world of cement and permeable pavement and Prof. Luiz Orsini to encourage me to cross the ocean to do research.

I also like to thank my colleagues of Politecnico di Milano (Claudia Destri, Mouna Feki, Anita Raimondi and many more to mention), Prof. Umberto Sanfilippo, Prof Stefano Mambretti, my colleagues on United States of University of Florida, Politecnico di Bari and Politecnico di Parma not only for the technical contributions but also for making this a really special and rich period.

And I must thank my parents Osmar Marchioni and Dirce M. L. Marchioni, my husband Adriano Gasaro and my family for their continuous support and patience and my children to give me the strength and driven to make an effort to contribute, even in a small way, to give them a better and sustainable world.

The author acknowledges the contribution from Capes for funding this work through the scholarship number BEX 9224/13-0.